48 V lead-acid/Li-ion battery charger

2 kW highly efficient natural convection-cooled design based on Infineon's CoolMOS™ P7 superjunction MOSFET

Authors: Eslam Alfawy and Rafael A. Garcia Mora

About this document

Scope and purpose

This document presents design considerations and results from testing a 2 kW industrial battery charger that is capable of charging 48 V based lead-acid and Li-ion batteries. The design is based on a dual-boost PFC and a half-bridge LLC DC-DC power supply solution, with natural convection cooling, using:

- 600 V CoolMOS™ P7 superjunction (SJ) MOSFETs for hard-switching and soft-switching topologies
- IDH16G65C6 CoolSiC™ Schottky diode 650 V G6 for an attractive price-performance ratio
- BSC030N08NS5 OptiMOS™ 5 80 V power MOSFET for reverse polarity protection
- IDB15E60 600 V silicon power diode
- ICE3PCS01G PFC controller IC for active Continuous Conduction Mode (CCM) power
- ICE2HS01G resonant mode controller
- ICE5QR2280AZ CoolSET™ QR Flyback controller
- 2EDN7524F EiceDRIVER™ 2EDN family of non-isolated dual gate drivers
- IRS21814 600 V high- and low-side gate driver IC
- XMC1403-Q064X0200 AA 32-bit XMC1000 industrial microcontroller

Intended audience

This document is intended for design engineers who want to realize a universal battery charger design that achieves a trade-off between performance targets and industrial production cost reduction to address cost-sensitive applications such as LSEV applications. The document also verifies the performance of the 600 V CoolMOS™ P7 SJ MOSFET technology in dual-boost PFC boost converters and resonant LLC converters along with EiceDRIVER™ ICs, 650 V CoolSiC™ Schottky diode G6 and XMC™ 1400 microcontroller.

48 V lead-acid/Li-ion battery charger
2 kW highly efficient natural convection-cooled design based on Infineon's
Table of contents

Table of contents

1   Summary of the 2 kW industrial battery charger

This application note provides a detailed description of the main features and operation under both steady-state and abnormal operating conditions of a 2 kW highly efficient natural convection-cooled industrial battery charger for 48 V lead-acid and Li-ion batteries. This demo board solidly confirms how different Infineon Technologies devices, ranging from power semiconductors to the controllers for the internal converters as well as for the accurate charging profile, perfectly fit a range of industrial applications.

Below is a summary of the key features that this demo board offers:

- Different battery types (chemistries) can be charged, as explained in section 3.1.
- Different battery charging capacities can be selected, as indicated in Table 4.
- Clear signalization of the operation status of the charger during normal operation, as described in section 3.3, and when an error is present, as described in section 3.4.
- Accurate charging profile according to the chemistry type selected as well as the measured temperature of the battery during the charging process, as described in the "Lead-acid and Li-ion charging profiles" section.
- In case larger batteries need to be charged or faster charge capability is needed, the battery charger can be connected in parallel with another unit to achieve this. This operation is clearly explained in section 5.
- High Power Factor (PF) and low Total Harmonic Distortion (THD) response at high-line, as shown in Figure 23.
- Efficiency higher than 92 percent from 20 percent of the rated load (2 kW) upward when V_{in} = 230 V AC, and efficiency higher than 91 percent of the rated load (1 kW) upward when V_{in} = 90 V AC, during CCM. Such results are clearly shown in Figure 28 and Figure 29.
- High performance achieved by using Infineon Technologies best-in-class devices:
  - TO-247 600 V CoolMOS™ P7 SJ MOSFETs for both dual-boost bridgeless PFC and half-bridge LLC topologies, along with single TO-220 650 V CoolSIC™ sixth-generation Schottky diodes.
  - EiceDRIVER™ 2EDN non-isolated gate driver as well as 600 V high- and low-side driver ICs.
  - QR Flyback controller ICE5QR4780AZ CoolSET™.
  - Super SO8 OptiMOS™ MOSFETs for battery management system control.
- Robust and realiable operation under different abnormal conditions:
  - Power Line Disturbance (PLD) events, like AC-Line Drop-Out (ACLDO) and voltage sag, as shown from Figure 30 to Figure 33.
  - Surge events that do not represent a serious threat to the integrity of the industrial battery charger according to what it is specified in the Surge immunity (EN61000-4-5)Surge immunity (EN61000-4-5) test in section 8.6.
- In case higher battery voltages are required, section 6 provides a list of changes that would be necessary to make at hardware level. Two different battery voltage ratings are considered: a) 72 V (range 67.2 V to 86.4 V at 30 A max.) and b) 144 V (range 134.4 V to 172.8 V at 15 A max.).

2 Introduction

The 2 kW industrial battery charger offers a charging solution that operates on any single-phase 90 V AC to 265 V AC grid worldwide with a 94.7 percent peak efficiency. The charger has two charging profiles implemented: one for Li-ion batteries and the other for lead-acid batteries. The respective charging profiles correspond to the latest trends of battery charging. With the selectable nominal battery capacity (C_{nom}) feature, the charging current can be automatically adjusted in order to charge different battery sizes and amp-hour ranges to help customers achieve battery charging flexibility.

The charger is designed based on a dual-boost PFC that provides high PF of greater than 0.9 and meets PFC regulation as per IEC61000-3-2 Class A, followed by a converter stage realized by a half-bridge LLC configuration. Infineon's latest 600 V CoolMOS™ P7 SJ MOSFET enables the design with natural convection cooling. The design has a battery management control system capable of charging both 48 V lead-acid and Li-ion batteries in the different charging modes – constant voltage and CCM.

The battery management control system implemented is designed to optimally charge lead-acid (WET, GEL, AGM, EFB and VRLA) as well as Li-ion (LiPo, Li_2MnO_3, $Li_2Mn_2O_4$, $Li_4Ti_5O_{12}$ and $LiFePO_4$) batteries used on electric vehicles including E-scooters, E-bikes and low-speed vehicles. Furthermore, an RS485 bus communication protocol feature allows for a master/slave operation that can extract 4 kW max. charging power when connecting two chargers in parallel configuration, ensuring seamless power distribution and a fast charging feature for Li-ion batteries.

2.1 Main features

Figure 1   Front panel of the industrial battery charger

48 V lead-acid/Li-ion battery charger
2 kW highly efficient natural convection-cooled design based on Infineon's

Some of the main features are listed below:

- Battery temperature monitor
- Auto-configures output power to 1000 W when connected to less than 127 V AC to prevent nuisance breaker trips
- RS485 bus communication for parallel operation
- Multi-colored LED indicator for battery status, charging, error and fault indication
- Convection cooled
- Battery Management System (BMS) integration
- Protected against short-circuit, reversed polarity, over- and under-AC-voltage, over-heating Without external fuses and with an automatic reset
- Control of the charge time and automatic detection of faulty batteries
- Thermal protection with internal probe
- Thermal probe for battery
- Dimensions: 258 × 123 × 80 mm
- Weight: 7.5 kg

2.2 Featured applications

- E-bikes – pedelecs battery charger
- E-rickshaws – E-scooters battery charger
- Forklifts – E-carts battery charger
- Micro E-cars – logistics EV battery charger

2.3 Specifications

Table 1   **Input requirements**

Parameter	Value
Input voltage range, V_{in_range}	90 V AC to 265 V AC
Nominal input voltage, V_{in}	200 V AC to 265 V AC
AC-line frequency range, f_{AC}	47 Hz to 63 Hz
Turn-on input voltage, V_{in_on}	80 V AC to 87 V AC, ramping up at low-line with limited power
Turn-off input voltage, V_{in_off}	75 V AC to 85 V AC, ramping down at low-line with limited power
Power Factor (PF)	Greater than 0.9 from 10 percent rated load
Hold-up time	10 ms after last AC zero point at P_{out_max} 20 ms after last AC zero point at $0.5 \times P_{out\_max}$
Total Harmonic Distortion (THD)	Less than 15 percent from 10 percent of the load at high-line, for Class A equipment

Table 2   **Output requirements**

Parameter	Value
Nominal output voltage, V_{out}	40 V DC to 60 V DC
Maximum output power, P_{out}	2 kW at V_{in} = 178 V AC to 265 V AC at I_{in_max} = 12 A AC
	1 kW at V_{in} = 90 V AC to 138 V AC
Peak output power, P_{out_max}	2 kW
Maximum output current, I_{out_max}	50 A
Output voltage ripple	Max. 20 V_{pk-pk} at V_{out} and I_{out}
Maximum output over-voltage threshold	60.9 V DC
Minimum output over-voltage threshold	60.2 V DC

Table 3   **Efficiency at different load conditions**

Value	Conditions
Greater than 94.7 percent at 50 percent of the load	V_{in} = 230 V AC, V_{out} = 48 V DC
Greater than 94.2 percent at 100 percent of the load	V_{in} = 230 V AC, V_{out} = 48 V DC
Greater than 91.7 percent at 100 percent of the load	V_{in} = 90 V AC, V_{out} = 48 V DC

3 Normal operation

3.1 Supported battery types

The battery charger is designed to charge lead-acid batteries and Li-ion batteries with a nominal voltage of 48 V. The maximum power is limited to 2000 W, which leads to charging currents from 35 A at 57 V up to 50 A at 40 V.

The charging voltage ranges from a minimum value of 40 V up to a maximum value of 62.5 V. In order to adapt the charging currents to the battery size, the battery capacity can be adjusted using an eight-step rotary switch.

The implemented charging profiles for lead-acid and Li-ion batteries are favored for universal charging to achieve a maximum number of battery types. There are no optimizations for fast charging or maximum capacity.

With the implemented charging profiles it is possible to charge lead-acid battery types such as WET, GEL, AGM, EFB and VRLA batteries, each with a nominal number of cells in series = 24 and Li-ion battery types like lithium-polymer (LiPo), lithium-nickel-manganese-cobalt (NMC), lithium-cobalt ($LiCoO_2$) or lithium-manganese (Li_2MnO_3), each with a nominal number of cells in series = 14.

It is also possible to charge Li-ion batteries with lithium-iron-phosphate (LFP) with a number of cells in series = 16 and lithium-titanium (LTO, SCiB) with a number of cells in series = 20 or 21.

The respective charging profiles correspond to the latest trends in battery charging.

3.2 Battery selection

For setting the optimal charging profile according to the battery type, the charger is equipped with a toggle switch to select the battery chemistry and an eight-step rotary switch to adjust the battery size (battery capacity). With the toggle switch it is possible to select either lead-acid batteries (white LED is on) or Li-ion batteries (blue LED lights).

With the rotary switch the battery capacity is selected according to the following steps:

Table 4   **Maximum battery capacity selection**

Position	Capacity	Max. charging current – I1		charging current	
		Lead-acid	Li-ion	Lead-acid (I1´)	Li-ion (I2)
0	40 Ah	8 A	20 A	0,8 A	4 A
1	60 Ah	12 A	30 A	1,2 A	6 A
2	80 Ah	16 A	40 A	1,6 A	8 A
3	100 Ah	20 A	50 A	2,0 A	10 A
4	125 Ah	25 A	65 A	2,5 A	12 A
5	150 Ah	30 A	75 A	3,0 A	15 A
6	200 Ah	40 A	100 A	4,0 A	20 A
7	250 Ah	50 A	125 A	5,0 A	25 A

The adjusted main charging current in the charging profiles is ($0.2 \times C_{nom}$) for lead-acid batteries and ($0.5 \times C_{nom}$) for Li-ion batteries.

For Li-ion batteries with fast charge capability (I_1 greater than or equal to $1.0 \times C_{nom}$) select a higher capacity value.

In single-operation mode the maximum current is limited to 50 A and 2000 W maximum power.In order to achieve the maximum performance (minimum charging time) particularly for Li-ion batteries use the parallel mode option with a maximum current of up to 100 A and 4000 W maximum power.

For further information about the charging profiles implemented see also chapter 4 "Lead-acid and Li-ion charging profiles".

To avoid mis-triggering/interruption during the charging process, the battery charger software is designed in such a way that it does not consider the change of the switches (toggle switch and rotary switch) during operation; the changes are only valid in the first 5 s after the mains is applied.This is before the charging process has started. Only at the end of the battery charging profile the green status LED is fully on again. In all other cases (while the charging process is executed) the changing of the switches has no effect.

If a valid change of battery type (chemistry or capacity) occurs, the 5 s interval is reset to zero and starts again.

3.3 Status signalization

For user information about the charger status and valid battery settings there are several LEDs positioned on the front side of the charger – see Figure 1.

Table 5 shows the blinking codes for different operating statuses. On the left-hand side there is a green LED to indicate the power status (mains on/off) and the mains capability (mains voltage). If the mains voltage goes below 170 Vrms the power LED will be blinking because the maximum power is reduced to 1000 W.

The next LED, also green colored, gives information about the charging process. When this LED blinks slowly, the charging process has started with the main charging current I_1. When the LED is blinking fast, the charging profile has changed to the constant voltage stage, reducing the main charging current.The charging process is finished when the LED is fully on.

The next two LEDs are signalizing error conditions. For temperature failures there is a separate orange-colored LED. If this LED is blinking, the charger works with reduced power because of the highly increased temperature. If the orange LED is fully on, then the charger is shut down.

For all other errors the red LED is used. If this LED is blinking, an error has occurred and the charger is switching off. All other LEDs are to indicate the currently valid settings (battery type and size).

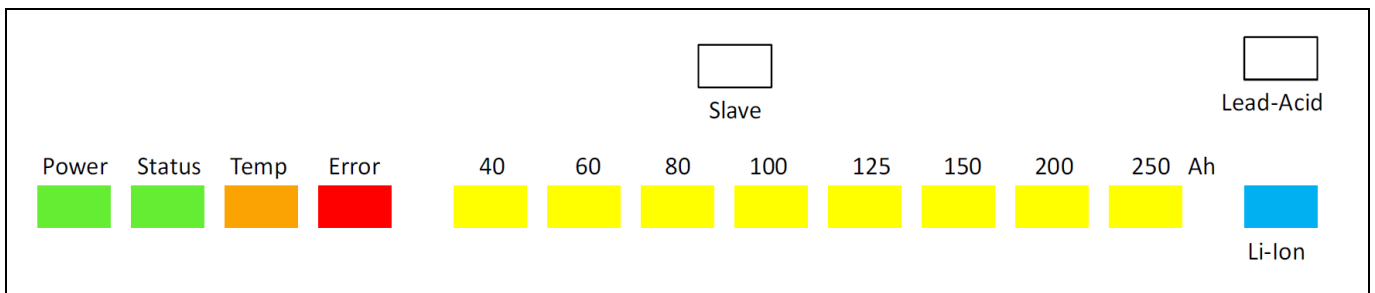For a detailed description of the blinking codes see 3.4 "Error signalization".

Figure 2   **LED indicators overview**

Table 5   **Blinking codes for operation status**

Status	Power LED (green)	Status LED (green)	Temperature LED (orange)	Error LED (red)	Eight battery capacity LEDs (yellow)	Li-ion LED (blue)	Lead-acid LED (white)	Slave LED (white)
Off	Battery charger is not powered	No charging	Temperature in normal range	No errors – normal operation	Slave mode	Lead-acid profile is active	Li-ion profile is active	Master mode
Blinking	Battery charger is powered on – reduced power	Time 2 s: constant current charge stage Time 1 s: constant voltage charge stage	Temperature in critical range – power derating	Error shutdown – blinking code for different errors				
Fully on	Battery charger is powered on – maximum power	Charging process finished	Over-temperature – error shutdown	Over-temperature error	Selected battery capacity – (40 Ah to 250 Ah respectively)	Li-ion profile is active	Lead-acid profile is active	Slave mode (all other LEDs are off)

3.4   Error signalization

For indication of which error is responsible for the shutdown of the charger, a dedicated blinking code is generated and signalized on the red error LED.
For details see Table 6.

Table 6   **Blinking codes for different errors**

Blinking code	Error description
2 × short/1 × long	Over-voltage error (62.8 V/59.8 V) – (lead-acid/Li-ion)
2 × short/2 × long	Under-voltage error (28.8 V/35.0 V) – (lead-acid/Li-ion)
2 × short/3 × long	Voltage gain error (voltage rise error) – (4.5 V/s)
2 × short/4 × long	Over-current error (52.5 A)
2 × short/5 × long	Under-current error (difference between current reference and measured current greater than 5.0 A)
Fully on	Over-temperature charger (+115°C)
3 × short/2 × long	Under-temperature charger (-20°C)
3 × short/3 × long	Over-temperature battery (+65°C/+60°C) – (lead-acid/Li-ion)
3 × short/4 × long	Under-temperature battery (-20°C)
4 × short/1 × long	Time-out pre-charging (2 h/1.5 h) – (lead-acid/Li-ion)
4 × short/2 × long	Time-out main charging current stage (10 h/8 h)
4 × short/3 × long	Time-out main charging voltage stage (12 h/10 h)

4 × short/4 × long	Exceedance of charging capacity ($1.2 \times C_{nom}$)	
5 × short/1 × long	Error auxiliary supply (9.5 V less than U_{aux} less than 15.5 V)	
5 × short/5 × long	Unspecified error	

4 Lead-acid and Li-ion charging profiles

4.1 Charging profiles

The battery charger software is implemented with two charging profiles – for charging Li-ion and lead-acid batteries. Furthermore it is possible to set the nominal battery capacity (C_{nom}) in order to adjust the charging currents to the battery size. The respective charging profile corresponds to the latest trends in battery charging.

4.1.1 Charging profile for Li-ion battery

The implemented charging profile for Li-ion batteries is valid for various types of Li-ion technologies.

You can charge:

- Lithium-cobaltdioxide ($LiCoO_2$), also known as Lithium polymer (LiPo)
- Lithium-manganese (Li_2MnO_3, $Li_2Mn_2O_4$)
- Lithium-titanium ($Li_4Ti_5O_{12}$), each of them with a nominal number of cells in series = 14
- Lithium-iron-phosphorus ($LiFePO_4$), with a nominal number of cells in series = 16

Attention: **It is not recommended to charge a LiFePO₄ battery with 15 cells in series.**
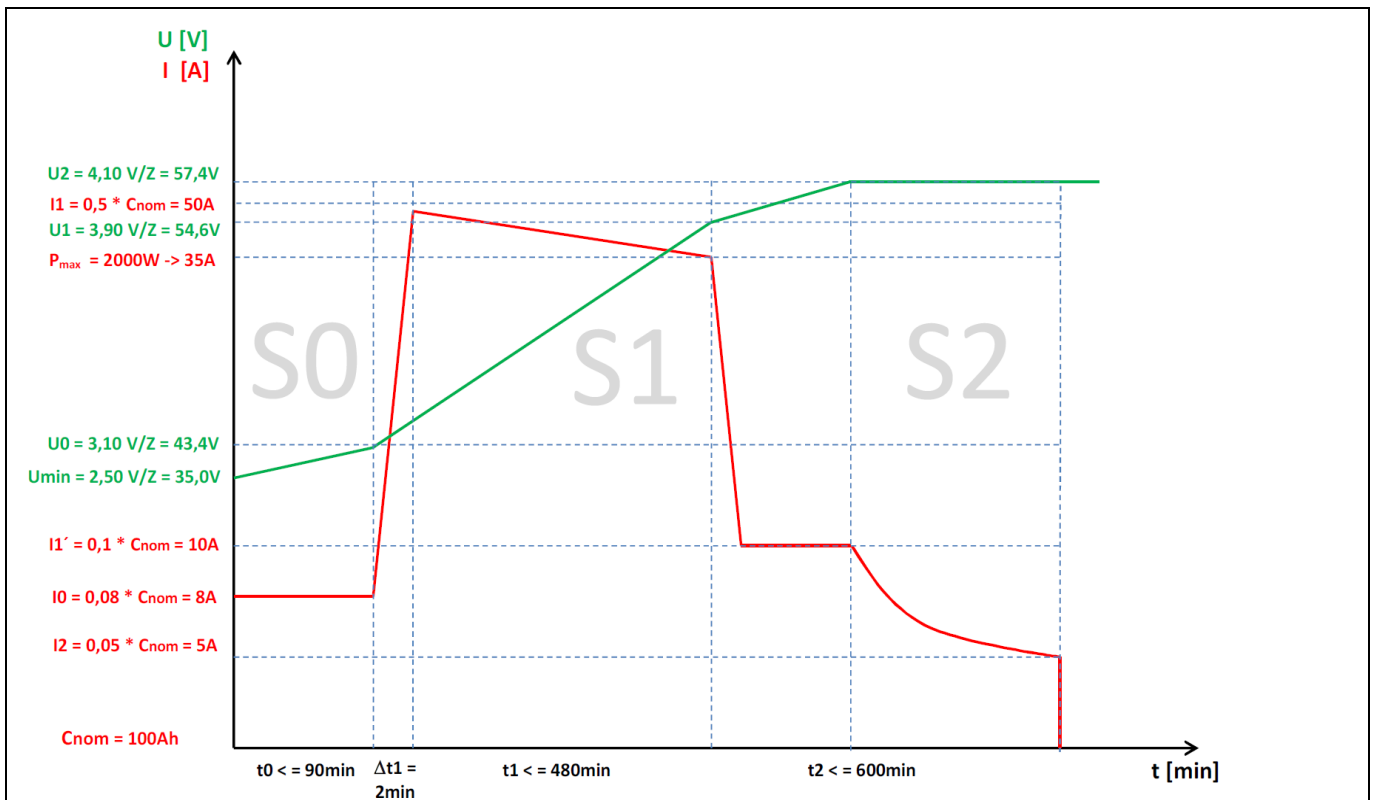

Figure 3   Charging profile of Li-ion battery

In case of a deep-discharged battery, the charging profile starts with a pre-charging state (S_0). In this state a low charging current is used to rebuild the cell voltage up to the normal range. If the cell voltage reaches the normal operating area in the given time, the main charging (S_1) starts with a current ramp (D_{t1} = 120 s).

The preset current value in the main charging state is $0.5 \times C_{nom}$. This value is valid for all Li-ion cells. For Li-ion batteries with a boost charge capability (I_1 greater than or equal to $1.0 \times C_{nom}$) you can choose a higher C_{nom} value and/or use the parallel charging option.

The S_1 state is divided into two sections. The main section is charging with the maximum current ($0.5 \times C_{nom}$) or the maximum power ($P_{max} = 2000$ W) up to a cell voltage of 3.9 V (equates to a capacity of ~ 90 percent). For the remainder of this state the charging current is reduced to $0.1 \times C_{nom}$.

If the charging voltage reaches a value of 4.1 V/cell, the battery charger switches to the saturation stage (S_2). Now the charging voltage remains constant until the charging current goes below the cut-off limit ($0.05 \times C_{nom}$).

In this case the charging profile is complete and the charging process is finished. The implemented charging profile for Li-ion batteries favors a gentle charging to achieve a maximum count.

4.1.2   Charging profile of lead-acid battery

The implemented charging profile for lead-acid batteries is also valid for various types of this battery.

So it is possible to charge:

- WET, GEL, AGM, EFB and VRLA batteries each with a nominal number of cells in series = 24
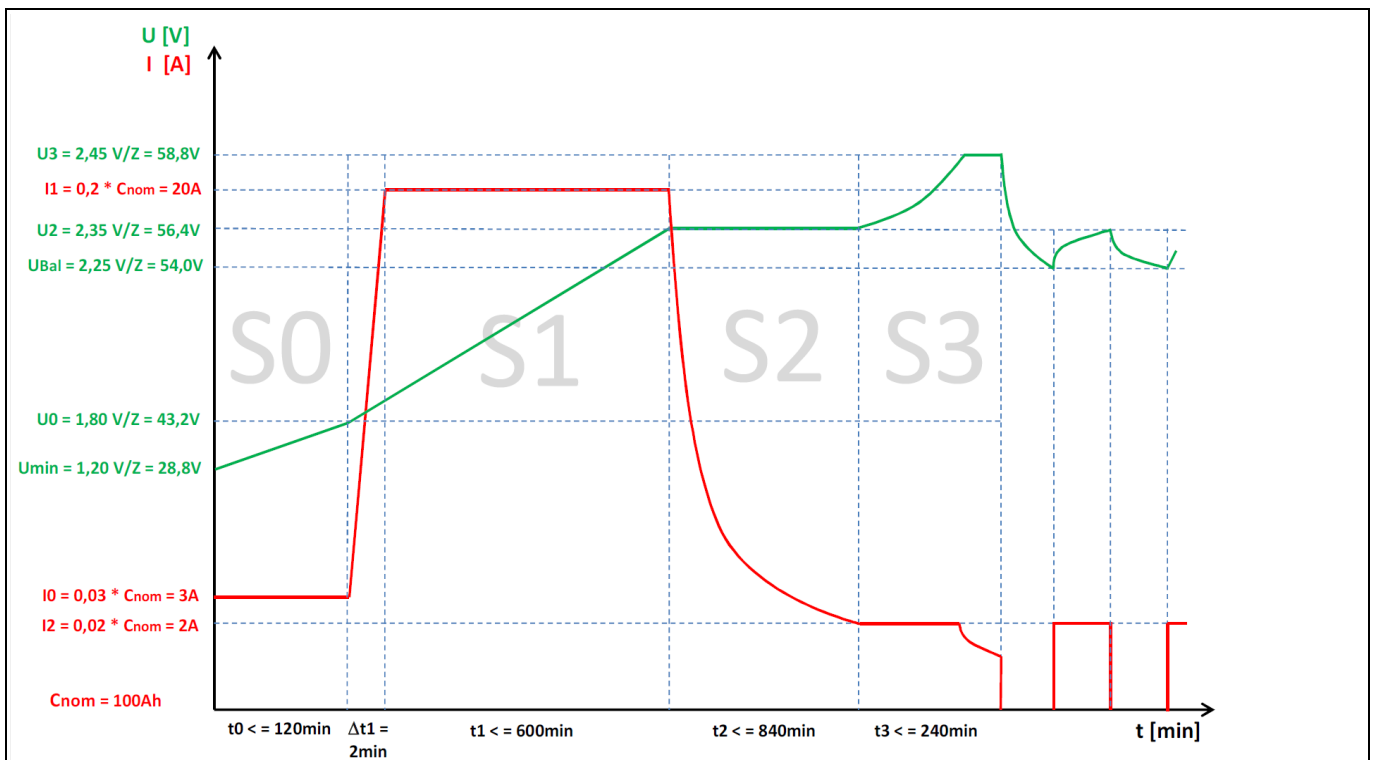

Figure 4   Charging profile of lead-acid battery

In case of a deep-discharged battery, the charging profile starts with a pre-charging state (S_0). In this state a low charging current is used to rebuild the cell voltage up to the normal range. If the cell voltage reaches the normal operating area in the given time, the main charging ($S_1 + S_2$) starts with a slow current ramp ($D_{t1} = 120$ s).

The preset current value in the main charging state is ($0.2 \times C_{nom}$). This value is valid for all lead-acid types. The main charging state is divided into two sections (S_1 and S_2).

The S_1 section is the constant current charging with the maximum current ($0.2 \times C_{nom}$) or the maximum power ($P_{max} = 2000$ W). Up to a cell voltage of 2.35 V/cell the charging current (or power) is to remain constant. The

battery charger then switches to the absorption stage (S_2). Now the charging voltage remains constant until the current goes below the switch-over limit ($0.02 \times C_{nom}$). If the main charging time t_1 (in S_1) is greater than 30 min the charger switches to the after-charging state (S_3); otherwise, the charging process is finished and the charger begins trickle-charging without after-charging.

After-charging state (S_3) the current remains constant ($0.02 \times C_{nom}$) and the battery voltage can rise up to 2.45 V/cell. The S_3 state is either finished by a time limitation [$t_3 = 1.0 \times (t_1 + t_2)$; with t_{3min} = 30 min and t_{3max} = 240 min] or by a DU/Dt condition [DU/Dt less than 0.2 V/15 min].

When the charging process has finished (S_0 to S_3), the charger enters a trickle-charging state (also called "balancing"). This state replaces the otherwise often-used float charging. Now the battery voltage is monitored and in case it falls below 2.25 V/cell a constant current charging starts ($0.02 \times C_{nom}$) until the battery voltage reaches 2.35 V/cell again. This can be done an unlimited number of times.

The implemented charging profile for lead-acid batteries favors universal charging to suit a maximum number of battery types. It is not optimized for fast charging or maximum capacity.

4.2 Charging profiles according to the temperature of the battery

For adaptation of the charging profiles according to the battery temperature, the charger is equipped with a simple two-pin connector. On this interface it is possible to connect a temperature-dependent resistor with a Negative Temperature Coefficient (NTC) and a nominal value of 10.000 Ω (NTC 10 k). See Table 7 for the precise temperature profile of the supported temperature sensor.

The charger is automatically detecting the existence of the battery temperature sensor. If the sensor is connected and the battery temperature is in the valid range from -30°C to +80°C, the charging profile is adjusted according to the measured temperature.

In all other cases – not connected, invalid range, broken or shorted wire – the charging profile is executed with the nominal battery temperature (+25°C) and without considering temperature correction.

The temperature-dependent modification of the charging profile is very different for lead-acid batteries and Li-ion batteries. A detailed description of the modifications performed is given in the following sections.

Table 7   **Temperature profile – battery temperature sensor – NTC 10 k**

Temperature [°C]	Resistance [Ω]
-50	667830
-40	335670
-30	176680
-20	96970
-10	55300
0	32650
10	19900
20	12490
30	8060
40	5320
50	3600
60	2490
70	1750
80	1260

90	920
100	680

4.2.1 Temperature profile of lead-acid battery

In the event of detection of a valid battery temperature the charging profile for lead-acid batteries is modified in the following way.

- Abort charging with error signalization when battery temperature is below -20°C.
- Abort charging with error signalization when battery temperature is over +65°C.
- Increase charging voltage in the range from +20°C down to -20°C with 3 mV per cell and Kelvin.
- Decrease charging current in the range from +55°C up to +65°C down to 50 percent of nominal value.

The supervision of the battery temperature and the correction of the charging voltage is done in all sectors of the charging profile. The derating of the charging current is done in the main charging sectors (S_1 and S_2).
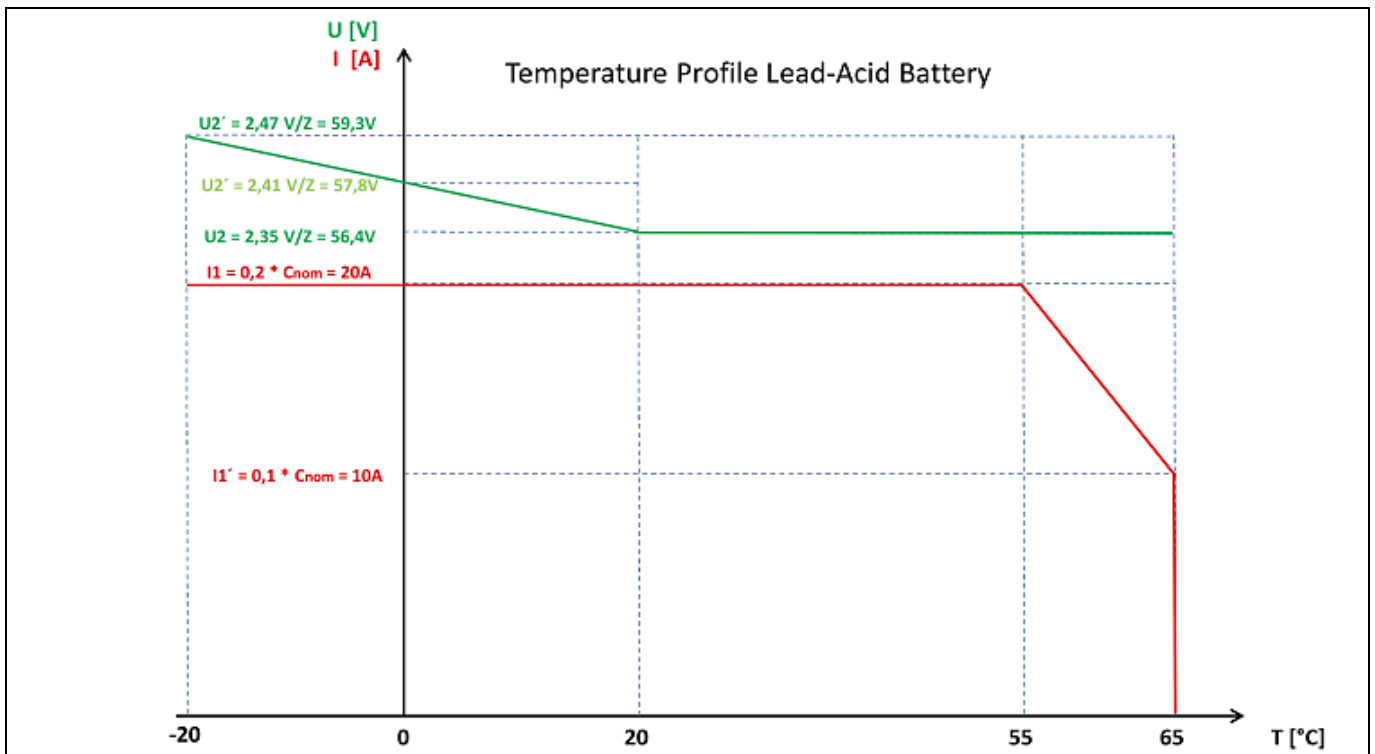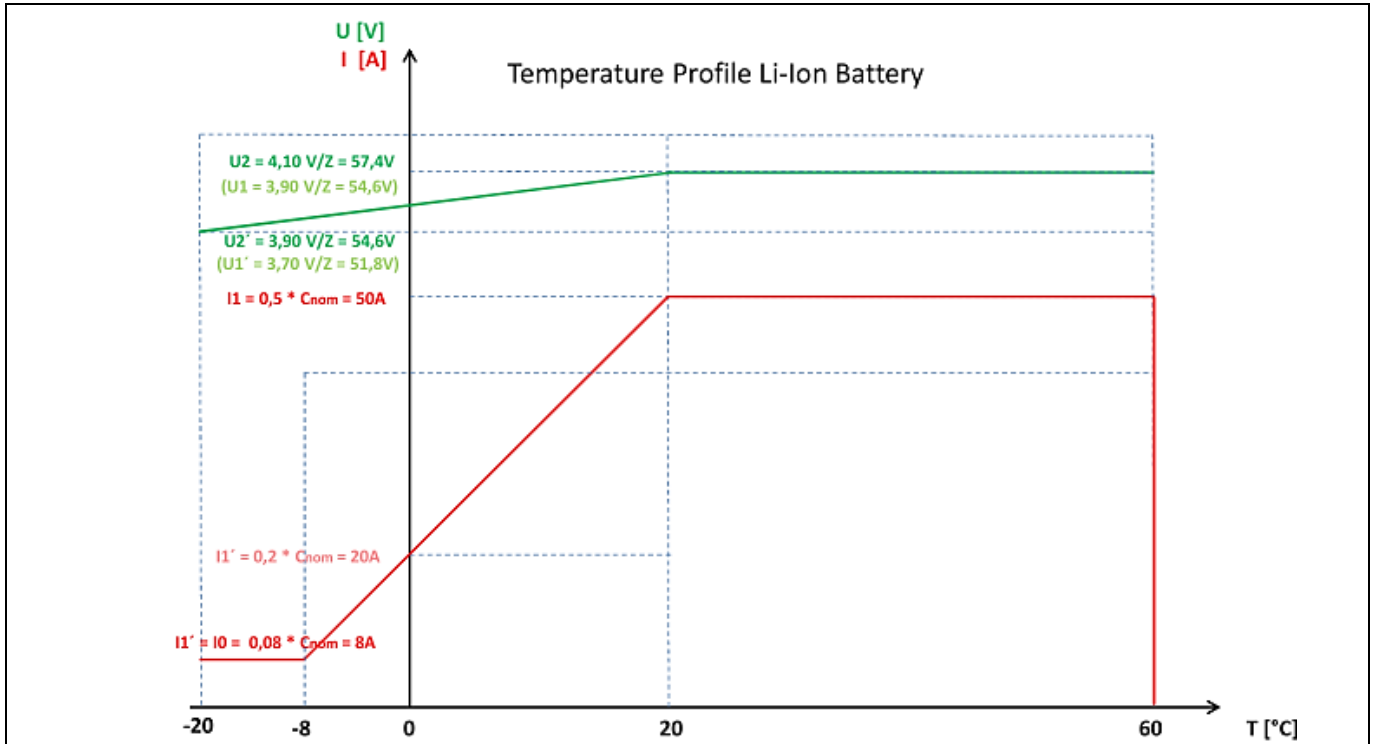

Figure 5   Temperature profile of lead-acid battery

4.2.2 Temperature profile of Li-ion battery

In the event of detection of a valid battery temperature the charging profile for Li-ion batteries is modified in the following way.

- Abort charging with error signalization when battery temperature is below -20°C.
- Abort charging with error signalization when battery temperature is over +60°C.
- Decrease charging voltage in the range from +20°C down to -20°C with 5 mV per cell and Kelvin.
- Decrease charging current in the range from +20°C down to -20°C down to 0 percent of nominal value, with a minimum limitation of $0.08 \times C_{nom}$ (I_0).

The supervision of the battery temperature and the correction of the charging voltage is done in all sectors of the charging profile. The derating of the charging current is done in the main charging sectors (S_1 and S_2).

Figure 6   Temperature profile of Li-ion battery

4.3   Flow diagram of the charging process

Figure 7 shows the flow diagram of the charging process, which describes the main software functions and the implemented structure.

Note: For further details about the state diagram of the charging process of both lead-acid and Li-ion batteries as well as the corresponding DAVE™ software and Doxygen documentation, please contact your local Infineon sales/technical office for assistance.
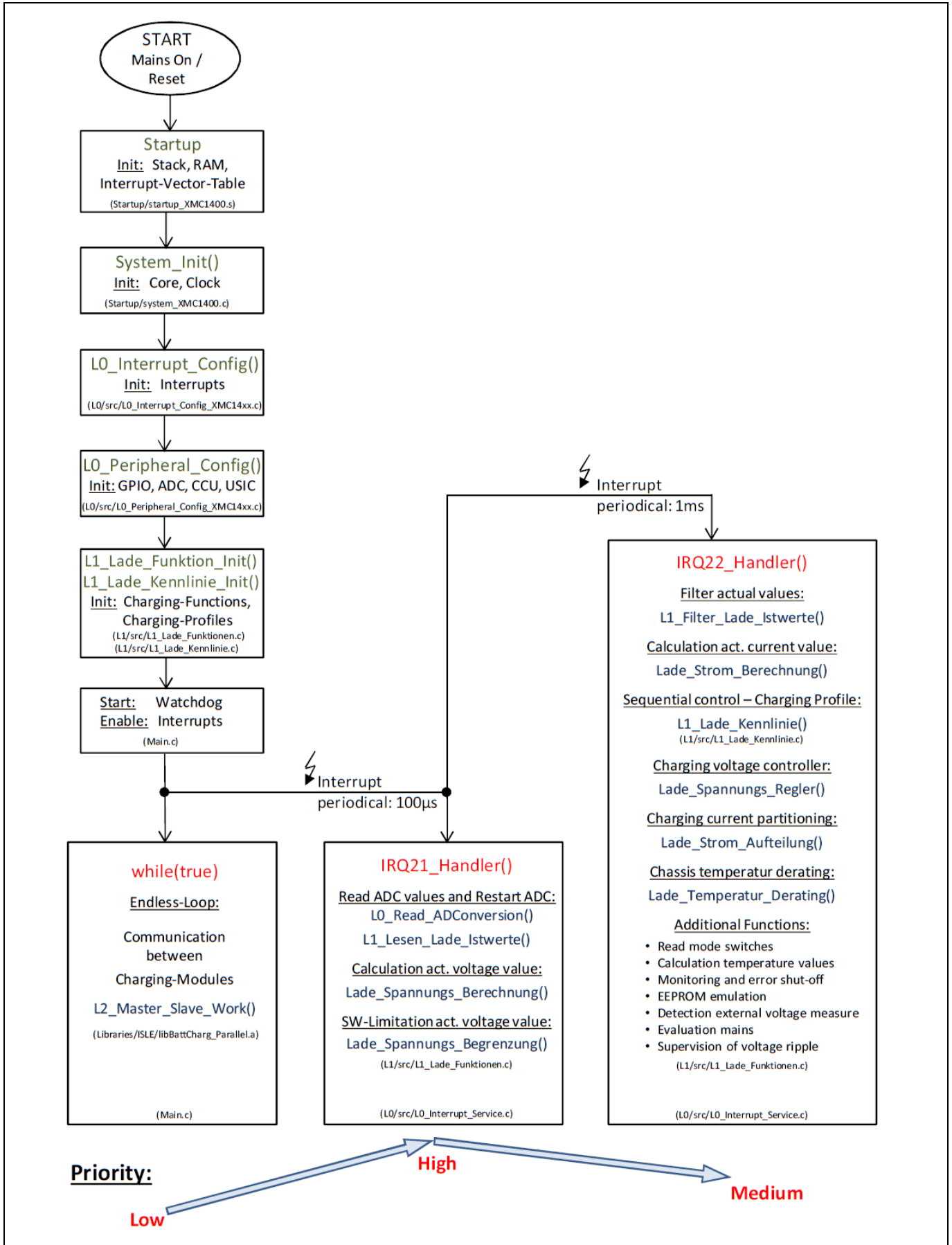
Figure 7   Flow diagram of the main software functions

5 Parallel operation

To charge large batteries or Li-ion batteries with fast-charge capability, the battery charger is equipped with a parallel mode option.

To use the parallel mode, you require only two battery charger units and the enclosed parallel mode cable. The current model is able to connect two charger units to work together.

For the battery connector it is sufficient to connect both units on the battery terminals (+) and (-). It is better to make this connection near the battery. For the mains supply you can also simply connect both charger units together, but you have to observe the maximum mains supply capability.

For proper parallel operation it is essential to connect the special parallel mode cable. Every battery charger is equipped with a simple four-pin connector to realize parallel mode operation. With the connection of the parallel mode cable the battery charger automatically changes its operation mode to parallel operation at the next mains off/on. The parallel mode cable includes the serial data connection and the master/slave selection. The cable determines which unit acts as the master and which as the slave. All battery chargers have the capability to work as both.

In parallel mode operation only the master unit displays the selected battery profile and capacity (in the same way as single mode operation). The slave unit is switching off the LEDs, except the power LED. Instead it switches on the white communication LED.

In parallel mode operation both units act as one charger with double the power, which can deliver a maximum power of 4 kW and a maximum current of up to 100 A.

The master unit decides in which way the required power will be supplied. The slave unit works as a simple current source and get its set-point value via communication from the master. The master and slave units are always monitoring the communication. In case of a failure in communication the slave unit switches off, but the master unit continues to work and takes over the slave current as far as possible.

5.1 Hardware

For parallel mode operation the battery charger is equipped with a serial interface and a master/slave switch.

The serial interface is composed of a RS485 transceiver, the internal bus termination and a transient limitation network. The master/slave switch-over consists of a simple input circuit with a current-dependent voltage interpretation. Both parts are merged in the four-pin interface connector.

The serial RS485 interface is working in half-duplex mode with a two-wire connection and a baud rate of 19200 baud. The RS485 transceiver is designed for low-speed operation and has implemented ESD protection up to 15 kV and a full fail-safe receiver.

The connection cable for the serial interface is a shielded and twisted pair cable (recommended type: UNITRONIC Li2YCY (TP)).

The master/slave selection is done by a simple wire strap in the connection cable.

5.2 Software

5.2.1 Communication protocol

For the data exchange between the charger units a proprietary communication protocol is implemented. This protocol is especially designed for battery chargers and limited to the required functions.

The used data frame consists of 11 bits – one start bit, one mode bit, eight data bits and one stop bit. The mode bit is to distinguish between address mode and data mode interpretation of the eight data bits.
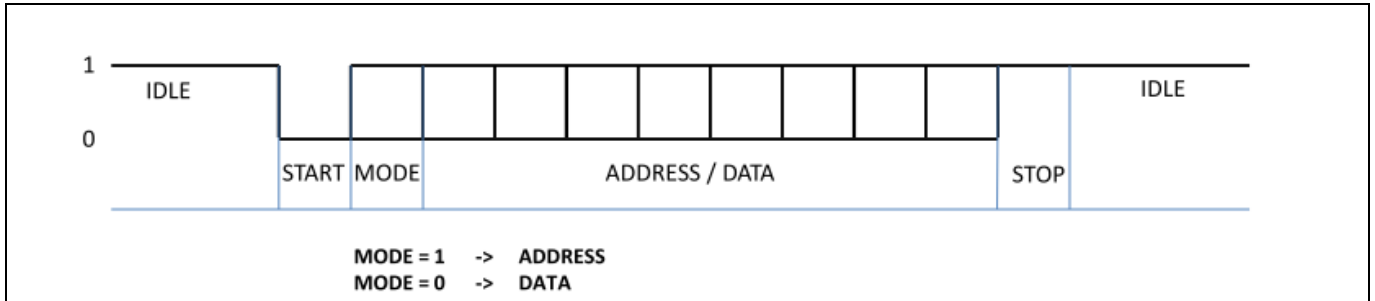

Figure 8 **Single data frame structure**

A characteristic communication protocol usually consists of five frames. The first frame contains the slave address (mode bit = 1), the second frame contains the command and the number of data bytes (mostly two data bytes), followed by the data frames and finished with a CRC8 checksum frame.
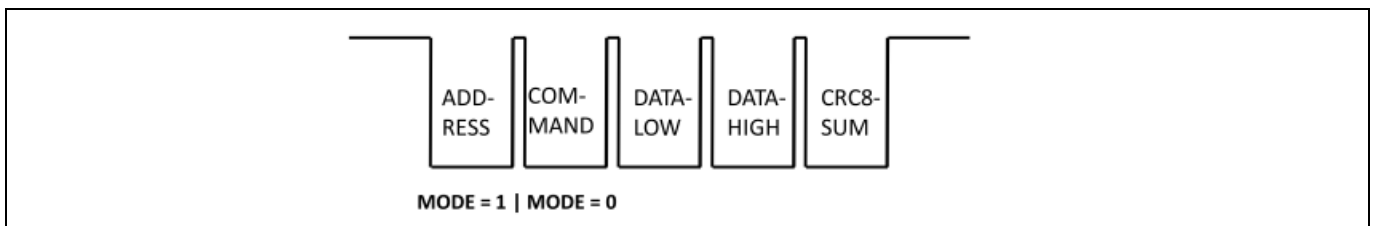
Figure 9 **Communication protocol consisting of five frames**

Every data exchange starts with a request protocol from the master unit, which directly responds to the addressed slave with a similarly constructed frame. Afterward the master sends the next request protocol to the slave(s). With the chosen baud rate of 19200 baud a complete data exchange requires a time period of approximately 10 ms.
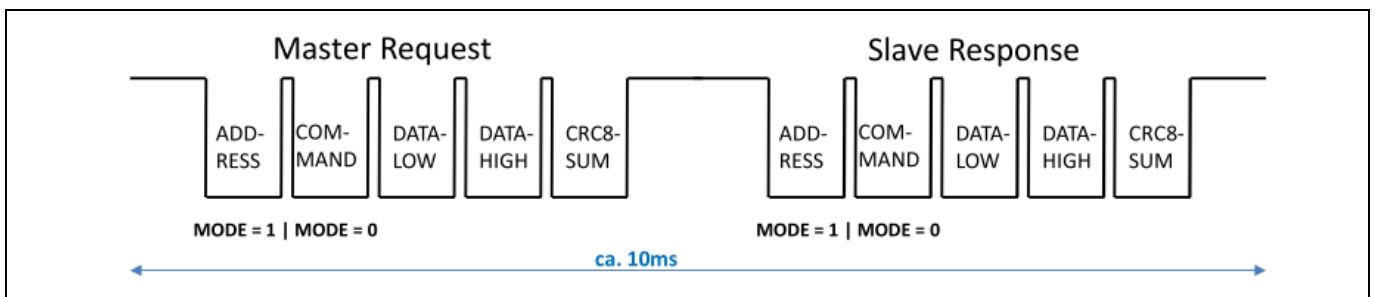

Figure 10 **Protocol structure between master and slave**

5.2.2 Parallel operation and data exchange

The data exchange starts with a lot of synchronization frames. The master checks the answers of the connected slave unit. When it finds valid response frames, the respective module is located as active, and in the next sequence the version and the current capability of the slave unit is fetched. If this part of communication is

successfully completed, the communication between master and slave unit is marked as synchronized and stable and the normal data exchange begins.

The most commonly used command in the communication between master and slave is the new current reference value for the slave unit, answered with the actual current value of the slave. Another often-used command is the control command for the slave, answered by the current status of the slave. Infrequently inserted are the commands for the present slave temperature and the maximum voltage prevention.

The master unit determines in which way the required power will be supplied. The slave unit works only as a simple current source.

For stable operation and good voltage regulation in low load ranges the master adds the slave, but not before the current reference exceeds a value of 10 A.Then the current is divided and both units (master and slave) are working together with a well-partitioned current value. If the current falls below a value of 6 A the master switches off the slave unit and takes over the whole current.

5.2.3   Communication error

The master and the slave unit are always monitoring for faultless communication.

In case of a disruption of the communication the slave unit tries to reset the internal communication module every 2 s. After three unsuccessful attempts the slave is shut down. The master detects the communication stoppage after 50 ms and begins to send new synchronization frames to the slave. This is done in several time intervals. If the communication remains disrupted, the master finishes the parallel operation after approximately 6 s and switches back to single operation.

In this mode, the master looks every 10 s for the recurrence of the slave unit and, when it detects the slave, it returns to parallel mode operation.

In case of a faulty communication (incomplete frame, noisy signal, checksum error, etc.) the slave doesn't transfer the new value but it sends its response as always.

Additionally an error flag in the slave status word is set. The master in such cases implements a dedicated error counter (every fault has its own error counter). If one error counter reaches a defined value, the master interrupts the data exchange with the slave and sends synchronization frames instead. If the communication remains defective the master finishes parallel operation and switches back to single operation.

If communication returns to normal operation (error counter down to zero) then the master continues the parallel operation with transmission of new data frames.In case the data exchange with the slave finishes, the master looks every 10 s for the recurrence of normal communication with the slave and returns to parallel mode operation when the communication is stable again.

6 Hardware modifications for higher battery voltages

In case higher battery voltages are required, below there is a list of changes that will be necessary to make at hardware level. Two different battery voltage ratings are considered:

I. 72 V (range 67.2 to 86.4 V), max. 30 A
II. 144 V (range 134.4 to 172.8 V), max. 15 A

6.1 Power circuit

6.1.1 Primary side

The whole primary side (PFC stage, LLC half-bridge) can remain unchanged.

6.1.2 Secondary side

6.1.2.1 Rectifier/transformer

I. 72 V (range 67.2 to 86.4 V)
The rectifier topology (center-tapped XFMR) can remain unchanged. Due to the higher output voltage, 300 V Si ultra-fast diodes are recommended (D26/D33, e.g. 2 × 15 A rated current each). The XFMR turns ratio should be 12:4:4 (with accordingly thinner litz wire for the secondary turns compared to the original 13:3:3 design).

II. 144 V (range 134.4 to 172.8 V)
a) The rectifier topology (center-tapped XFMR) can remain unchanged. Due to the higher output voltage, 600 V Si ultra-fast diodes are recommended (D26/D33). The use of SiC SBD (600 V/650 V) can improve efficiency.

The XFMR turns ratio should be 13:9:9 (with accordingly thinner litz wire for the secondary turns compared to the original 13:3:3 design).

b) Most likely, a topology change toward "voltage doubler rectifier" is the better option. While this change is more drastic, there are some advantages:
- 300 V Si ultra-fast diodes can be applied, the diode voltage is not doubled and is clamped to the output voltage (max. 172.8 V).
- The relative amount of additional voltage spikes is supposed to be significantly smaller compared to the center-tapped rectifier (due to lower stray inductance).
- The XFMR structure is simpler (no center tap). The recommended turn ratio is 12:4.
The disadvantage of high current stress of output caps is less significant at higher output voltages.
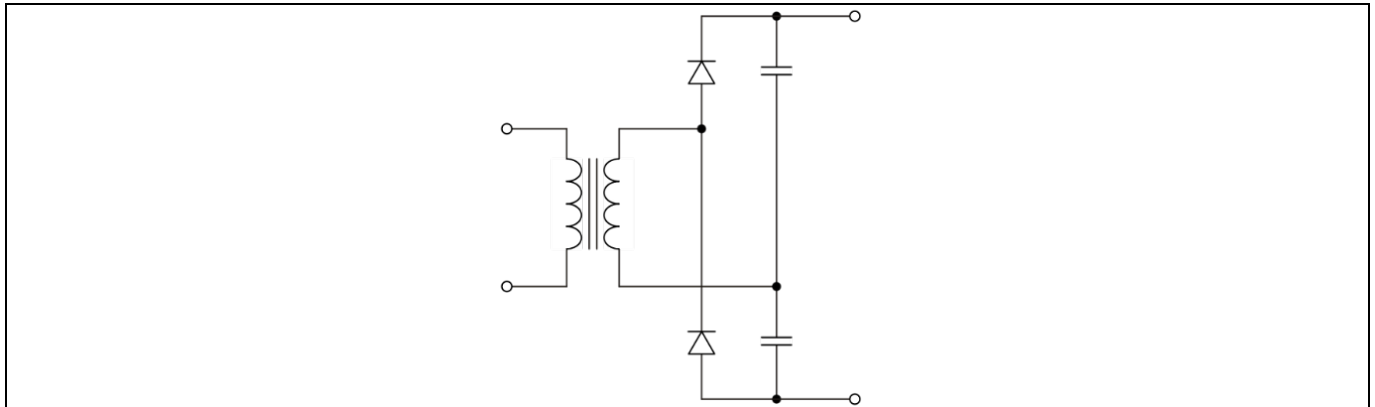
Figure 11   Voltage doubler rectifier

6.1.2.2   Output filter

The selection of filter components is subject to EMI results. Suggestions for the initial design are as follows:

I.   72 V (range 67.2 to 86.4 V)
       The caps C37, C38, C39 as well as C41 and the inductors L5 and L6 can remain unchanged; maybe one cap of the parallel connection can be removed.

II.   144 V (range 134.4 to 172.8 V)
       One cap of C37, C38, C39 can be removed. C41 must have a voltage rating of 250 V. L5 and L6 should be changed (approximately three times thenumber of turns, and accordingly thinner wires).
       In case of topology change toward "voltage doubler rectifier", please consider the current capability of the voltage doubler capacitors!

6.1.2.3   Reverse polarity protection MOSFETs (Q8, Q9, Q10, Q11, Q19)

A higher voltage rating of the MOSFETs is recommended (100 V minimum for the 72 V version and 200 V for the 144 V version). The total number of paralleled devices is subject to thermal behavior.

Note: Please refer to our latest OptiMOS™ portfolio to choose the proper devices.

6.1.2.4   Battery Current Sense (CS) resistor (R67)

The original (48 V system) resistor value is 0.5 mΩ. Recommendations for high voltage systems:
I.   72 V: 1 mΩ
II.   144 V: 2 mΩ

Please note the adaptations in the control circuit!

6.2   Control circuit

6.2.1   Current sense

Based on the recommended changes of CS resistors, the amplification of the CS op-amp should be adapted, in order to achieve a good resolution of measured current.

Only **R76** (original: 13 kΩ) is to be changed:
  I.   72 V: 13 kΩ
  II. 144 V: 13 kΩ

6.2.2 Voltage sense

The amplifications of the voltage sense op-amps should be adapted. R118, R119, R120, R121 as well as R124, R125, R126, R127 are to be changed (from 100 kΩ each in the original 48 V system) to:
  I.   72 V: 150 kΩ
  II. 144 V: 300 kΩ

6.2.3 µC daughter board

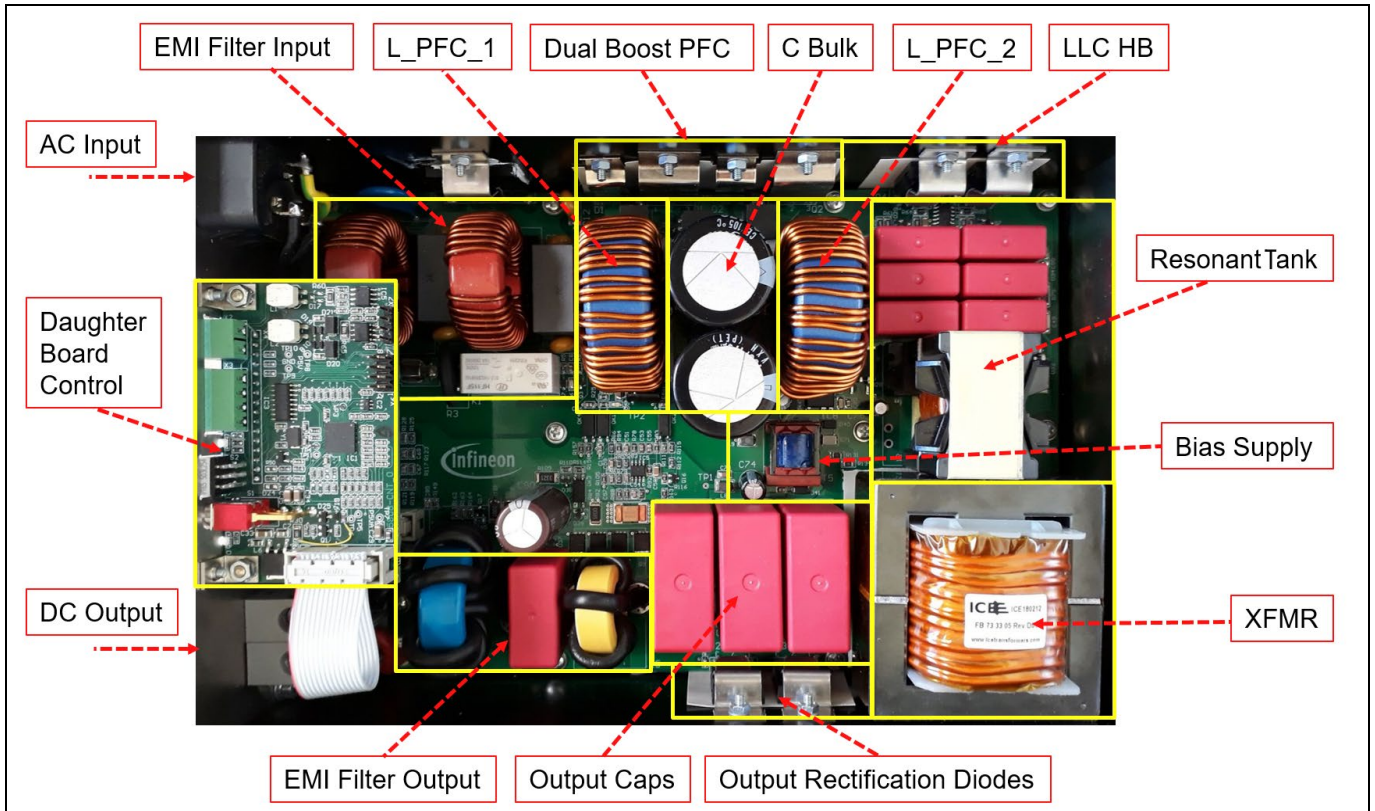There's no need to change the hardware of the board.

7 Functional groups

Figure 12   Functional groups of the 2 kW industrial battery charger design

7.1 Input line filter

The EMI filter is implemented as a two-stage filter, which provides sufficient attenuation for both Differential Mode (DM) and Common Mode (CM) noise.
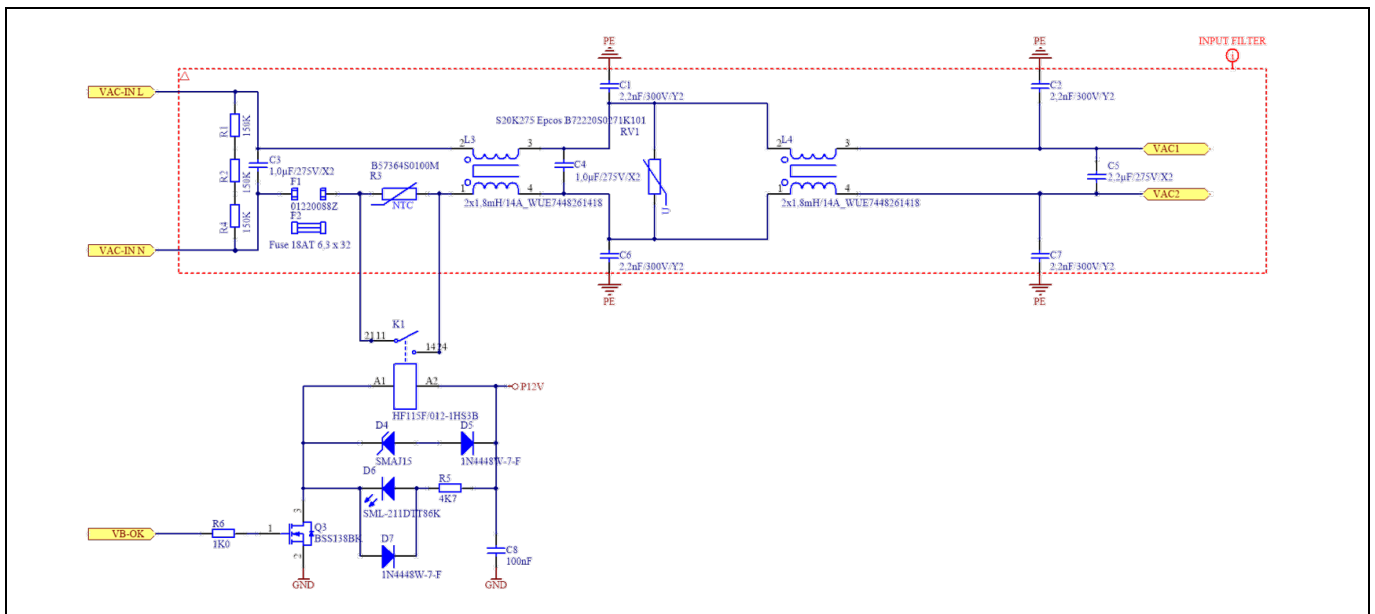
Figure 13   Two-stage EMI filter and inrush limit circuitry

The two high-current CM chokes L3 and L4 are based on high-permeability toroid ferrite cores. Each of these has 2 × 1.8 mH inductance.

The relatively high number of turns causes a considerable amount of stray inductance, which ensures sufficient DM attenuation.

In case the fuse is blown due to any abnormal conditions during the operation of the converter, the C3 X-capacitor is fully discharged through resistors R1, R2 and R4 in order to prevent any electric shock injuries to the operator of the demo board.

The line filter includes circuitry that limits the start-up inrush current on the first half-cycle to 25 A. During normal operation the inrush current limit impedance is bypassed by a relay contact K1. The relay K1 is controlled by the PFC controller.

7.2 Dual-boost semi-bridgeless PFC
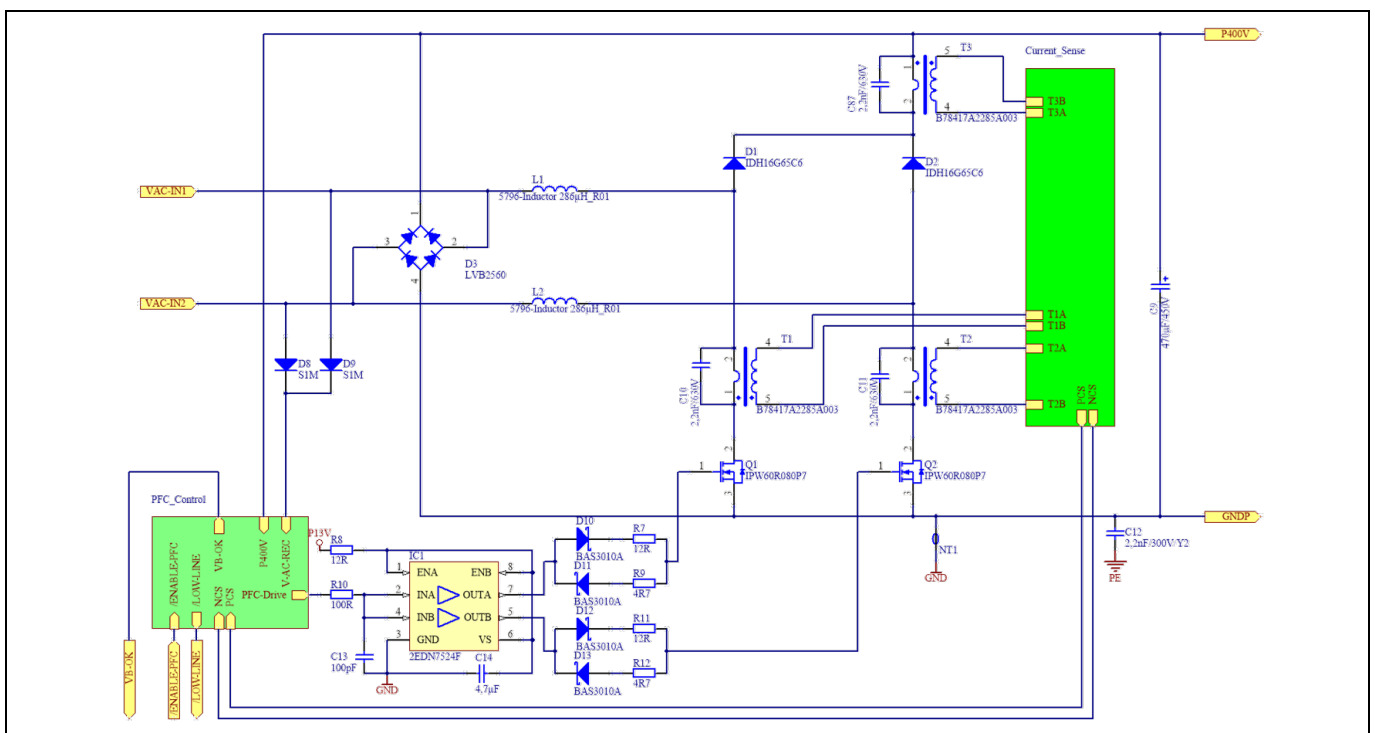
Figure 14 **Dual-boost semi-bridgeless PFC converter**

Although active PFC can be achieved by several topologies, the dual-boost semi-bridgeless converter is a very attractive solution for high-power supply solutions for the following reasons:

- Compared to the standard/classic PFC rectifier based on a diode bridge (with two active rectification diodes at all times), a single PFC MOSFET and a PFC diode, the dual-boost has lower conduction losses because there are always two power semiconductors in the current path per AC semi-cycle (e.g. Q1 or Q3 + complementary low-side diode from D3). However, for ease of control and taking into account impedance on the returning path, even three can be active (e.g. Q1 + complementary low-side diode from D3 || Q2 or Q2 + complementary low-side diode from D3 || Q1).
- Higher efficiency at a higher power density compared to the same rated power standard/classic PFC rectifier, due to less cooling effort and better heat spot distribution.
- More efficient and easier to control compared to an interleaved PFC rectifier, as this is a bridgeless topology with no need for phase shedding between the PFC legs.

7.2.1   PFC boost inductor

The PFC choke design is based on a toroidal high-performance magnetic powder core. Toroidal chokes have a large surface area and allow a good balance, minimizing core and winding losses, and achieving a homogeneous heat distribution without hot spots. Hence they are suitable for systems that are targeting the highest power density without forced air cooling.

Figure 15   PFC choke

The chosen core material is HS from Chang Sung Corporations (CSC), which has an excellent DC bias and good core loss behavior. The part number is HS467075, which indicates an outer diameter of the core of 47.6 mm, with a corresponding height of 18.92 mm, and a 75 µ permeability. The winding was implemented using enameled copper wire AWG 14 (1.8 mm diameter). The winding covers approximately 1.5 layers. This arrangement allows a good copper fill factor, while still having good AC characteristics, and is a preferred fill form factor for high-power toroidal inductors. There are 46 turns, taking advantage of the high permitted DC bias. The resulting small-signal bias inductance is 358 µH.

Table 8   **Calculated losses (per choke)**

Operating conditions	P_{Core} [W]	$P_{winding}$ [W]	P_{Total} [W]
200 V AC/10.5 A	1.8	1.9	3.7
178 V AC/12 A	1.8	2.4	4.2

7.3   The LLC resonant half-bridge converter

The design of the half-bridge LLC is described in the configuration shown in Figure 16. The LLC resonant converter design is realized by two clamping diodes across the two split resonant capacitors. This configuration offers a couple of important benefits.

1- Greatly reduced input current ripple, switch current and resonant capacitor voltage stress. This will protect the converter from destructive damage. Another benefit of this method is that it doesn't need an active control, and is very simple to implement. Its response speed is fast, which can provide cycle-by-cycle current protection.

2- The voltage stress on the resonant capacitor is limited so that a low-voltage capacitor can be used; another benefit is that by limiting the voltage on the resonant capacitor, it automatically limits how much current can go through the resonant tank during each half switching cycle, which in turn will limit the output current. Thus cost reduction and extended lifetime are achieved.
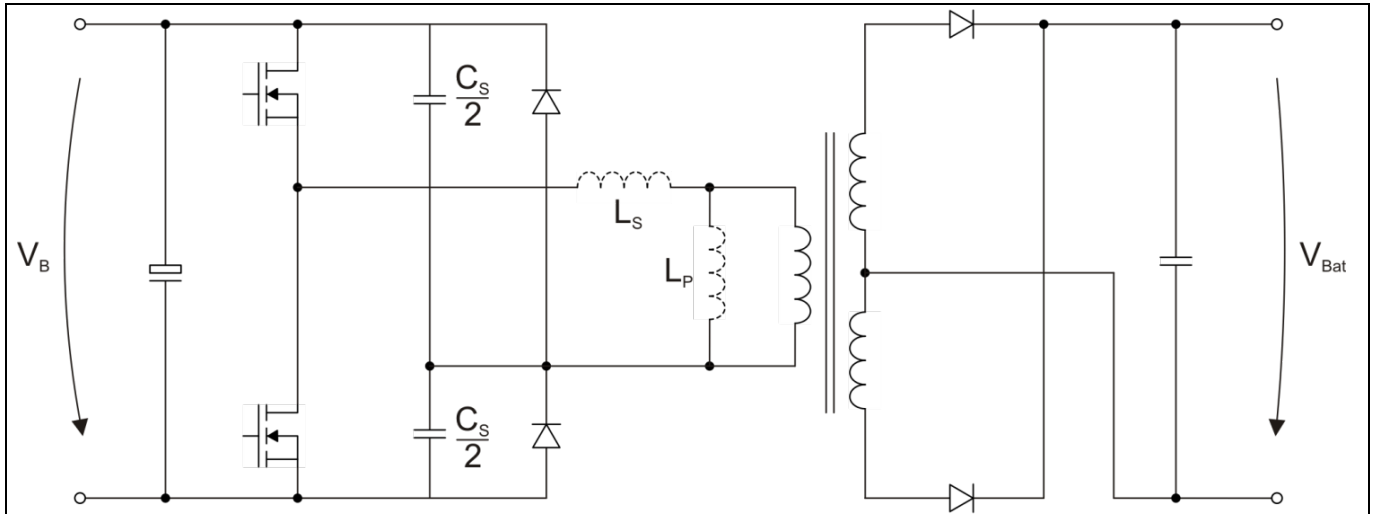
Figure 16 **Half-bridge LLC converter. L_p is integrated into the transformer (adj. by Air Gap). L_s is a discrete inductor.**

7.3.1 The main transformer design

The final structure of the main transformer is shown in Figure 17; the selected core used is E65/32/27 and the core material is the ferrite TDK PC47. This has been developed so that the primary is realized in a "sandwich" technique using 16 turns of four layers of litz wire, 45 strands and 0.1 mm diameter. This minimizes the AC losses due to skin and proximity effect. The secondary is done with a copper band 20 × 0.5 mm.

The transformer is built with the following specifications:

- Turns ratio (n): 13:3:3
- Primary terminal voltage: 400 V AC
- Primary windings: min. 630 × 0.071 mm, 2 × parallel
- Secondary terminal voltage: 46 V AC
- Secondary windings: min. 2000 × 0.071 mm, 2 × bifilar
- Frequency at no load: 140 kHz
- Frequency at full load: 90 kHz
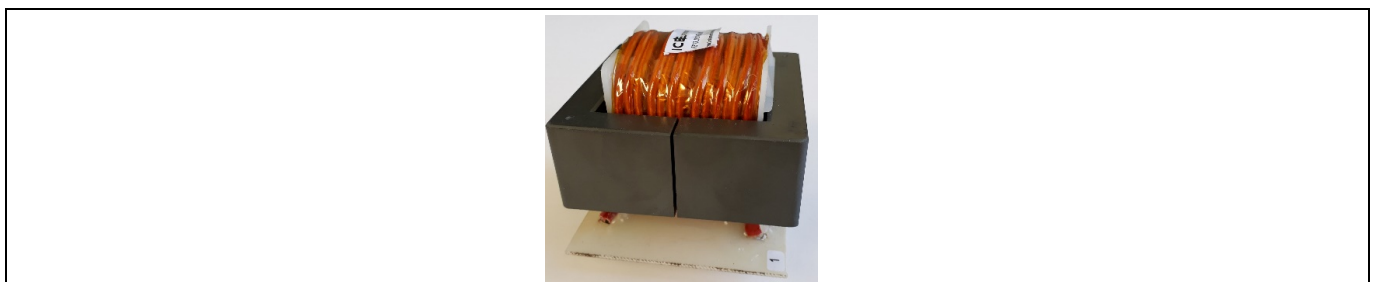
Figure 17 **Main LLC transformer**

Table 9 **Transformer calculated losses**

Operating conditions	P_{Core} [W]	$P_{winding}$ [W]	P_{Total} [W]
2 kW/40 V	0.8	6.2	7.0
2 kW/46 V (res.)	1.4	5.0	6.4
2 kW/60 V	3.4	4.8	8.2

7.3.2 Resonant choke design

In the case of the current design, it has been decided to use an external resonant inductor L_s. This is because the demo board is intended to be modified for higher output battery voltages, so having the resonant inductance externally enables changing the resonant tank in a more flexible way. The overall value of L_s including the contribution of the transformer primary leakage inductance shall be:

[L_s = 7.5 µH + 1.5 µH (XFMR leakage) = 9 µH] The external resonant choke is realized using a PQ40/40 core with TDK PC47 ferrite core material and air gap approx. 6 mm whose winding construction is shown in Figure 18.
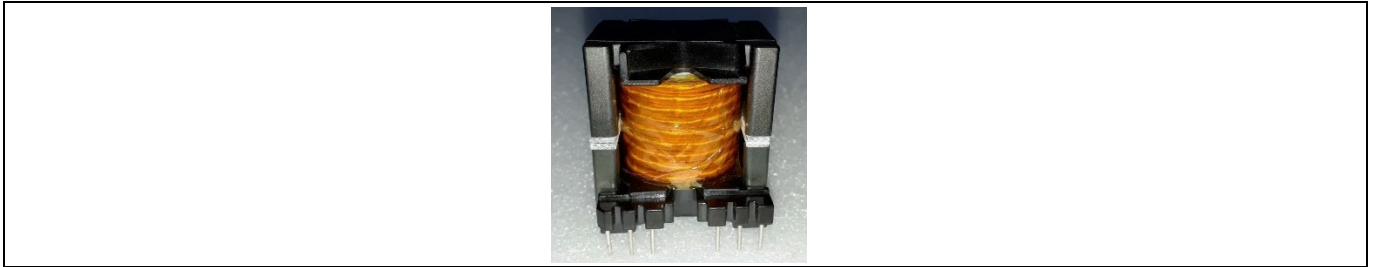
Figure 18   Winding: nine turns – HF litz wire 840 × 0.071 mm

Table 10   **Calculated losses (resonant choke)**

Operating conditions	P_{Core} [W]	$P_{winding}$ [W]	P_{Total} [W]
2 kW/40 V	2.2	1.5	3.7
2 kW/46 V (res.)	1.2	1.2	2.4
2 kW/60 V	1.1	1.4	2.5

7.3.3 Control loop of the LLC converter
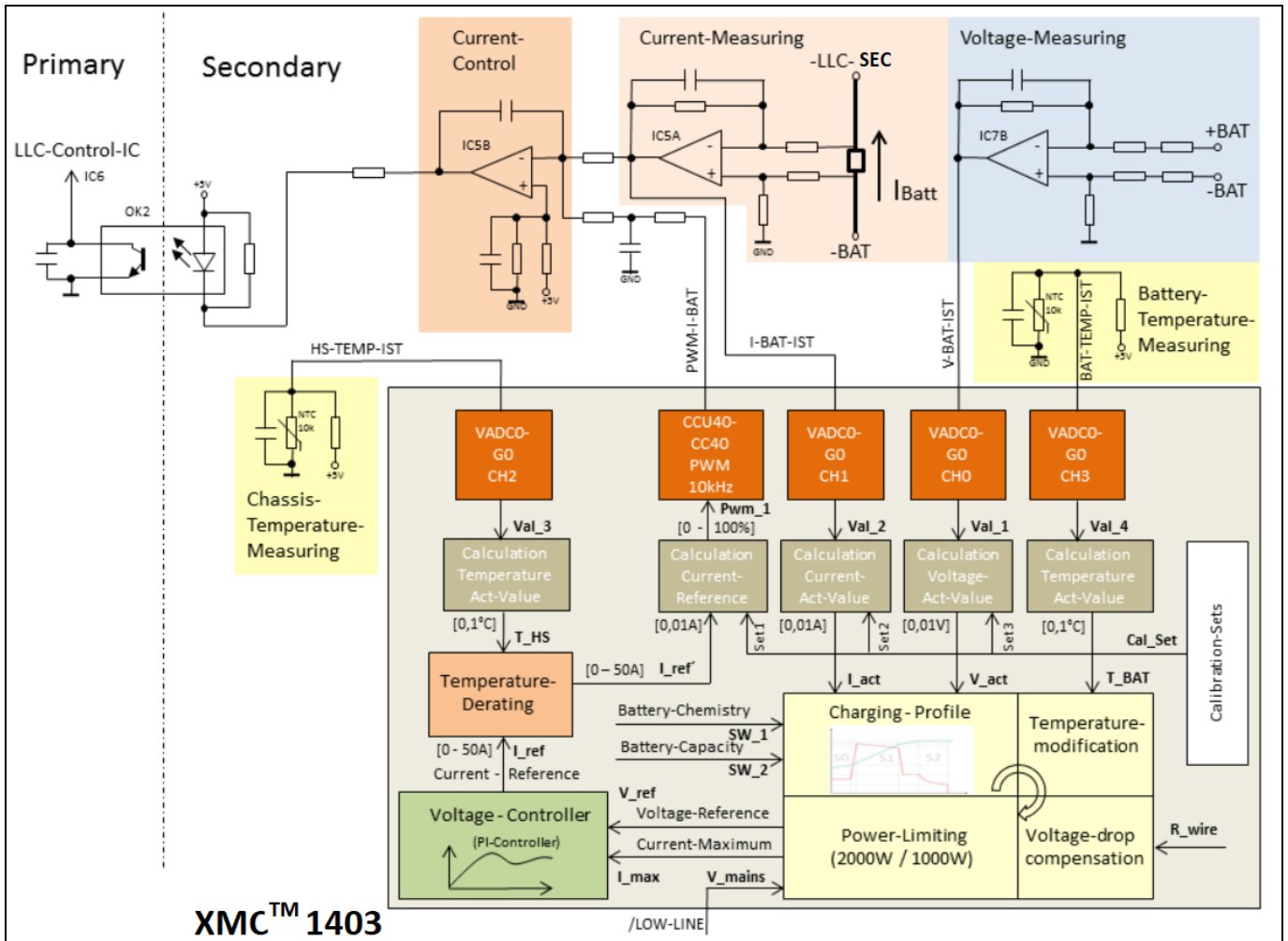
Figure 19 **Interface between the LLC converter and the XMC™ microcontroller**

Figure 19 shows the control block diagram of the LLC converter and the interface to the XMC™ 1403 microcontroller. The dark orange blocks mark the hardware units that are necessary to handle the different inputs (V-BAT-IST, BAT-TEMP-IST, I-BAT-IST, HS-TEMP-IST) and output (PWM-I-BAT) signals, respectively. The rest of the boxes inside the XMC™ show the calculation functions and the handed variables. Detailed information about each of the functions can be found in the Doxygen documentation.

Note: *For further details about the corresponding DAVE™ software and Doxygen documentation, please contact your local Infineon sales/technical office for assistance.*

7.4 Bias power supply

The PFC and LLC controllers and gate drivers as well as the control board need an auxiliary power supply for start-up and operation. An auxiliary power supply of 6 W is designed on-board using the ICE5QR4780AZ QR DCM Flyback controller with primary-side control.This controller offers a low part count and relatively low-cost solution, eliminating the need for optocoupler and feedback circuitry. In addition, QR topology ensures high efficiency, and optimizes losses. The converter is powered from the output of the PFC stage and must be able to start up prior to the PFC stage being operational. For this reason, the circuit is designed to operate over a wide input voltage range, 125 V DC to 450 V DC.
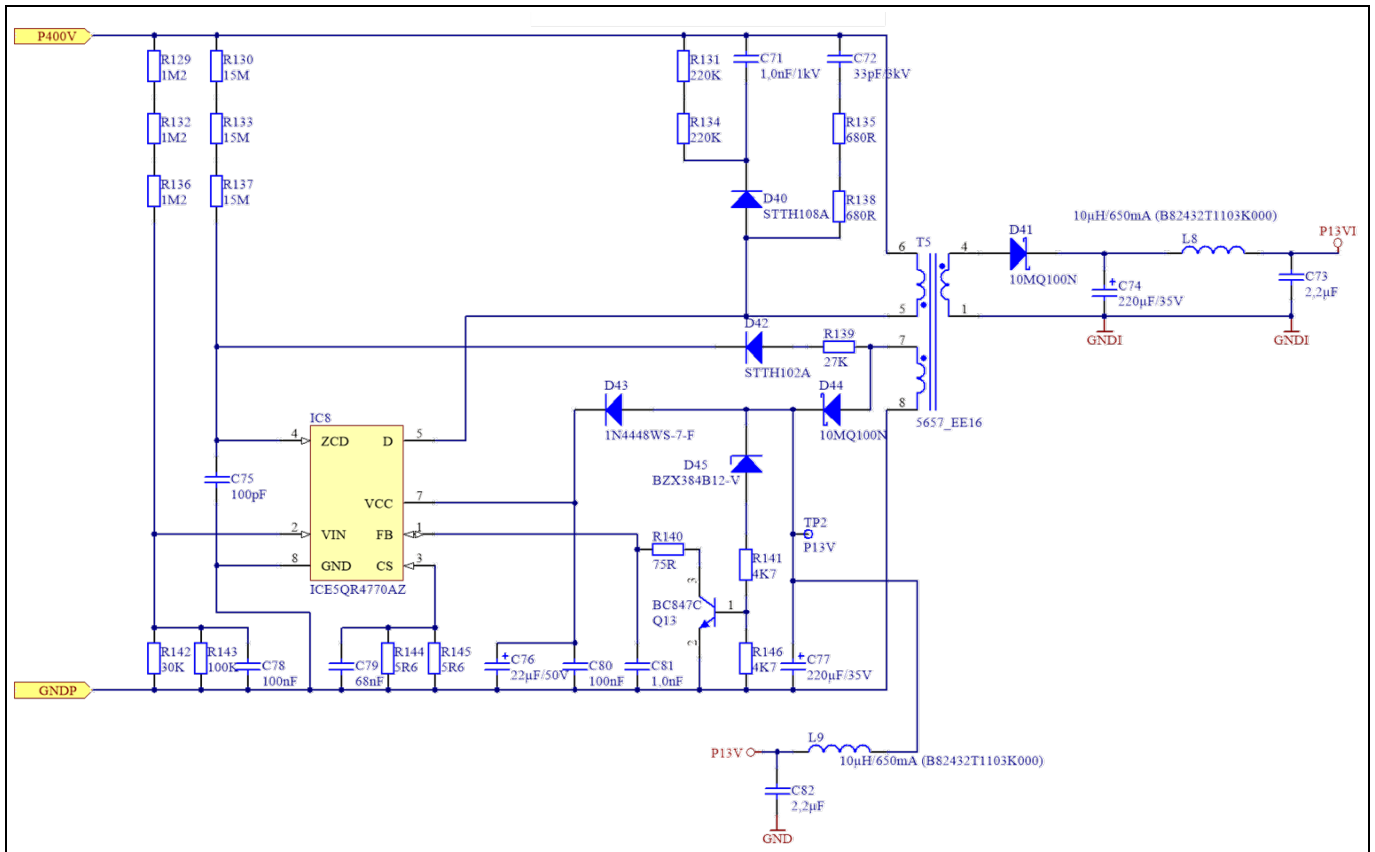
Figure 20   Auxiliary power supply design

7.4.1 Input and output requirements

The voltages needed throughout the whole system are provided by the dedicated Flyback DC-DC converter ICE5QR4780AZ. The specifications are shown in Table 11.

Table 11

Parameter	Value
Input voltage range, $V_{aux\_in\_range}$	125 V DC to 450 V DC
Nominal primary output voltage, V_{aux_pri}	13 V DC +/-10 percent
Nominal secondary output voltage, V_{aux_sec}	13 V DC +/-10 percent
Maximum output power, P_{aux_out}	6 W

7.4.2 Flyback transformer

The transformer design is based on a gapped ferrite core EE 16/8/5 with a horizontally arranged bobbin. The total air gap is 0.2 mm. The selected core material is TDK N87 or equivalent.

The turns ratio was chosen to be 184:15:15, resulting in 150 V (approximately) reflected primary transformer voltage.
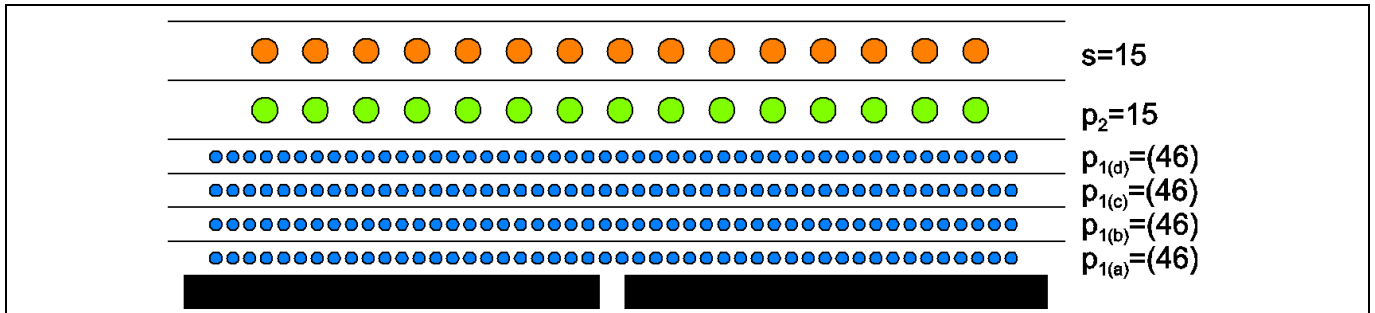
Figure 21   Winding arrangement

The secondary winding (S) has safety insulation from the primary side, which is implemented using triple-insulated wire. The other windings are made of standard enameled wire. The high-voltage primary winding (P1) is split into four layers.
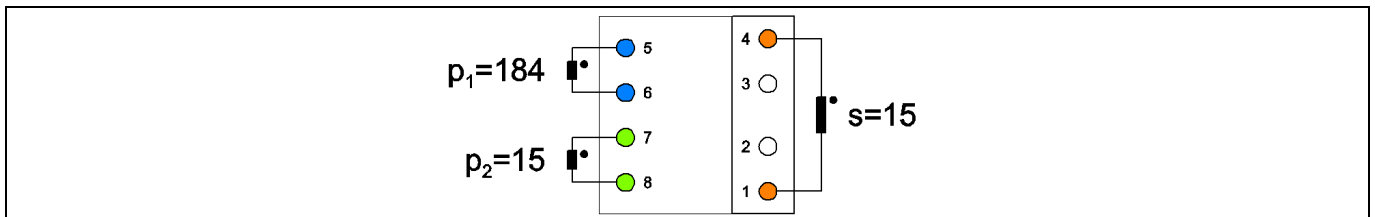
Figure 22   Pin arrangement, top view

7.5 Infineon semiconductors

7.5.1 600 V CooMOS™ P7

The Infineon Technologies 600 V CoolMOS™ P7 series is a revolutionary step forward, providing the world's lowest R_{DS_ON} per package and, thanks to its low switching losses, efficiency improvements over the full load range. The main features of this technology are:

- Increased MOSFET dv/dt ruggedness
- Better efficiency due to best-in-class Figures-of-Merit (FOM) $R_{DS\_ON} \times E_{oss}$ and $R_{DS\_ON} \times Q_g$
- Easy to use/drive due to driver source pin for better control of the gate

Such features bring meaningful benefits to the final application, including:

- Enabling higher system efficiency, as the parasitic inductance of the power source pin does not interfere in the driving PWM signal at the gate – as a result, undesired re-turn-off events are completely avoided
- Enabling increased power density solutions
- System cost/size savings due to reduced cooling requirements
- Higher system reliability due to lower operating temperatures

7.5.2 Gate driver for MOSFETs

7.5.2.1 EiceDRIVER™ 2EDN non-isolated gate driver for MOSFETs

The 2EDN7524 is a non-inverting fast dual-channel driver for low-side switches. Two true rail-to-rail output stages with very low output impedance and high current capability are chosen to ensure the highest flexibility and cover a wide variety of applications.

All inputs are compatible with low voltage TTL signal levels. The threshold voltages (with a typical hysteresis of 1 V) are kept constant over the supply voltage range.

Since the 2EDN7524 is particularly aimed at fast-switching applications, signal delays and rise/fall times have been minimized. Special effort has been made to minimize delay differences between the two channels to very low values (typically 1 ns).

The 2EDN7524 driver used in this demo board comes in a standard PG-DSO-8 package.

7.5.2.2 600 V high- and low-side driver for MOSFETs

The IRS21814 is a high-voltage, high-speed power MOSFET driver with independent high-side and low-side referenced output channels. Proprietary HVIC and latch-immune CMOS technologies enable ruggedized monolithic construction. The logic input is compatible with standard CMOS or LSTTL output, down to 3.3 V logic. The output drivers feature a high pulse current buffer stage designed for minimum driver cross-conduction. The floating channel can be used to drive an N-channel power MOSFET in the high-side configuration which operates up to 600 V.

7.5.3 Sixth-generation CoolSiC™ Schottky diode

Because CoolSiC™ Schottky diodes have a capacitive charge, Q_c, rather than a reverse recovery charge, Q_{rr}, their switching loss and recovery time are much lower than a silicon ultra-fast diode, leading to enhanced performance. Moreover, SiC diodes allow higher switching frequency designs. Hence, higher power density converters are achieved. The capacitive charge for SiC diodes is not only low, but also independent of di/dt, current level and temperature, which is different from silicon diodes that have a strong dependency on these conditions.

The recommended diode for CCM boost applications is the 650 V CoolSiC™ fifth-generation Schottky diode, which includes Infineon's leading-edge technologies, such as a diffusion soldering process and wafer thinning technology. The result is a new family of products that show improved efficiency over all load conditions, resulting from the improved thermal characteristics. Even with the high surge current capability of SiC Schottky diodes, it is still preferable to use bulk pre-charge diodes. These are high-side diodes of the bride rectifier (D1 and D2 in Figure 14) with a high I^2t rating to support pre-charging the bulk capacitor to the peak of the AC-line voltage; this is a high initial surge current stress (which should be limited by a series NTC) that is best avoided for the PFC boost rectifier diode.

7.5.4 XMC™ 1400 microcontroller for charging profile implementation

32-bit microcontrollers with ARM® Cortex®-M0 focus on low-cost embedded control applications. The XMC1400 series devices are optimized for motor control, power conversion and LED lighting applications and Human-Machine Interfaces (HMIs). Increasing complexity and demand for computing power of embedded control applications requires microcontrollers to have a significant CPU performance, integrated peripheral functionality and rapid development environment, enabling short time-to-market, without compromising cost efficiency. The performance of XMC1400 is increased by 70 percent over the existing XMC1000 due to the 48 MHz of the core frequency and the two CAN node interfaces.

Some of the XMC1400 features are listed below:

- 128.0 kB Flash, 16 kB RAM
- Core frequency: 48 MHz
- Peripherals clock: 96 MHz
- 8 × 16-bit timers
- 12-channel 12-bit ADC
- MultiCAN: two CAN nodes, 32 message objects
- Four-channel USIC (configurable to SPI, UART, IIC, IIS)
- Real-time clock
- Watchdog timer

7.5.5 ICE3PCS01 standalone CCM PFC controller

ICE3PCS01G is a 14-pin wide input range (85 V AC to 265 V AC) controller IC for active CCM PFC converter. Compared to the first and second generation of ICE1PCS0x and ICE2PCS0x, the third generation PFCs have the lowest internal reference trimmed at 2.5 V and integrated digital control voltage loop. They also have other advantages such as low peak current limit at 0.2 V, adjustable gate switching frequency range from 21 kHz to 100 kHz, and the ability to synchronize with external frequency range from 50 kHz to 100 kHz. They are now able to achieve 95 percent efficiency at full load across the input voltage range.

7.5.6 ICE2HS01G resonant mode controller

Infineon ICE2HS01G is a high-performance resonant mode controller designed especially for high-efficiency half-bridge or full-bridge LLC resonant converters with synchronous rectification at the secondary side. With its driving techniques, the synchronous rectification can be realized for LLC converters operated with secondary switching current in both CCM and DCM conditions. No special synchronous rectification controller IC is needed at the secondary side. The maximum switching frequency is supported up to 1 MHz. Except for the patented SR driving techniques, this IC provides very flexible design and integrates full protection functions as well. It is adjustable for maximum/minimum switching frequency, soft-start time and frequency, dead-time between primary switches, and turn-on and turn-off delay for secondary SR MOSFETs. The integrated protections include input voltage brown-out, primary three-level over-current, secondary over-load protection and no-load regulation.

8 Experimental results

8.1 Equipment needed

- Isolated AC source
- Single-phase power analyzer
- Digital oscilloscope
- Electronic DC load to simulate a battery

8.2 Standby power consumption with battery fully charged

Measurements performed with a "WT3000" Yokogawa digital power meter showed the following results for standby power consumption of the demo board at no load:

Table 12

Charging profile	V_{in} = 230 V AC	V_{in} = 115 V AC
Lead-acid/ Li-ion	I_{IN} less than 162 mA RMS	I_{IN} less than 320 mA RMS
	P_{IN} < 3.1Watt	P_{IN} < 3.1 Watt

8.3 PF and THD measurements
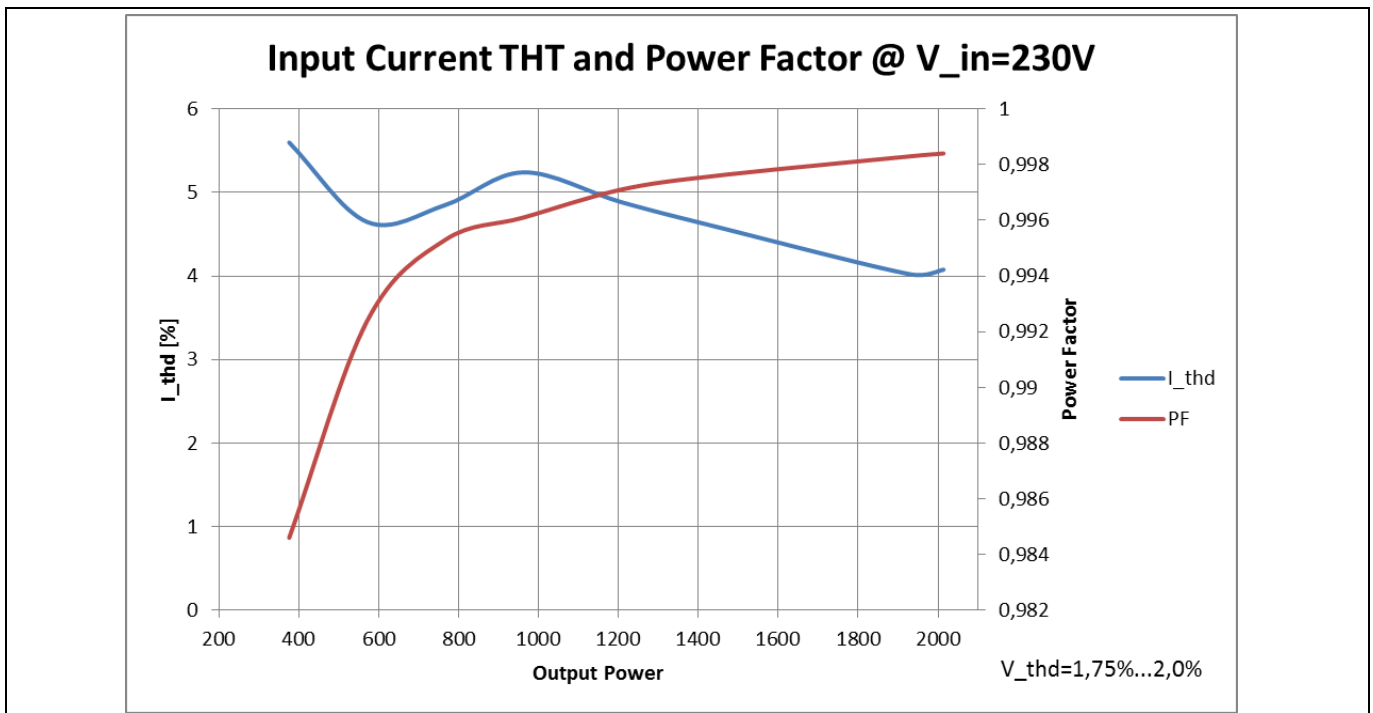
Figure 23   Input PF and THD at 230 V AC

Power factor is higher than 0.9 above 20 percent of load. Input current distortions are below 6 percent above 20 percent of load at 230 V AC.

8.4 Battery charging profile test

In order to verify the implemented charging profiles two diffirent measures were performed; one for a Li-ion battery and another for a lead-acid battery. For that purpose two different nominal battery capacities (C_{nom}) was set, a lower 60 Ah and a higher 200 Ah C_{nom} value.The measured data was recorded by a power analyzer (Yokogawa WT3000).

For simulating the battery an electronic load in constant resistance mode was used along with a greater than 10 mF electrolytic capacitor bank. The different resistance values are adjusted by hand with a gear potentiometer.

8.4.1 Charging profile of lead-acid batteries

The charging profile for lead-acid batteries was tested with a nominal battery capacity of 200 Ah. This results in a main charging current of 40 A and a beginning power regulation at ~ 50.0 V.

The recorded chart begins in pre-charging state, with a constant current of $0.03 \times C_{nom} = 6.0$ A. After reaching the switch-over point (43.2 V), the main current ramp starts. After reaching the maximal charging current of 40 A, the current is constant and the voltage begins to increase. When the charging voltage is to approach a value of ~ 50.0 V the power regulation ($P_{max} = 2000$ W) starts and reduces the charging current accordingly. At a charging voltage of 2.35 V/cell = 56.4 V the current is reduced to ~ 35.5 A. Now this charging state is completed and the next section (constant voltage section (S_2)) starts. The charging voltage remains constant at 2.35 V/cell = 56.4 V and charges the battery until the current goes below $0.02 \times C_{nom} = 4.0$ A (in Figure 24). Due to the fact that the constant current charging (S_1) was longer than 30 min, the after-charging state is executed and a constant current of $0.02 \times C_{nom} = 4.0$ A is impressed. The charging voltage in this state is rising up to 2.45 V/cell = 58.8 V. In the given measurement the after-charging is finished by the dv/dt condition after a duration of 2×15 min = 30 min. The charging process is finished at this point and the trickle-charging (balancing) would be started if the battery voltage goes below 2.25 V/cell = 54.0 V. But this is not shown in this chart.
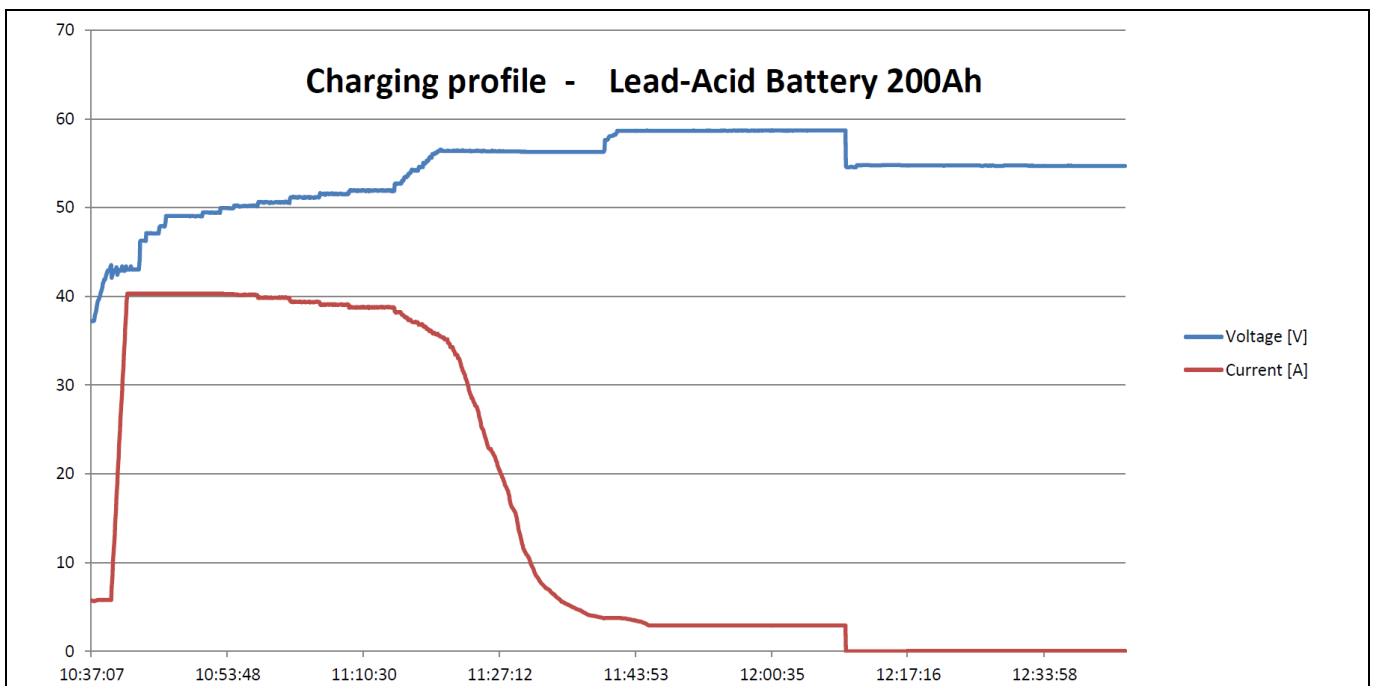
Figure 24   Charging profile of a 200 Ah lead-acid battery

8.4.2 Charging profile of Li-ion batteries

The test of the charging profile for Li-ion batteries was done with a nominal battery capacity of 60 Ah. This results in a main charging current of 30 A. The recorded chart begins in pre-charging state with a constant current of $0.08 \times C_{nom} = 4.8$ A. After reaching the switch-over point of 43.4 V the main current ramp starts. After reaching the maximal charging current (30 A), the current is constant and the voltage begins to increase (voltage steps are caused by hand regulation). When the charging voltage approaches the end of the linear range of the Li-ion charging characteristic (~3.9 V/cell), the current is reduced to $0.1 \times C_{nom} = 6.0$ A. With this current the rest of the capacity is slow-charged in the strong non-linear area of the charging characteristic.

Up to a battery voltage of 4.1 V/cell (57.4 V), the current is constant and afterward the battery voltage remains constant at 4.1 V/cell. The current is now decreasing and the charging process finishes at a current of less than $0.05 \times C_{nom}$ less than = 3.0 A (in Figure 25).
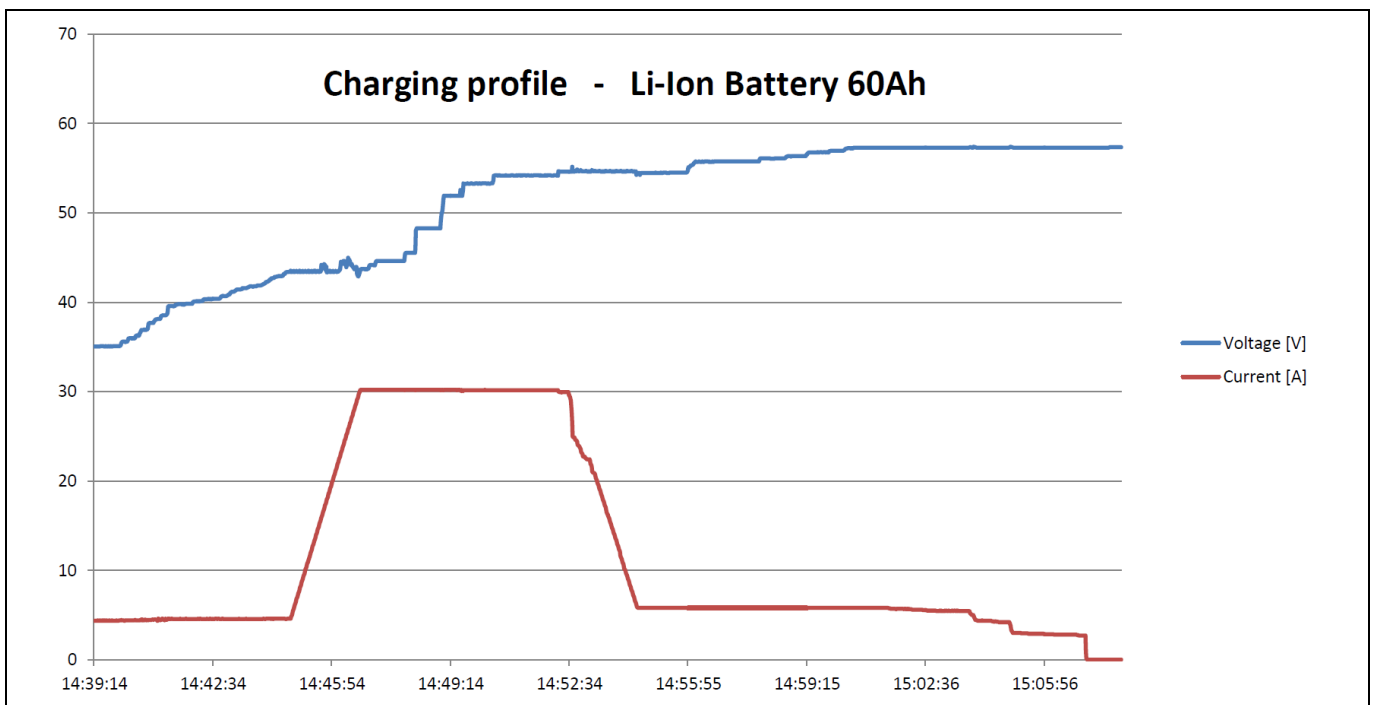
Figure 25   **Charging profile of a 60 Ah Li-ion battery**

8.5   EMI measurements

8.5.1   Radiated EMI

Table 13   **Radiated EMI test conditions**

Standard specification	EN55011, Group 1, Class A
Input voltage	230 V AC
Output voltage	48.8 V
Output current	42.5 A
Load type	Resistive
Charger position	Horizontal
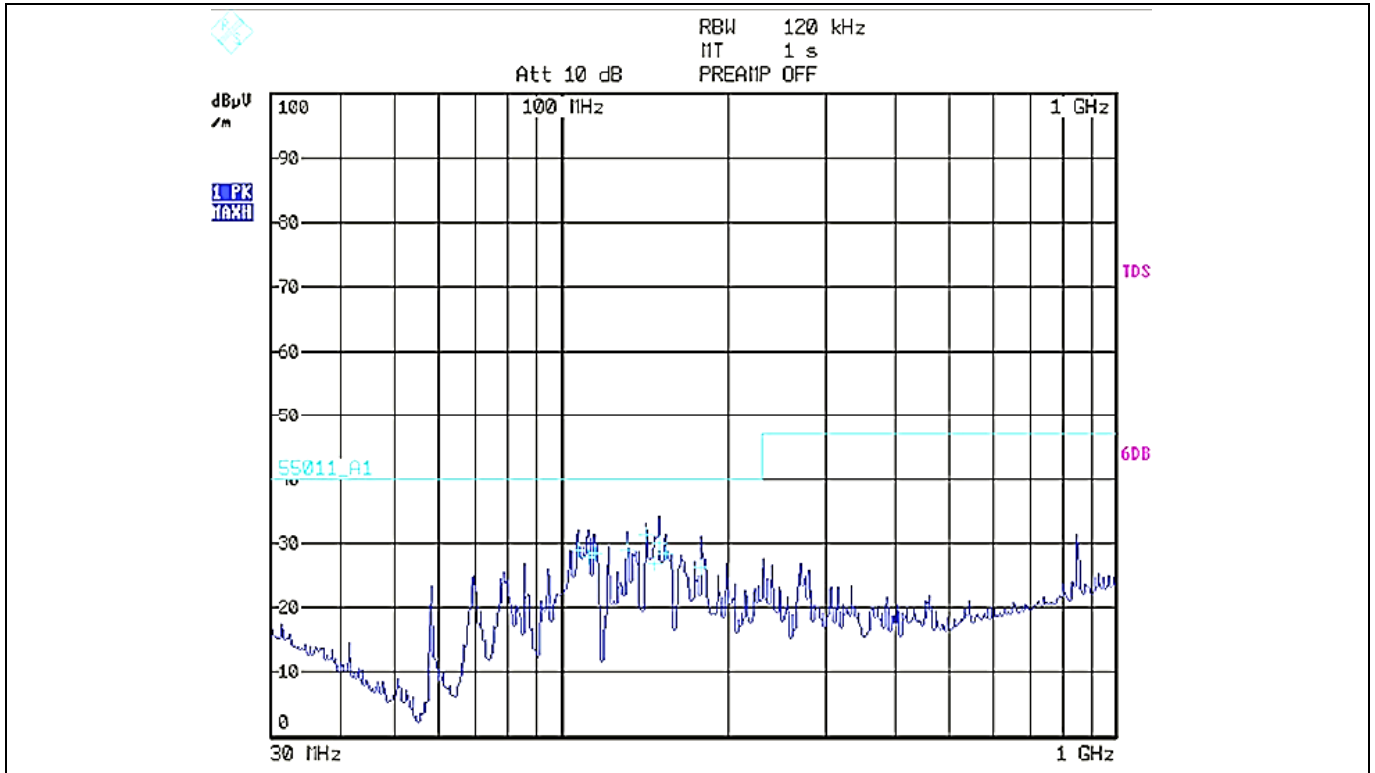
Figure 26   Radiated EMI according to EN55011, Group 1, Class A limits

The dark blue line represents peak measurements; light blue plus signs shows detailed quasi-peak results.

8.5.2   Conducted emissions

8.5.2.1   Emissions at full load

Generally conducted emissions will be more critical at full-load condition. So, this operating point is chosen for measuring conducted EMI.

Table 14   **Conducted EMI test conditions**

Standard specification	EN55011, Group 1, Class A
Input voltage	230 V AC
Output voltage	48.8 V
Output current	42.5 A
Load type	Resistive

The conducted peak and average emissions in a pre-compliance test set-up were compared against EN55022 Class-A quasi-peak and average limits and found to be meeting them comfortably, as shown in Figure 27.
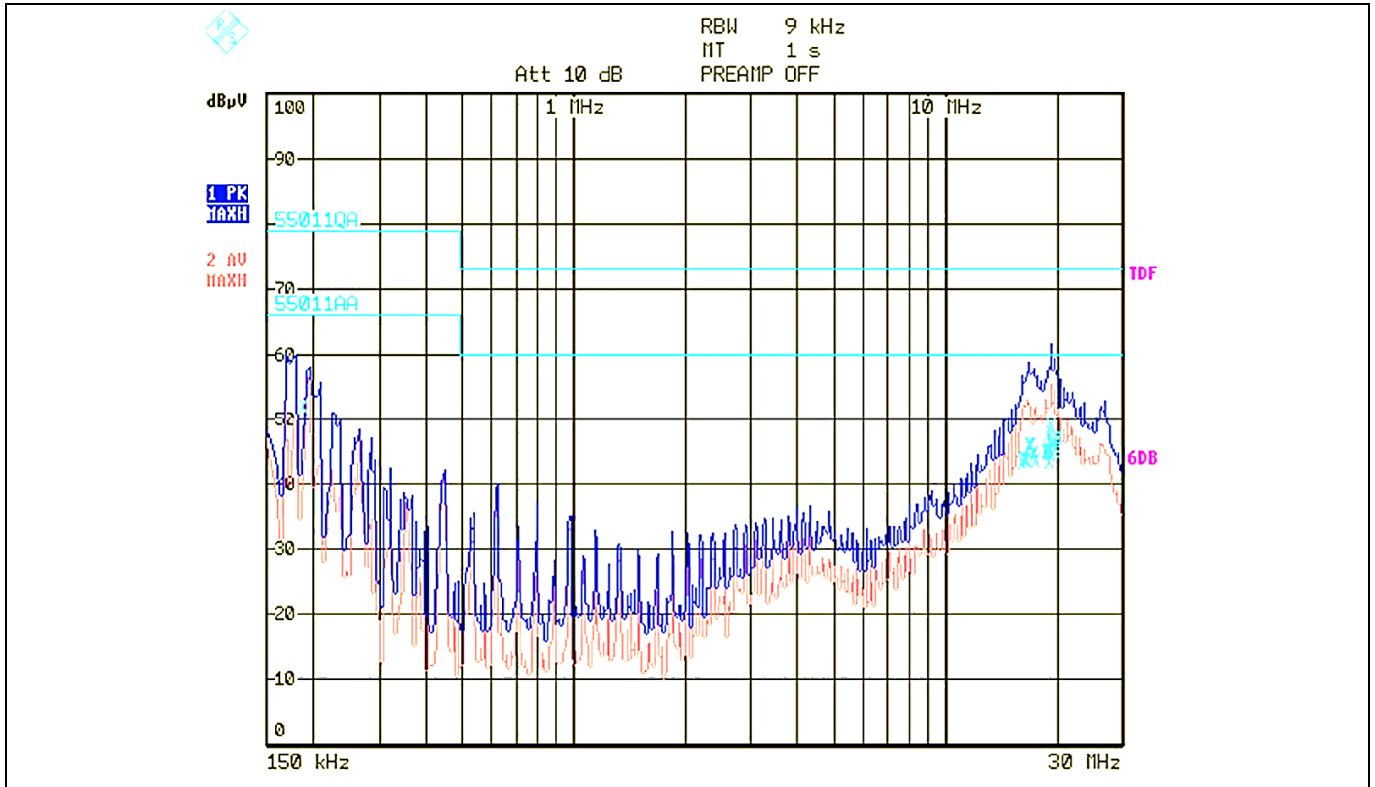
Figure 27   Conducted EMI according to EN55011, Group 1, Class A limits

The blue line represents peak and the red line represents average measurements.

8.6   Surge immunity (EN61000-4-5)

The battery charger 48 V/50 A design complies with the EN61000-4-5 installation Class 3 (±1 kV for line-to-N and ±2 kV for line-to-earth).

8.7   Short-circuit and inverse polarity detection

The detection circuitry of the short-circuit and inverse polarity can be found in Figure 39 formed by the Q8, Q9, Q10, Q11 and Q19 OptiMOS™ MOSFETS, the R67 sensing resistor and controlled by BMS.

Please be aware that the short-circuit and inverse polarity detection events are detected only when these conditions are present before powering the chargers.

As a result, the following recommendations MUST BE FOLLOWED at all times:

1. Do not attach any battery when the charger is powered on. First, proceed to connect the battery and then plug the charger into the mains.

2. In case the battery is reverse connected or if there is a short-circuit due to cabling matters, then after plugging the charger(s) into the mains, there will be the red LED error blinking indication as 2 × short/2 × long = under-voltage error (lead-acid /Li-ion).

3. In this case, please unplug the charger(s) and check correct polarity or neat cabling.

8.8 Overall system efficiency

8.8.1 Different output power (output voltage as parameter)
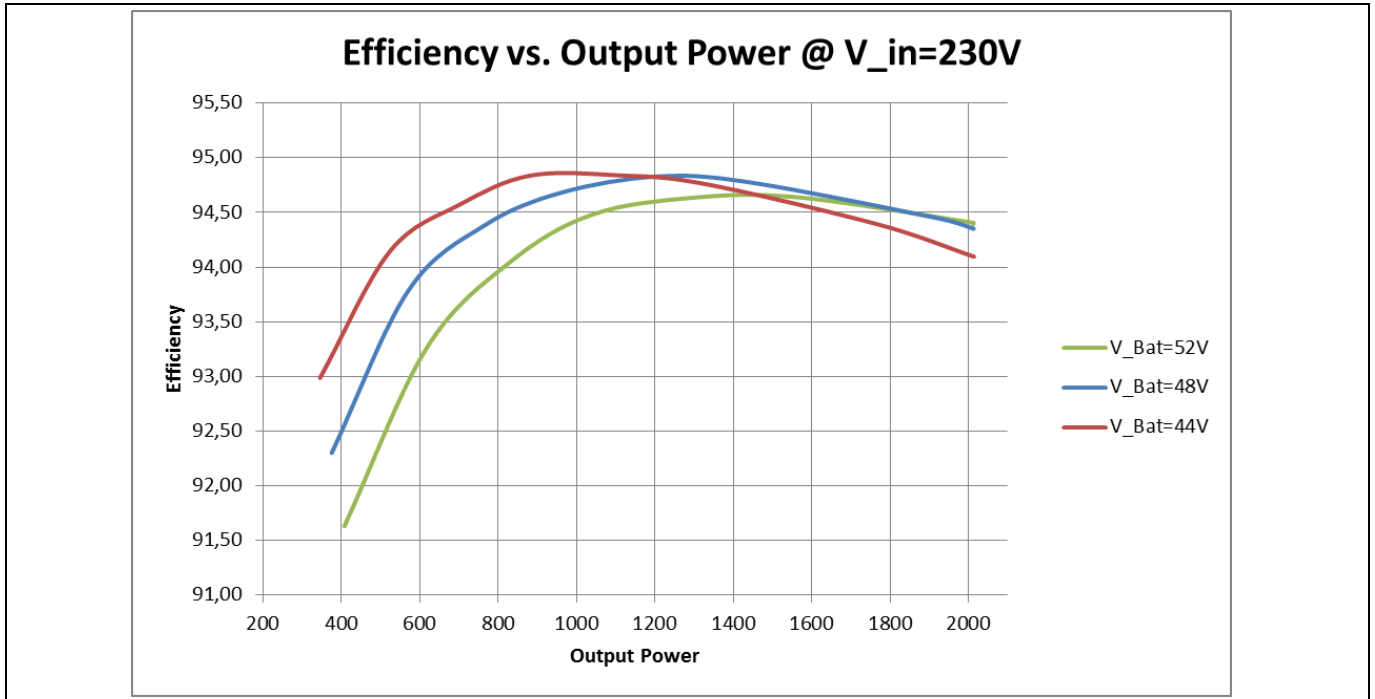
Figure 28   **Efficiency with a constant input voltage of 230 V AC**

8.8.2 Full load at different output voltages (input voltage as parameter)
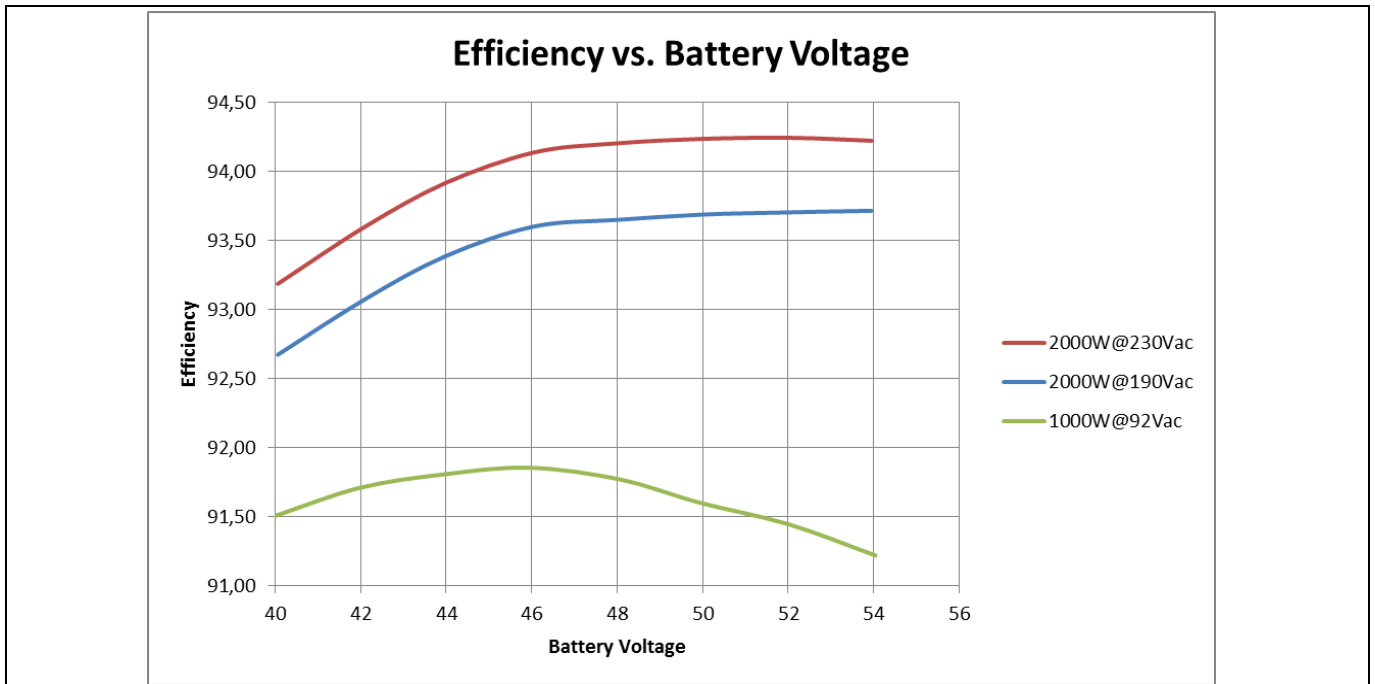
Figure 29   **Efficiency is best at high inpnut and output voltages**

At low power and low battery voltage the effect of magnetizing current losses of LLC transformer decreases the efficiency below 92 percent.

8.9 AC-Line Drop-Out (ACLDO)

To demonstrate the robustness of the hold-up time design of the 2 kW industrial battery charger demo board, ACLDO events can be tested in the worst operating conditions, i.e. no AC voltage from the grid during 10 ms working at full load. Key to the following figures:

- C1 (yellow): DC output voltage
- C2 (blue): AC input voltage
- C3 (purple): Output DC current
- C4 (green): AC input current of the demo board

		Value	Mean	Min	Max	St Dev	Count	Info
C4	Max	24.42A	24.415625	24.42	24.42	0.0	1.0	
C1	Min	49.55	49.55	49.55	49.55	0.0	1.0	
C3	Max	49.88A	49.878125	49.88	49.88	0.0	1.0	
C3	Min*	33.63A	33.628125	33.63	33.63	0.0	1.0	
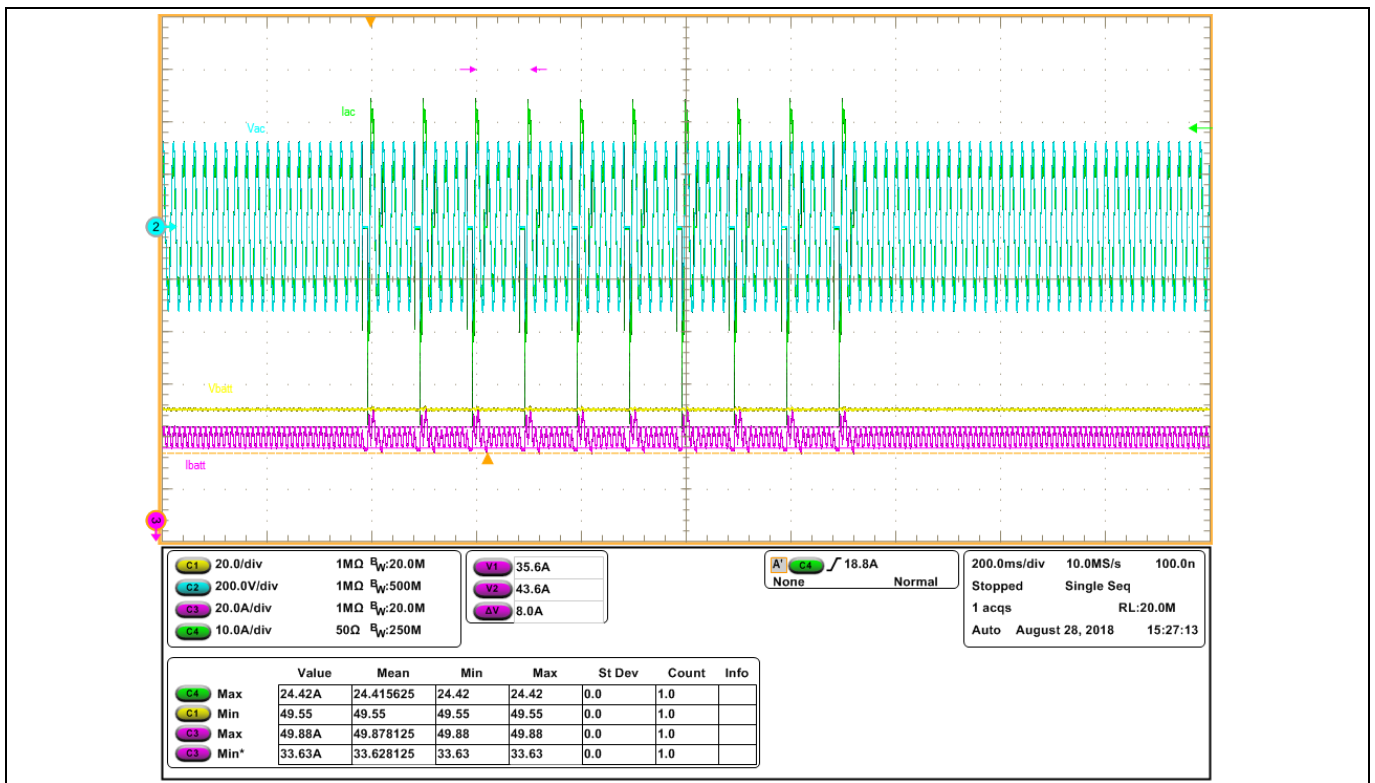
Figure 30 **Ten times 10 ms ACLDO events when V$_{in}$ = 230 V AC at P$_{out}$ = 2 kW**

As can be seen in Figure 30, the charger maintains error-free operation when subjected to the ten ACLDO events. Worth noting is that during this time-slot the output voltage is regulated even when the output current spikes considerably, but still within the permitted limits.

		Value	Mean	Min	Max	St Dev	Count	Info
C4	Max	24.42A	24.415625	24.42	24.42	0.0	1.0	
C1	Min	49.55	49.55	49.55	49.55	0.0	1.0	
C3	Max	49.88A	49.878125	49.88	49.88	0.0	1.0	
C3	Min*	33.63A	33.628125	33.63	33.63	0.0	1.0	
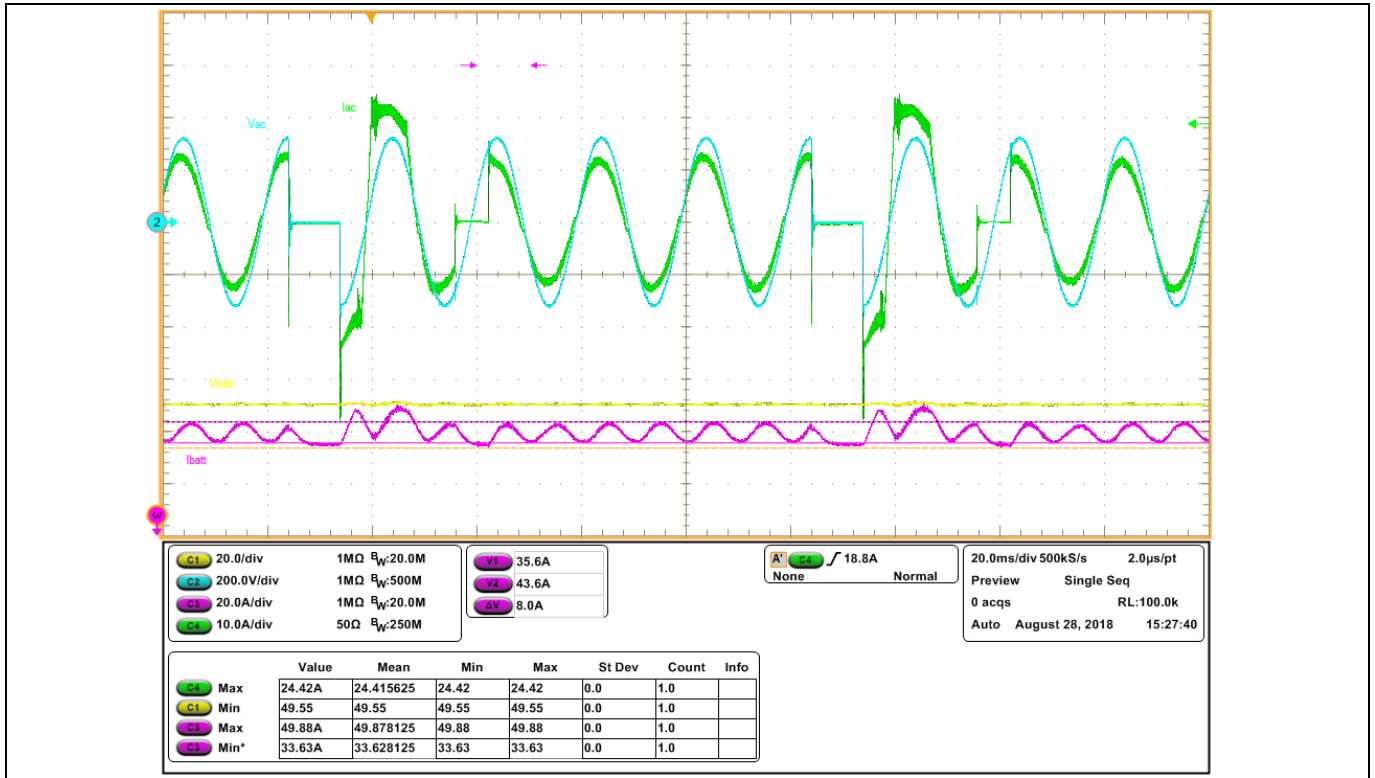
Figure 31   Detail view during two ACLDO events for 10 ms each when V_{in} = 230 V AC at P_{out} = 2 kW

As can be seen in Figure 31, the ACLDO event happens at 90 degrees with a black-out of 10 ms. The return happens at the most critical point, i.e. 270 degrees, when the current has its highest (or lowest) value. When the AC-line voltage returns, the PFC controller boosts in current limit operating mode. This results in the sinusoidal-like truncated current waveform at the input.

It is worth noticing that during this ACLDO, the output voltage remains unaffected (as expected due to the type of load), which assures an unchanged charging condition to the battery even during this abnormal event. The ripple current, however, doubles during this period. At the end, the charger starts operating normally again after 1.5 AC cycles.

Figure 32 and Figure 33 show power line disturbance events, commonly known as voltage dips or sags. In Figure 32, the input voltage decreases to 130 V AC during 500 ms. As expected, the input current is increased and during the first 200 ms the charger tries to maintain the same power. Due to thermal and electric protection, the charger enters power limitation of 1.6 kW for the rest of the time until the input voltage is restored to its rated value. Worth noticing is that during this period, the charger keeps the regulation voltage but at a lower charging current.

The same principle of operation is observed in Figure 33, when the input voltage decreases to 150 V AC for 2 s. Similarly to the previously explained PLD event, the input current is increased and for approximately 950 ms the charger enters power limitation of 1.6 kW. Due to thermal protection, the charger further limits its operation to 1.2 kW. Once the input voltage is restored to its rated value, the charger automatically and linearly restores its operation at the selected rated power.

Figure 32 500 ms voltage dip with a voltage decrease down to 130 V AC
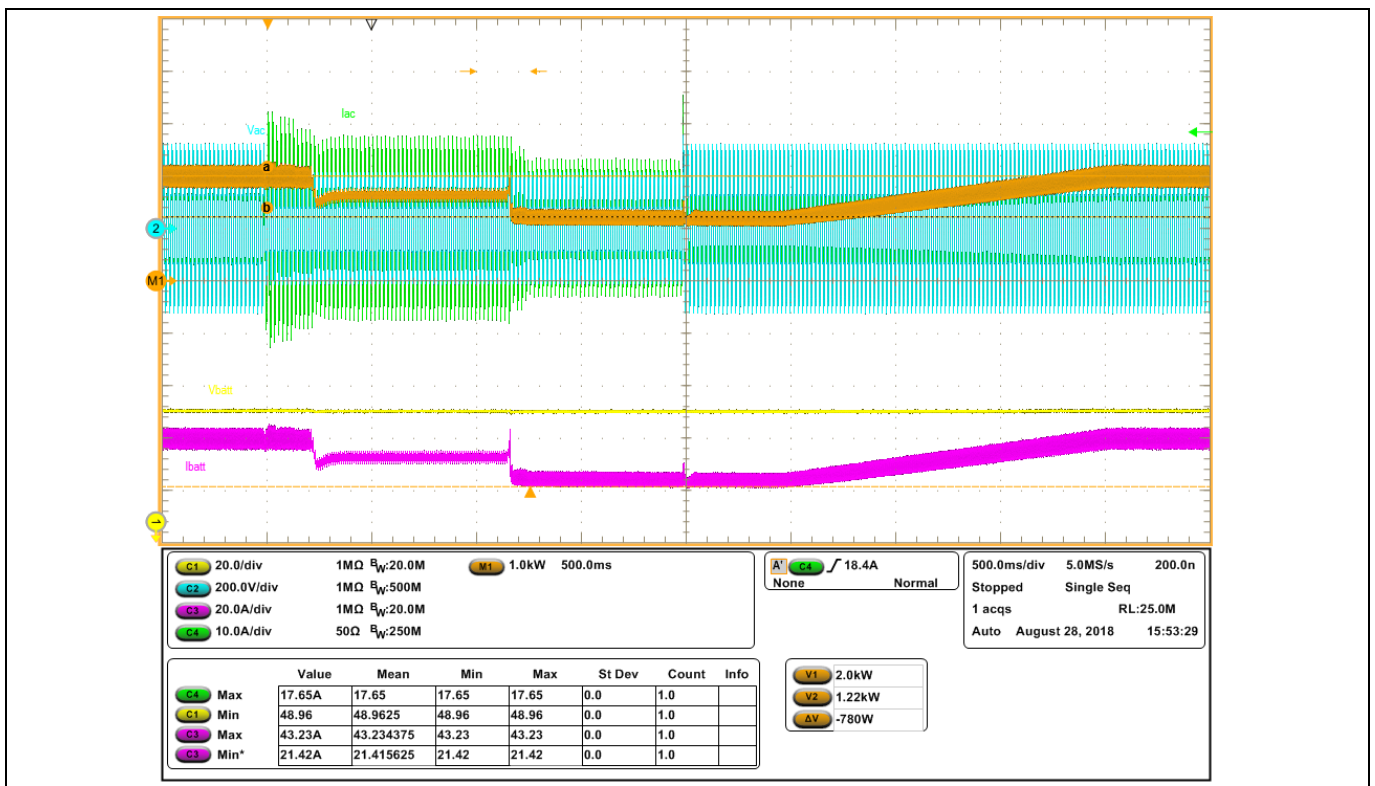
Figure 33 2 s voltage dip down to 150 V AC

9   Schematics, layout and Bill of Materials (BOM)

9.1   Power board schematic
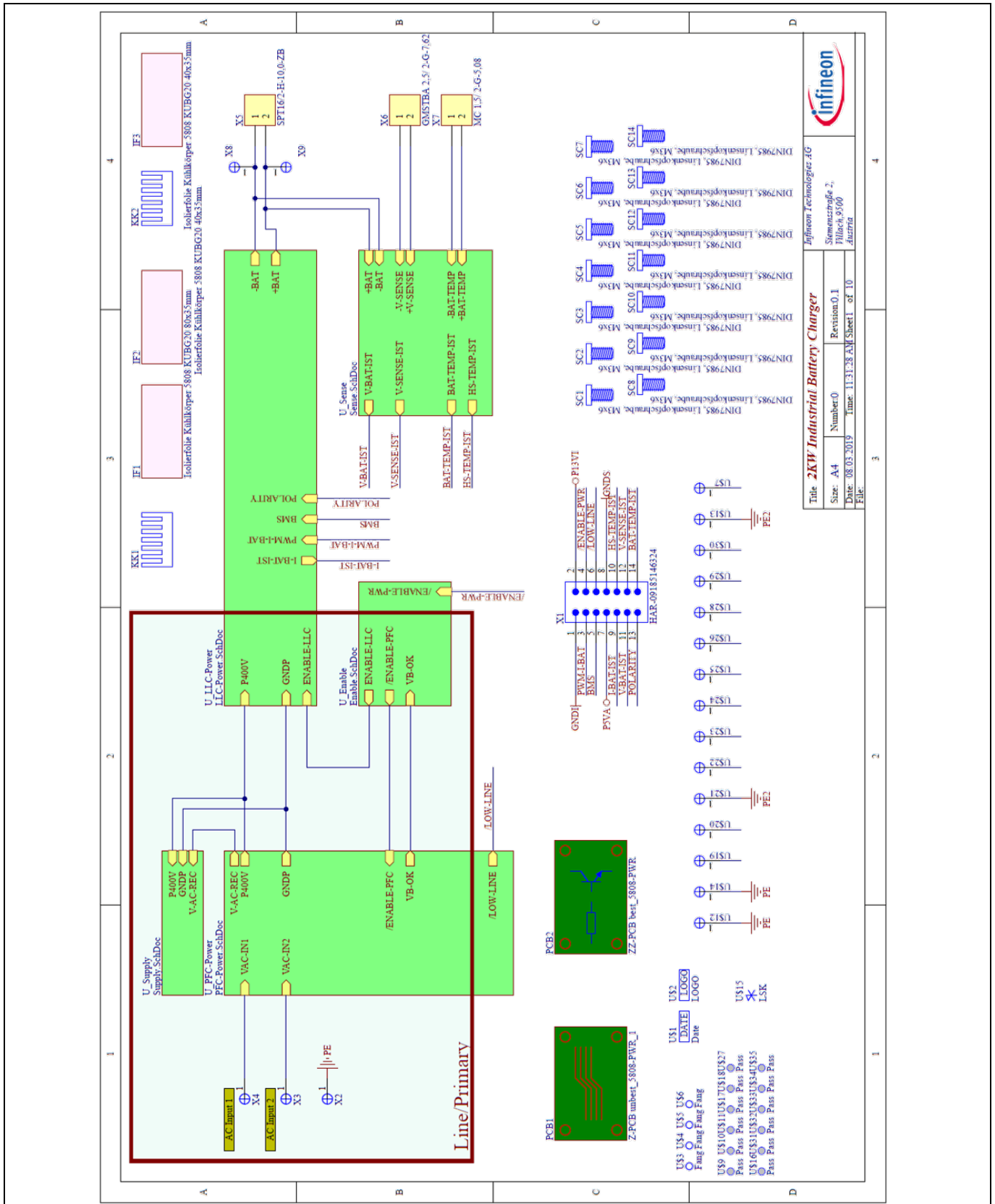
Figure 34   Main board block diagram
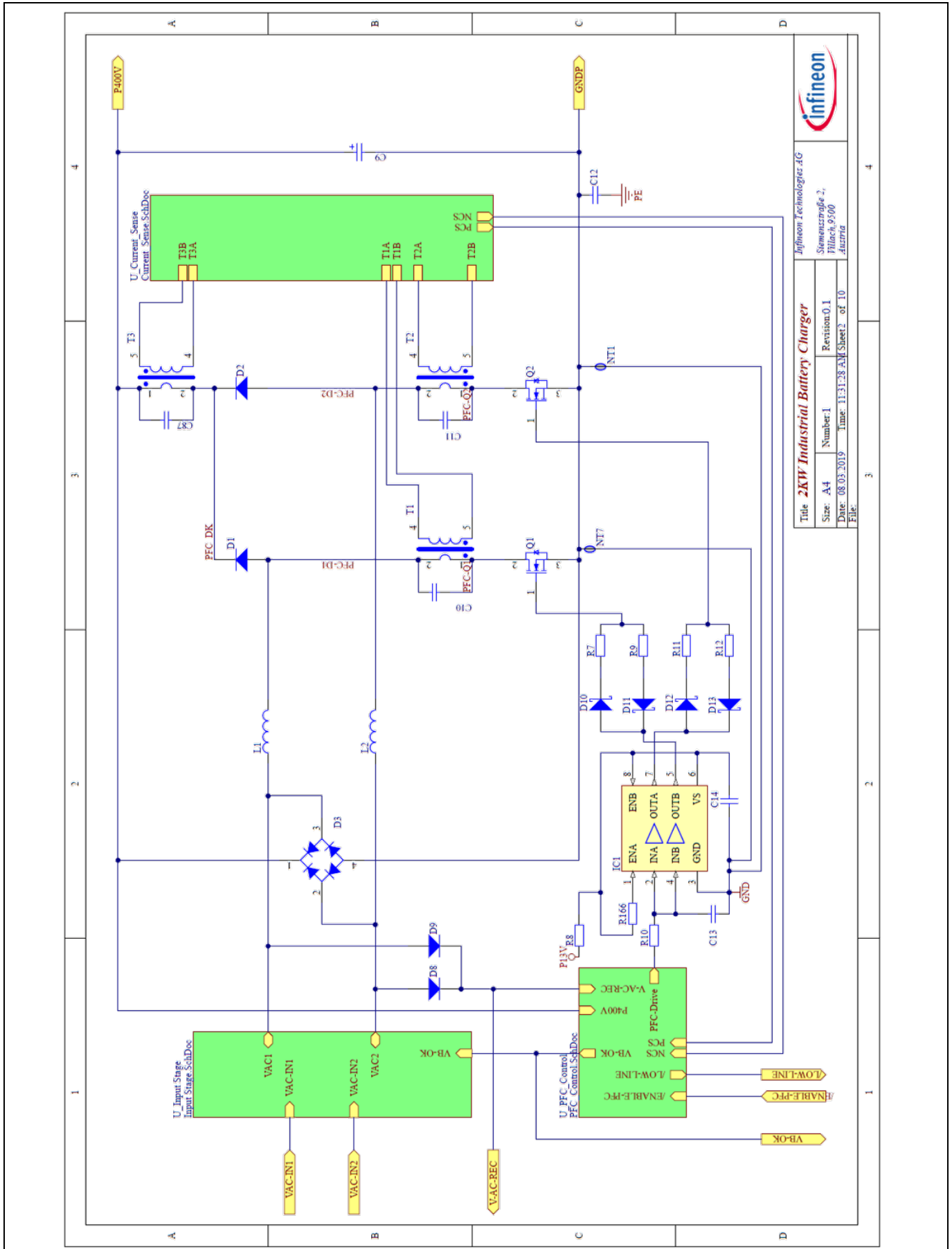
Figure 35   Dual PFC boost circuitry with controller interface
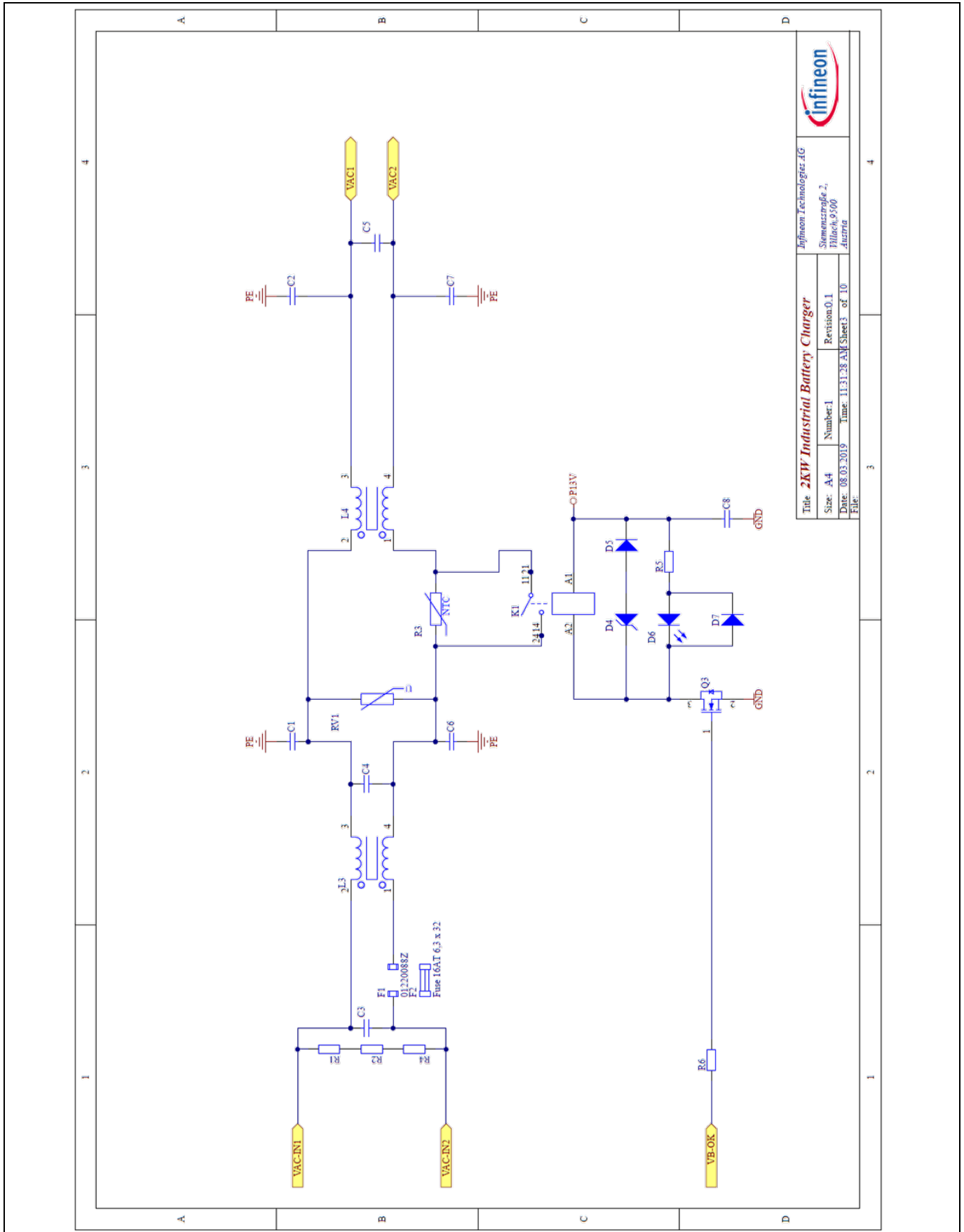
Figure 36 EMI filter and inrush current limit circuitry
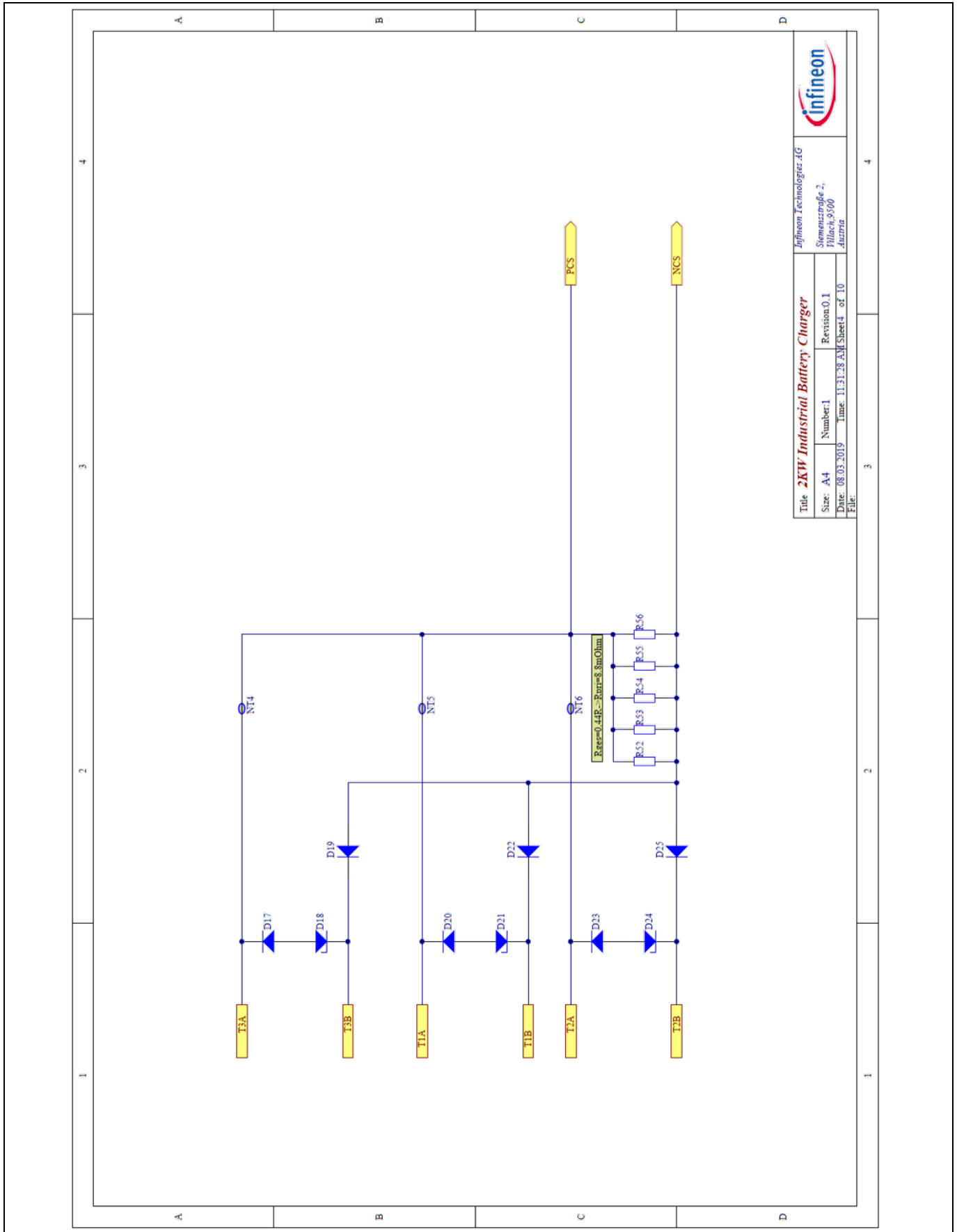
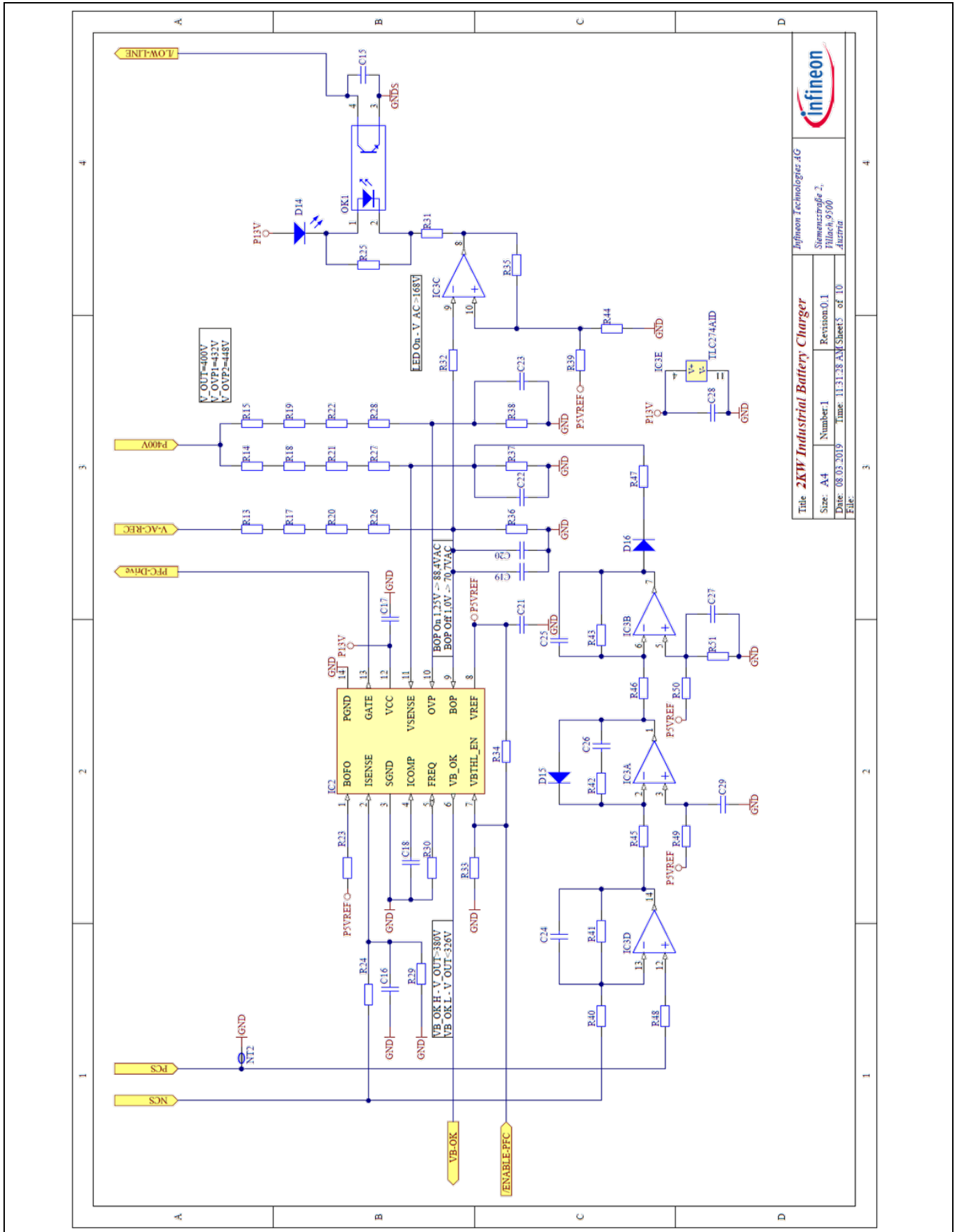**Figure 37** **Sensing circuitry on the secondary side of the current transformers for the PFC control**

Figure 38   PFC controller circuitry
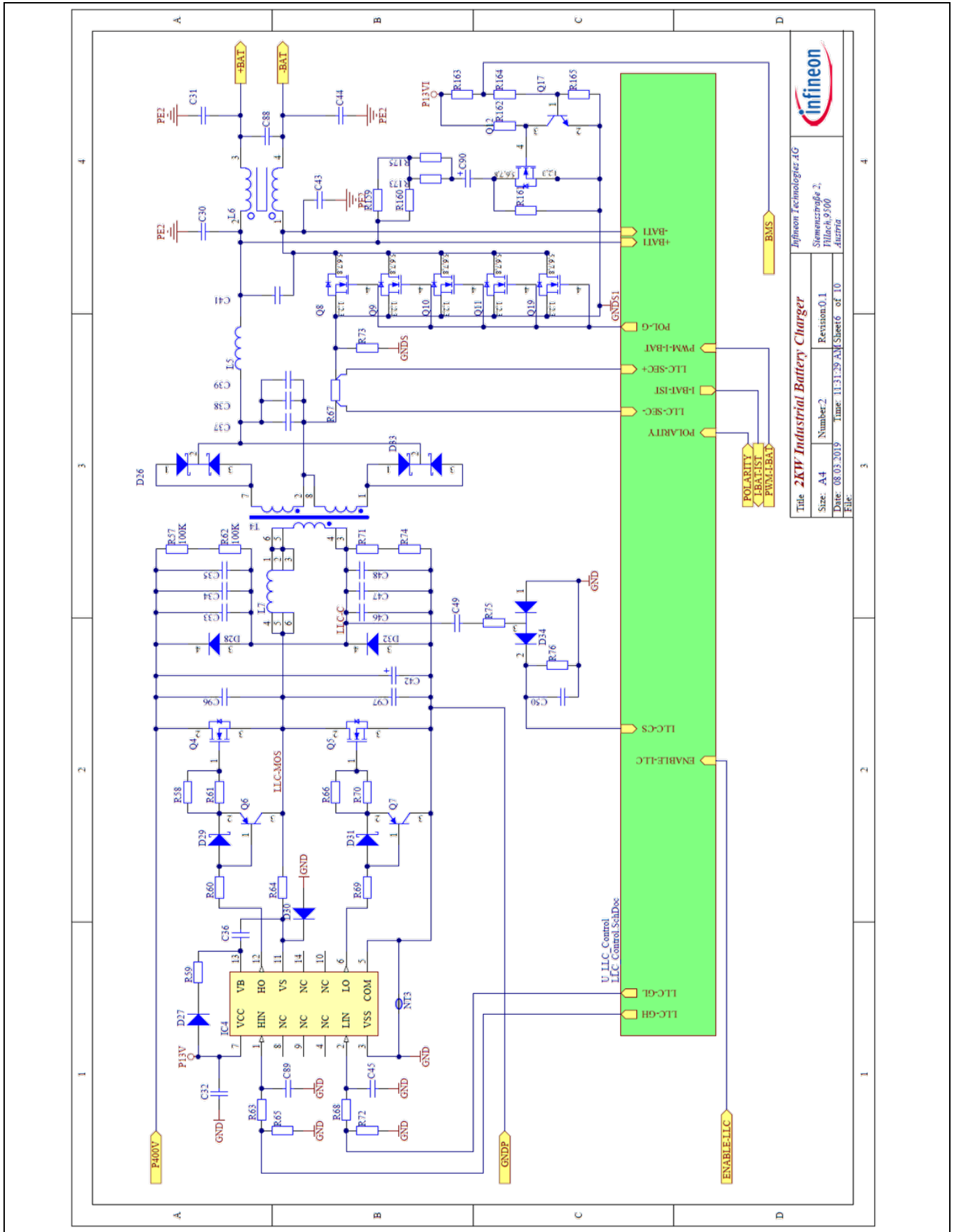
Figure 39   LLC half-bridge converter primary- and secondary-side circuitry with controller interface
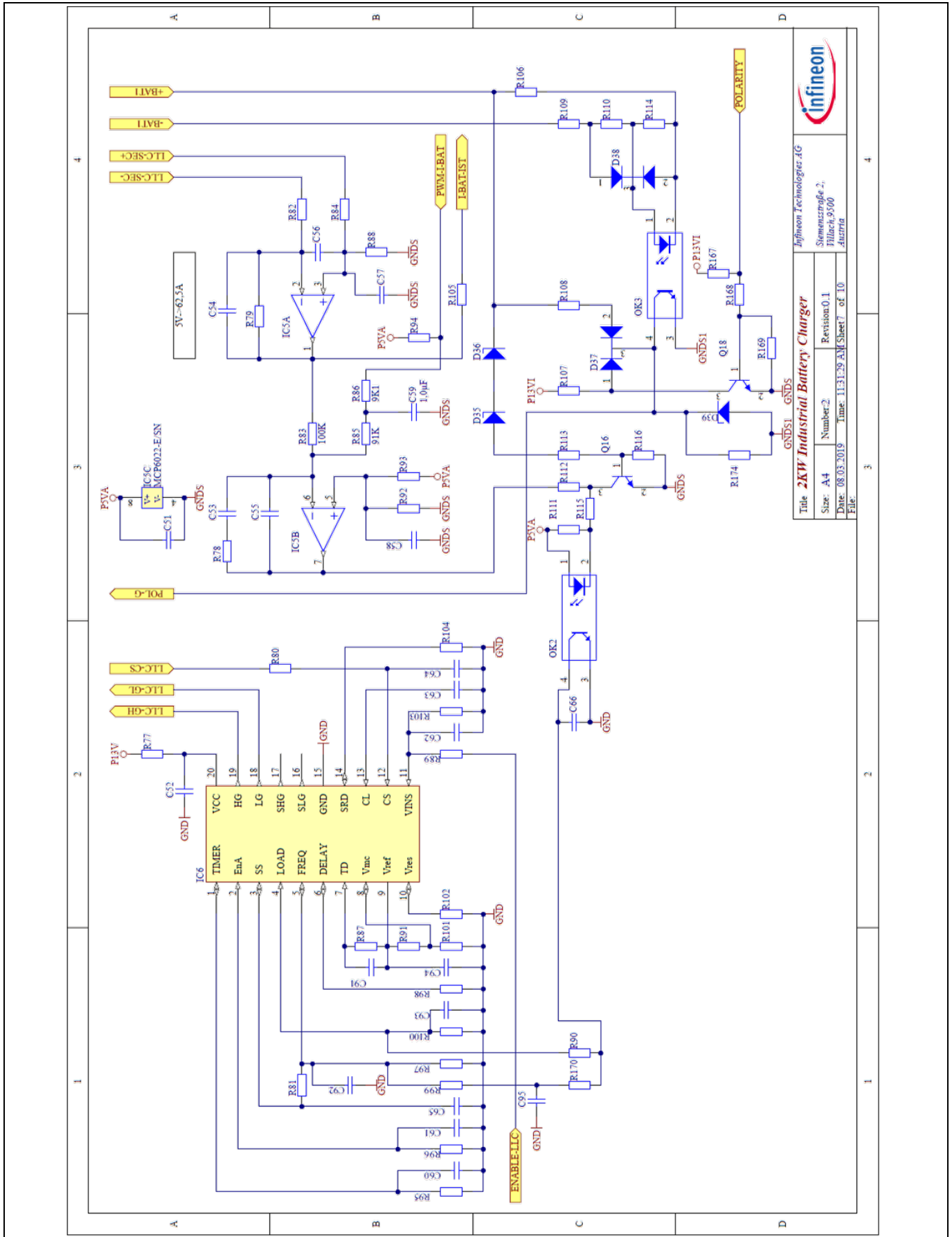
Figure 40   LLC controller including feedback loop control circuitry

Figure 41   Battery sensing circuitry

Figure 42   Bias supply circuitry
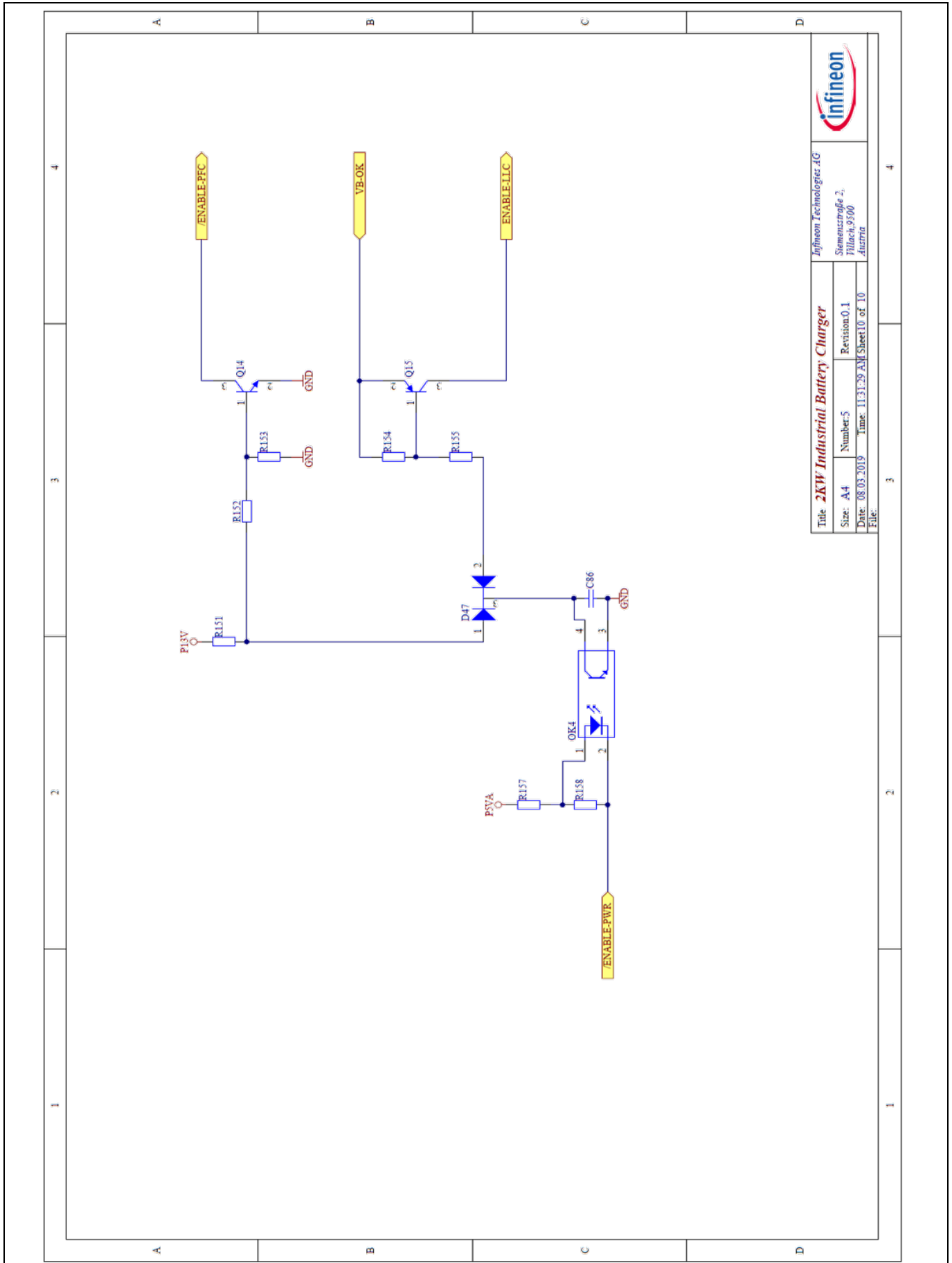
Figure 43   Enabling circuitry

9.2 Power board PCB layout
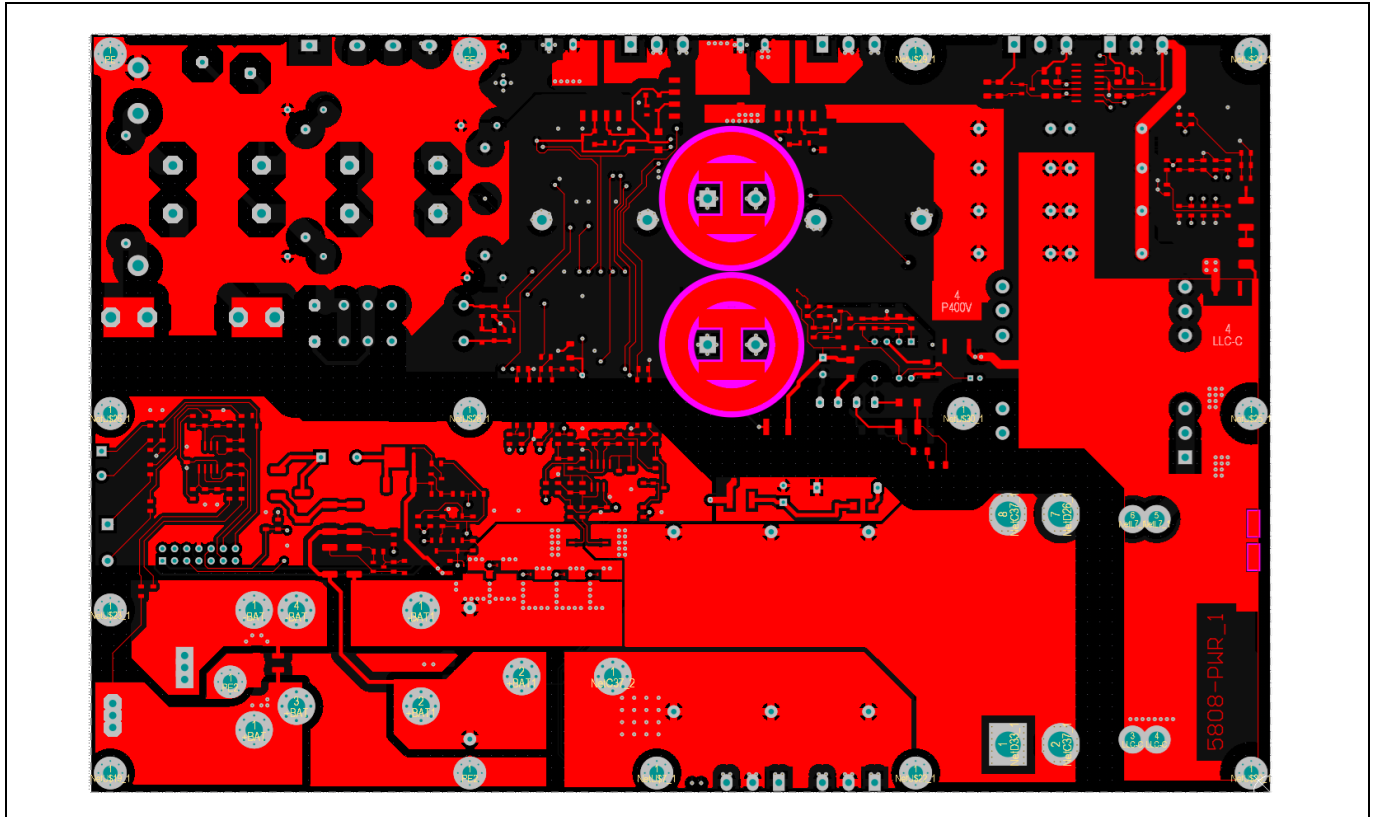
Figure 44 **View of the power PCB top layer**
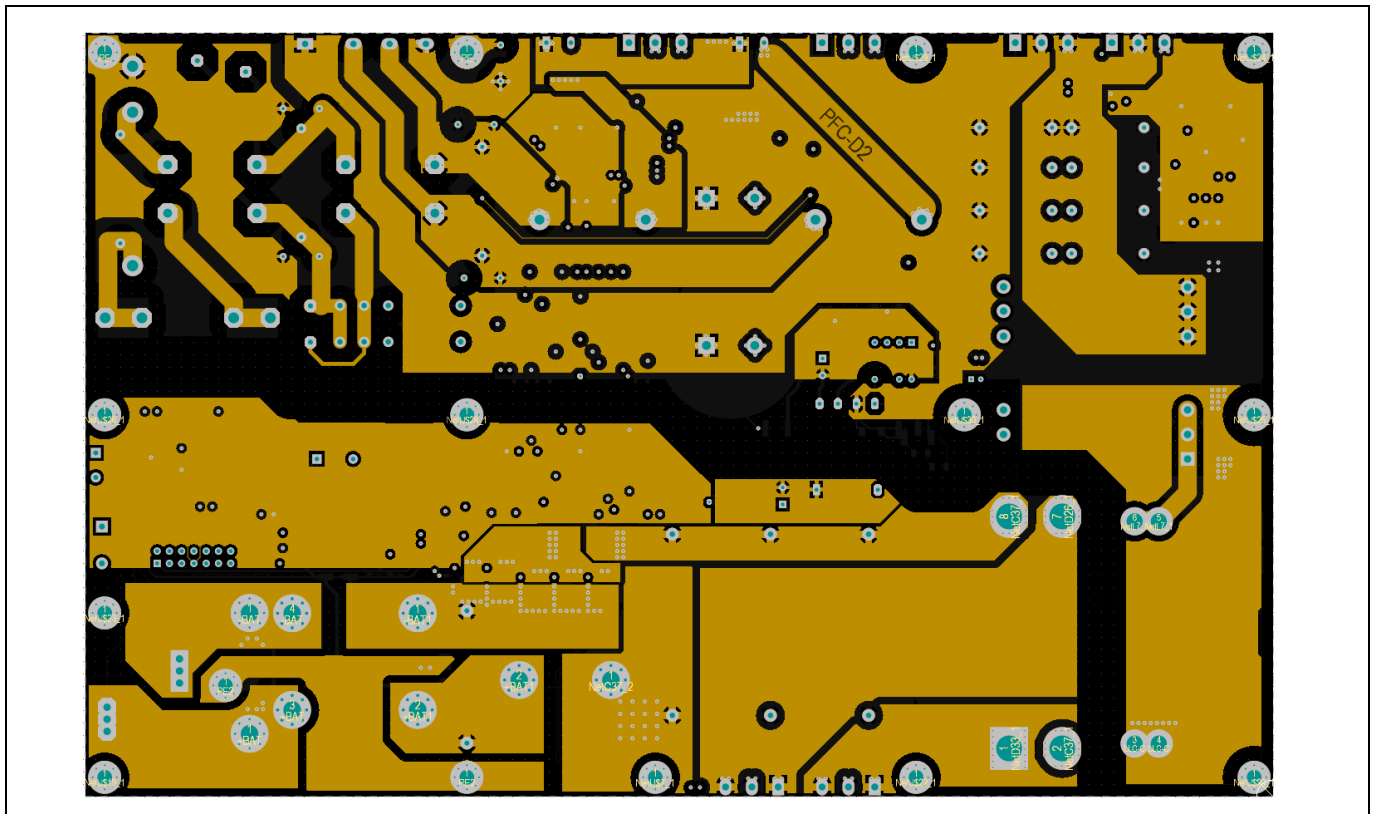
Figure 45 **View of the power PCB inner 1 layer**
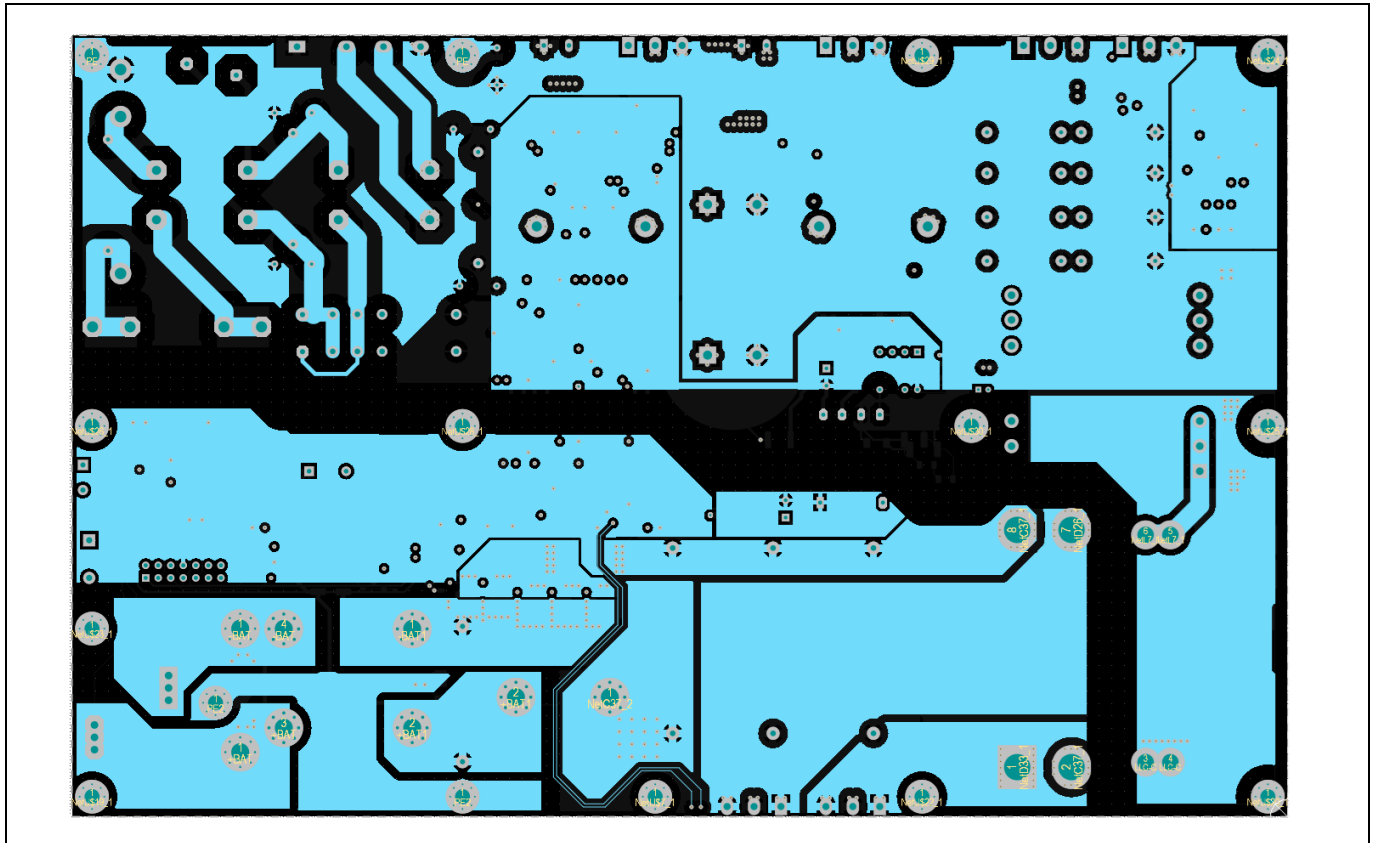
Figure 46   View of the power PCB inner 2 layer
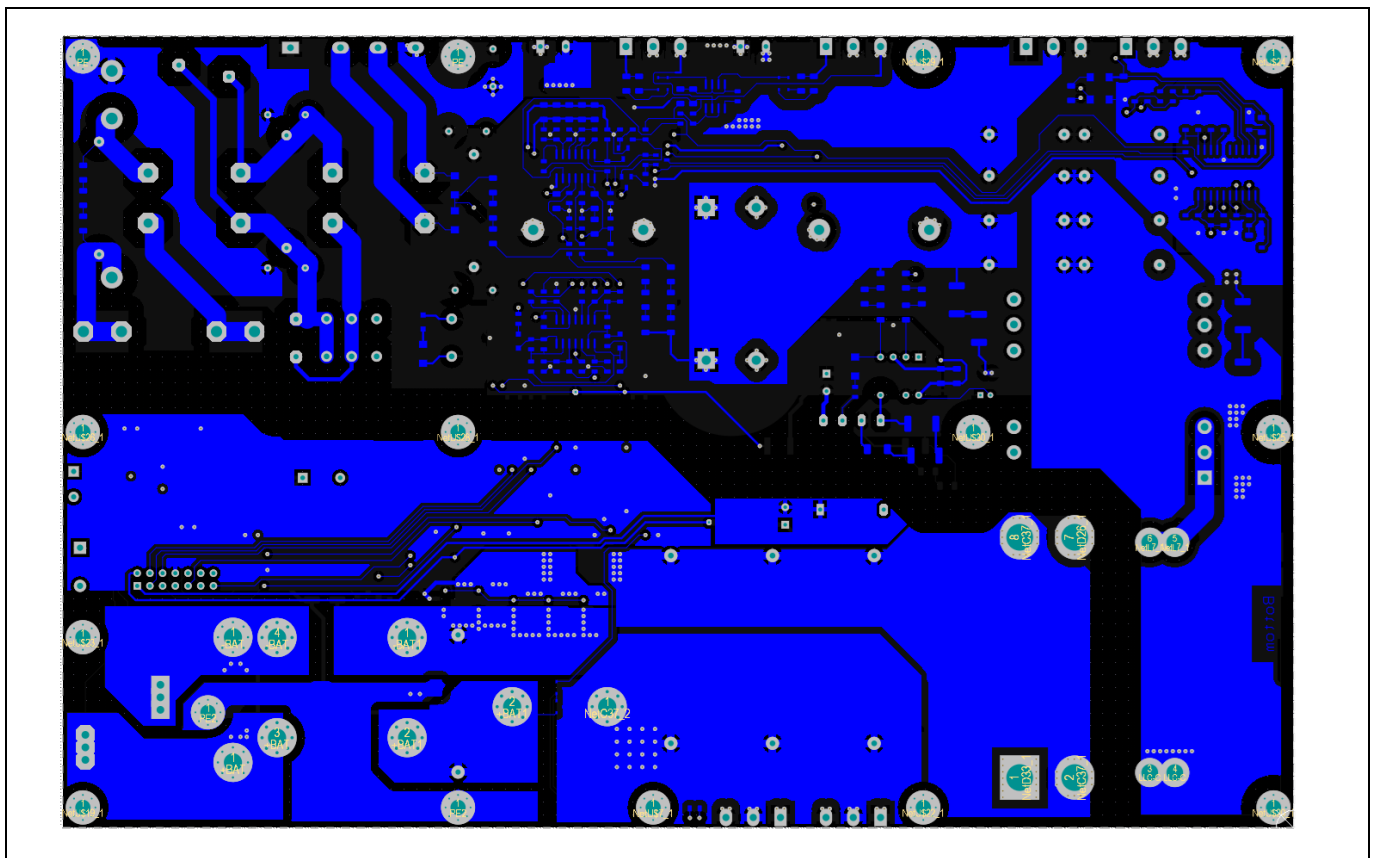
Figure 47   View of the power PCB bottom layer

9.3 Power board BOM

Table 15 **Power board BOM**

Comment	Description	Designator	Quantity
2.2 nF/300 V/Y2	Capacitor	C1, C2, C6, C7, C12	5
1.0 µF/275 V/X2	Capacitor	C3, C4	2
2.2 µF/275 V/X2	Capacitor	C5	1
100 nF	Capacitor	C8, C21, C27, C28, C29, C40, C51, C80, C83, C94, C98	11
470 µF/450 V	Polarized capacitor	C9, C42	2
2.2 nF/630 V	Capacitor	C10, C11, C87	3
100 pF	Capacitor	C13, C45, C62, C75, C89	5
4.7 µF	Capacitor	C14, C17, C58, C65	4
1.0 nF	Capacitor	C15, C61, C64, C66, C67, C68, C69, C70, C81, C86, C93	11
3.3 nF	Capacitor	C16	1
6.8 nF	Capacitor	C18	1
2.2 µF	Capacitor	C19, C20, C32, C36, C73, C78, C82	7
10 nF	Capacitor	C22, C23, C25, C55, C95, C99	6
1.0 µF	Capacitor	C24, C26, C52, C59, C84, C85	6
100 nF	Capacitor	C30, C43, C88	3
4.7 nF/630 V/NP0	Capacitor	C31, C44	2
47 nF/1 kV DC	Capacitor	C33, C34, C35, C46, C47, C48	6
10 µF/250 V	Capacitor	C37, C38, C39	3
22 µF/100 V/MKS4	Capacitor	C41	1
330 pF/1 kV	Capacitor	C49	1
470 nF	Capacitor	C50, C60	2
330 nF	Capacitor	C53	1
220 pF	Capacitor	C54, C56, C57, C91, C92	5
47 nF	Capacitor	C63	1
1.0 nF/1 kV	Capacitor	C71	1
33 pF/3 kV	Capacitor	C72	1
220 µF/35 V	Polarized capacitor	C74, C77	2
22 µF/50 V	Polarized capacitor	C76	1
68 nF	Capacitor	C79	1
1000 µF/80 V	Polarized capacitor	C90	1
470 pF/2 kV/FKP1	Capacitor	C96, C97	2
IDH16G65C6	Diode	D1, D2	2
LVB2560	Full-wave diode bridge	D3	1
SMAJ15	Diode	D4	1

Comment	Description	Designator	Quantity
1N4448W-7-F		D5, D7, D15, D16, D17, D20, D23, D43	8
HSMG-C170	LED	D6	1
S1M		D8, D9	2
BAS3010A		D10, D11, D12, D13, D29, D31	6
SML-211DTT86K 605 nm	LED	D14	1
BZX84/C75	Z-diode SOT23	D18, D21, D24	3
STTH102A		D19, D22, D25, D42	4
DSSK60-02A	Schottky double diode TO220/247	D26, D33	2
STTH1L06A		D27, D30	2
IDB15E60		D28, D32	2
BAV99	Double diode SOT23	D34	1
BZX384B33-V		D35, D36	2
BAV70	Double diode SOT23 common cathode	D37, D38, D47	3
BZX84/C15	Z-diode SOT23	D39	1
STTH108A		D40	1
10MQ100N		D41, D44	2
BZX384B12-V		D45	1
PLVA650A	Z-diode SOT23	D46	1
01220088Z	Double fuse clip	F1	1
Fuse 16 AT 6.3 × 32	Fuse	F2	1
2EDN7524F	Dual non-inverting MOSFET driver	IC1	1
ICE3PCS01G	PFC controller	IC2	1
TLC274AID	Micropower quad op-amp	IC3	1
IRS21814	High- and low-side driver	IC4	1
MCP6022-E/SN	Micropower dual op-amp	IC5, IC7	2
ICE2HS01G	High-performance resonant mode controller	IC6	1
ICE5QR4780AZ	QR CoolSET™ controller	IC8	1
Insulated heatsink 5808 KUBG20 80 × 35 mm	Insulation	IF1	1
Insulated heatsink 5808 KUBG20 40 × 35 mm	Insulation	IF2, IF3	2
HF115F/012-1HS3B	Single-pole single-relay	K1	1
5808-Ind 358 µH/20 A	Inductor	L1, L2	2
2x1,8mH/14A_WUE7448261418	Magnetic-Core Inductor Common Mode	L3, L4	2

Comment	Description	Designator	Quantity
5808-Ind 2.3 µH/55 A	Inductor	L5	1
5808-CMC sek	Magnetic core CM inductor	L6	1
5808-LLC-L 9 µH	Inductor	L7	1
10 µH/650 mA (B82432T1103K000)	Inductor	L8, L9	2
TCLT1003	Optoisolator	OK1, OK2, OK3, OK4	4
Z-PCB unbest_5808-PWR_1	Unsoldered board	PCB1	1
ZZ-PCB best_5808-PWR	Soldered board	PCB2	1
IPW60R080P7	CoolMOS™ SJ MOSFET	Q1, Q2	2
BSS138BK	N-CH power MOSFET	Q3	1
IPW60R060P7	CoolMOS™ SJ MOSFET	Q4, Q5	2
FMMT718	Amplifier transistor PNP silicon	Q6, Q7	2
BSC030N08NS5	OptiMOS™ MOSFET	Q8, Q9, Q10, Q11, Q12, Q19	6
BC847C	Amplifier transistor NPN silicon	Q13, Q14, Q16, Q17, Q18	5
BC857C	Amplifier transistor PNP silicon	Q15	1
150 K	Resistor	R1, R2, R4	3
B57364S0100M	NTC inrush	R3	1
4K7	Resistor	R5, R29, R111, R141, R146, R162	6
1K0	Resistor	R6, R80, R104, R112, R116, R147, R148	7
12 R	Resistor	R7, R8, R9, R11, R12, R69	6
100 R	Resistor	R10, R63, R68, R82, R84, R105, R166	7
2M0	Resistor	R13, R17, R20	3
1M0	Resistor	R14, R15, R18, R19, R21, R22	6
12 K	Resistor	R16, R102, R117, R122, R123, R128, R168, R169	8
33 K	Resistor	R23, R39, R91	3
75 R	Resistor	R24, R76, R140	3
2K7	Resistor	R25, R31, R149	3
330 K	Resistor	R26, R90	2
180 K	Resistor	R27, R171, R172, R174	4
560 K	Resistor	R28	1
68 K	Resistor	R30	1
10 K	Resistor	R32, R42, R65, R72, R93, R94, R103, R153, R154, R165, R176	11
110 K	Resistor	R33	1

Comment	Description	Designator	Quantity
160 K	Resistor	R34	1
1M5	Resistor	R35, R96	2
100 K	Resistor	R36, R50, R51, R83, R100, R108, R118, R119, R120, R121, R124, R125, R126, R127, R143	15
20 K	Resistor	R37, R38	2
470 R	Resistor	R40, R48, R115	3
24 K	Resistor	R41, R107, R164, R167	4
47 K	Resistor	R43, R45, R46, R47, R49, R98, R110, R142, R163	9
30 K	Resistor	R44	1
2R2	Resistor	R52, R53, R54, R55, R56, R59, R64, R77	8
100 K	Resistor	R57, R62, R71, R74	4
10 R	Resistor	R58, R60, R61, R66, R70	5
LRMAP3920B-R0005	Shunt resistor four-wire	R67	1
1R0	Resistor	R73, R159, R160, R173, R175	5
220 R	Resistor	R75	1
3K3	Resistor	R78, R99, R170	3
16 K	Resistor	R79, R88	2
6K2	Resistor	R81	1
91 K	Resistor	R85	1
9K1	Resistor	R86, R92	2
270 K	Resistor	R87	1
1K2	Resistor	R89, R101	2
470 K	Resistor	R95	1
27 K	Resistor	R97, R139	2
3K32	Resistor	R106, R109	2
1K5	Resistor	R113, R114, R157, R158	4
1M2	Resistor	R129, R132, R136	3
15 M	Resistor	R130, R133, R137	3
220 K	Resistor	R131, R134	2
680 R	Resistor	R135, R138	2
5R6	Resistor	R144, R145	2
B57421V2103J062	NTC resistor	R150	1
22 K	Resistor	R151, R152, R155	3
1K0	Resistor	R161	1
S20K275 Epcos B72220S0271K101	Industrial high-energy metal-oxide varistor	RV1	1
DIN7985, Linsenkopfschraube, M3 × 6	Screw	SC1, SC2, SC3, SC4, SC5, SC6, SC7, SC8, SC9,SC10, SC11, SC12, SC13, SC14	14

Comment	Description	Designator	Quantity
B78417A2285A003	SMT CS transformers, EP7	T1, T2, T3	3
5808-LLC-X	LLC transformer EE65	T4	1
5808 transformer EE16 184_15_15_R01	Transformer Flyback converter	T5	1
HAR-09185146324	Flat cable connector (IDC), standard male header, pin, 14 contacts	X1	1
SPT16/2-H-10.0-ZB	Header, two-pin	X5	1
GMSTBA 2.5/2-G-7.62	Header, two-pin	X6	1
MC 1.5/2-G-5.08	Header, two-pin	X7	1

9.4 Control board schematic
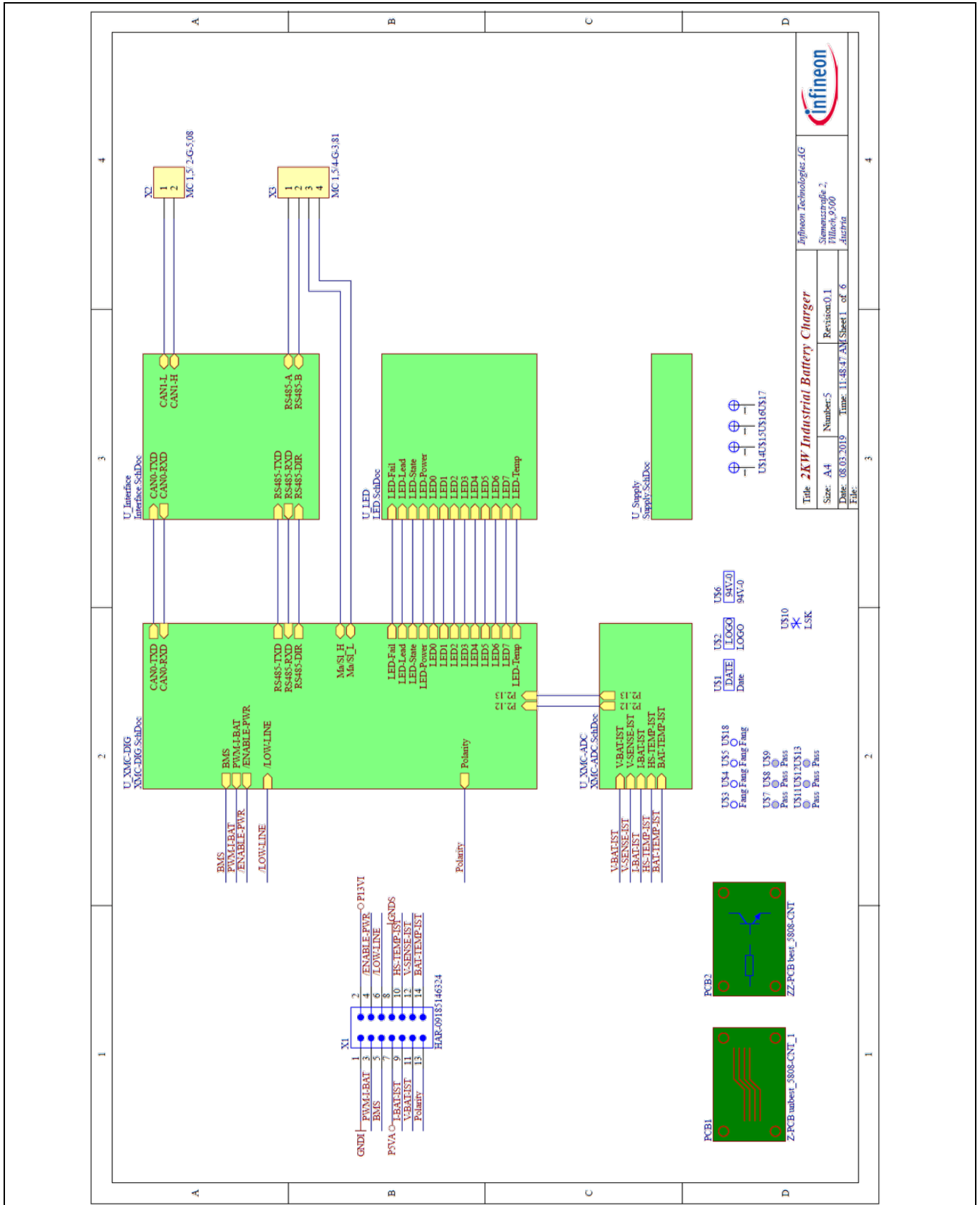
Figure 48 Block diagram of the control board

Figure 49   ADC-related circuitry
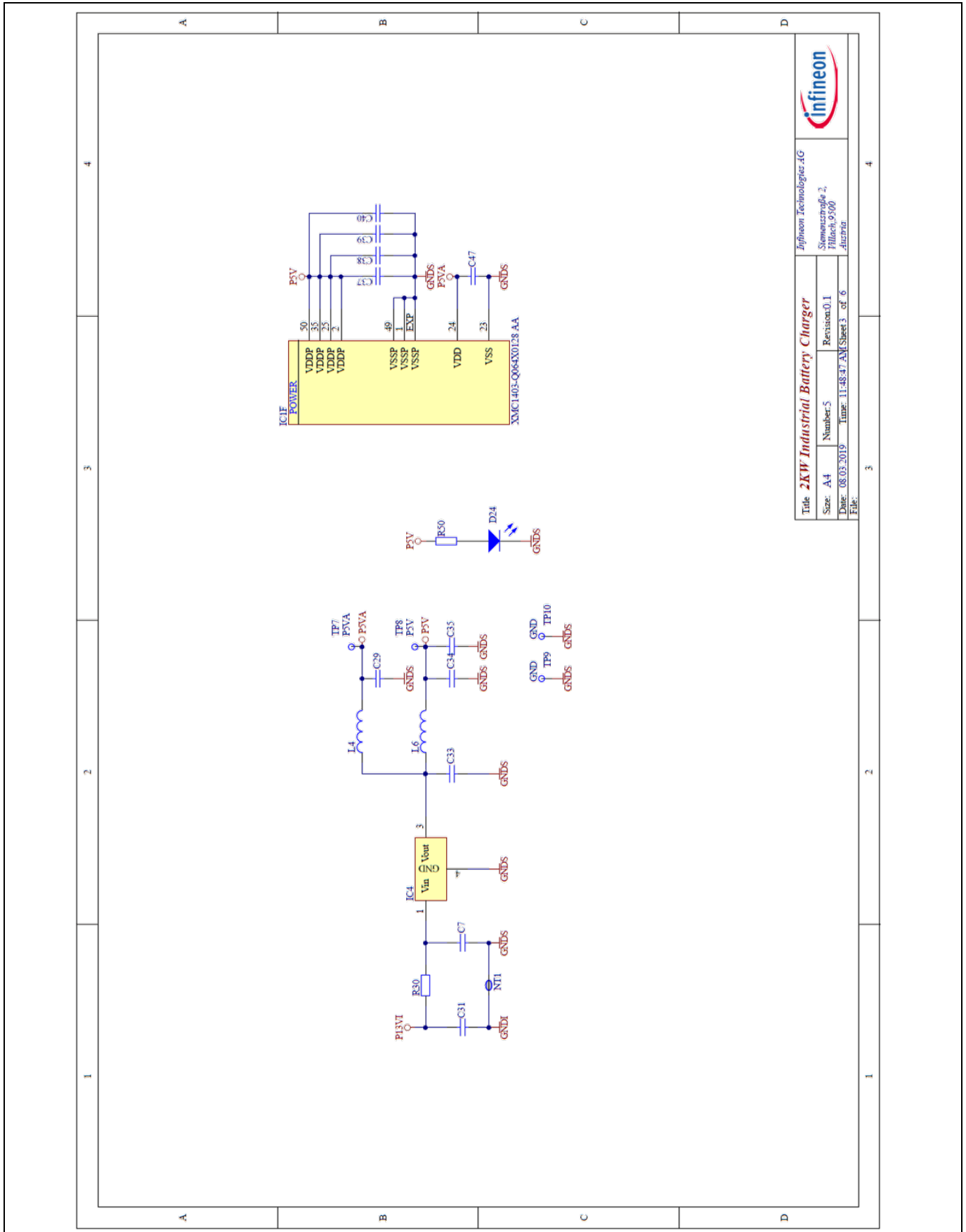
Figure 50   Supply input voltage to the XMC™ microcontroller

Figure 51   Communication interface ports circuitry

Figure 52   Main digital XMC™ 1400-based interface circuitry
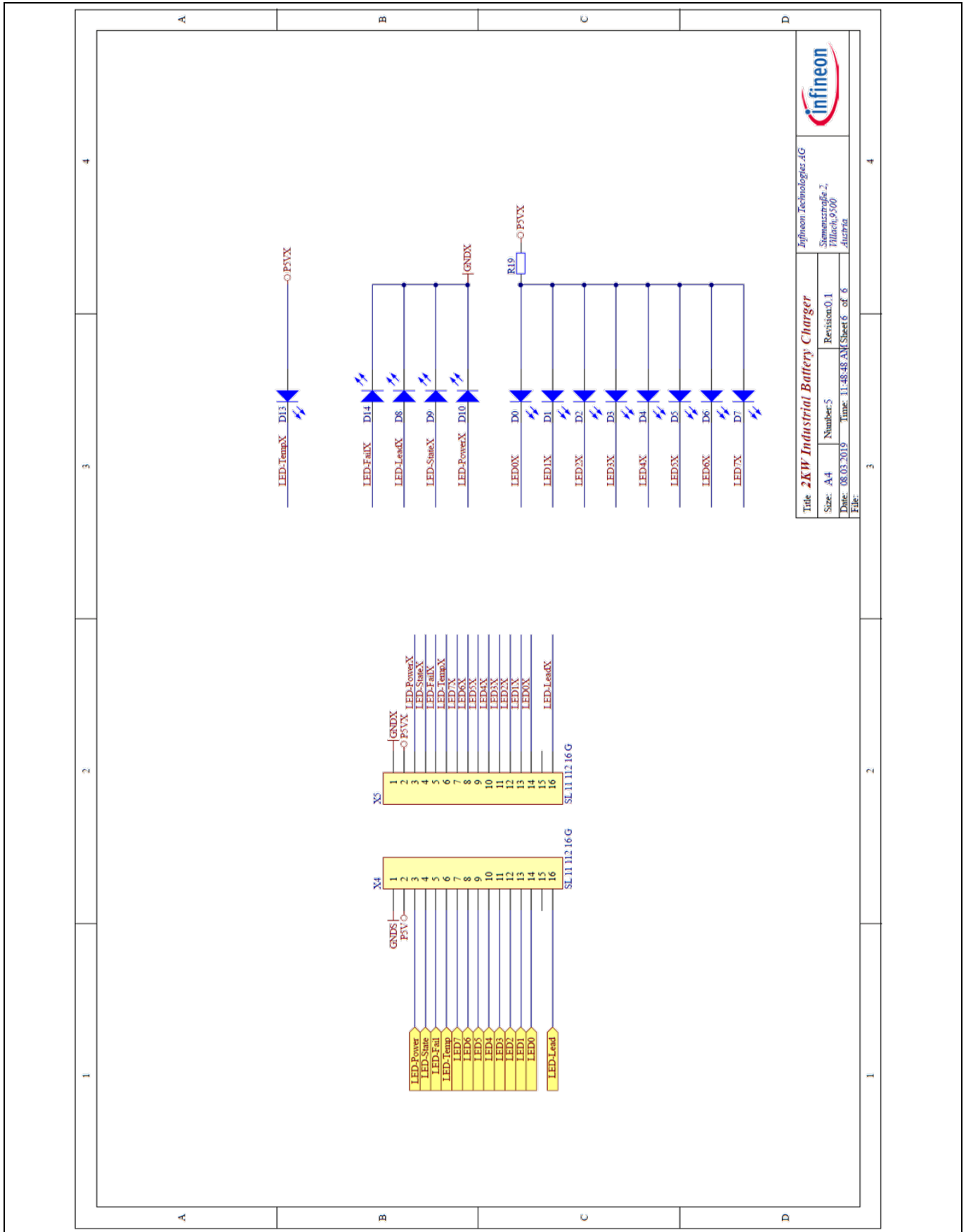
Figure 53   LED indicator circuitry

9.5   Control board PCB layout
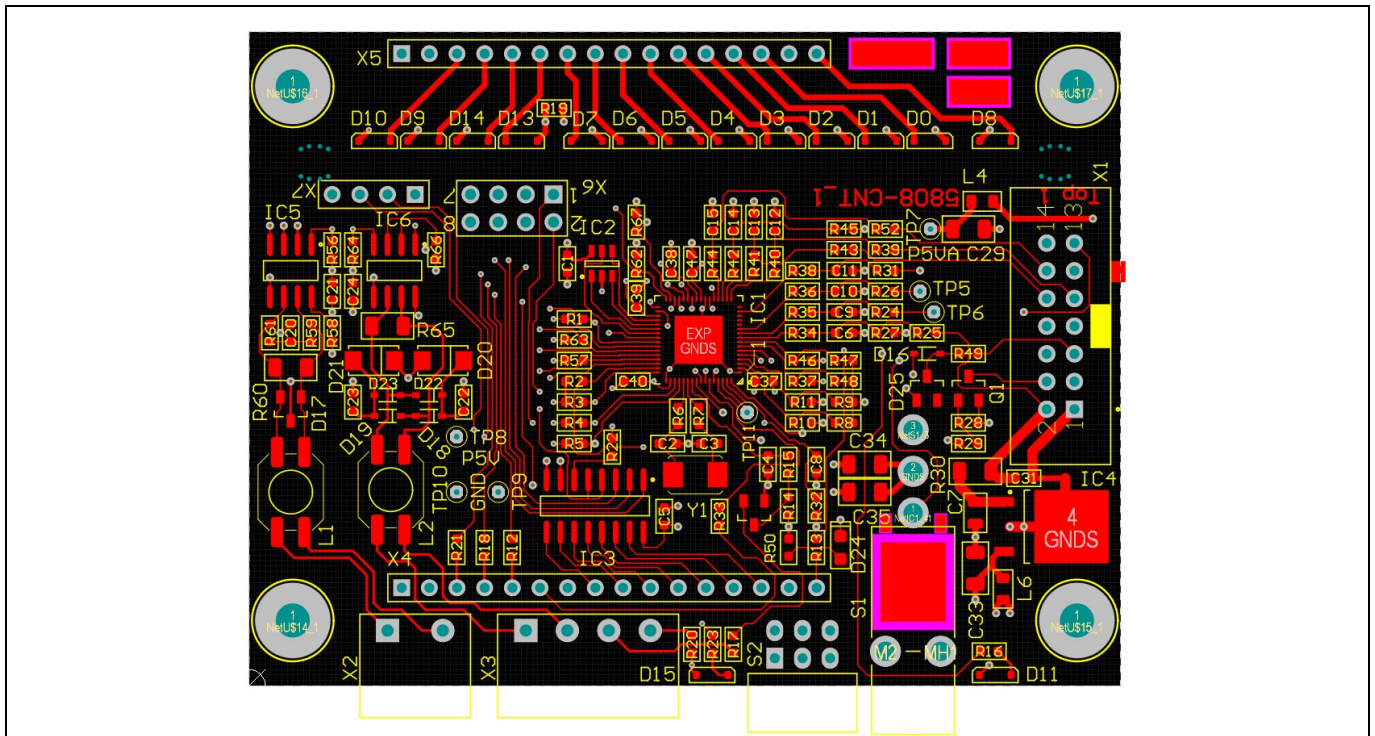
Figure 54   View of control PCB top layer
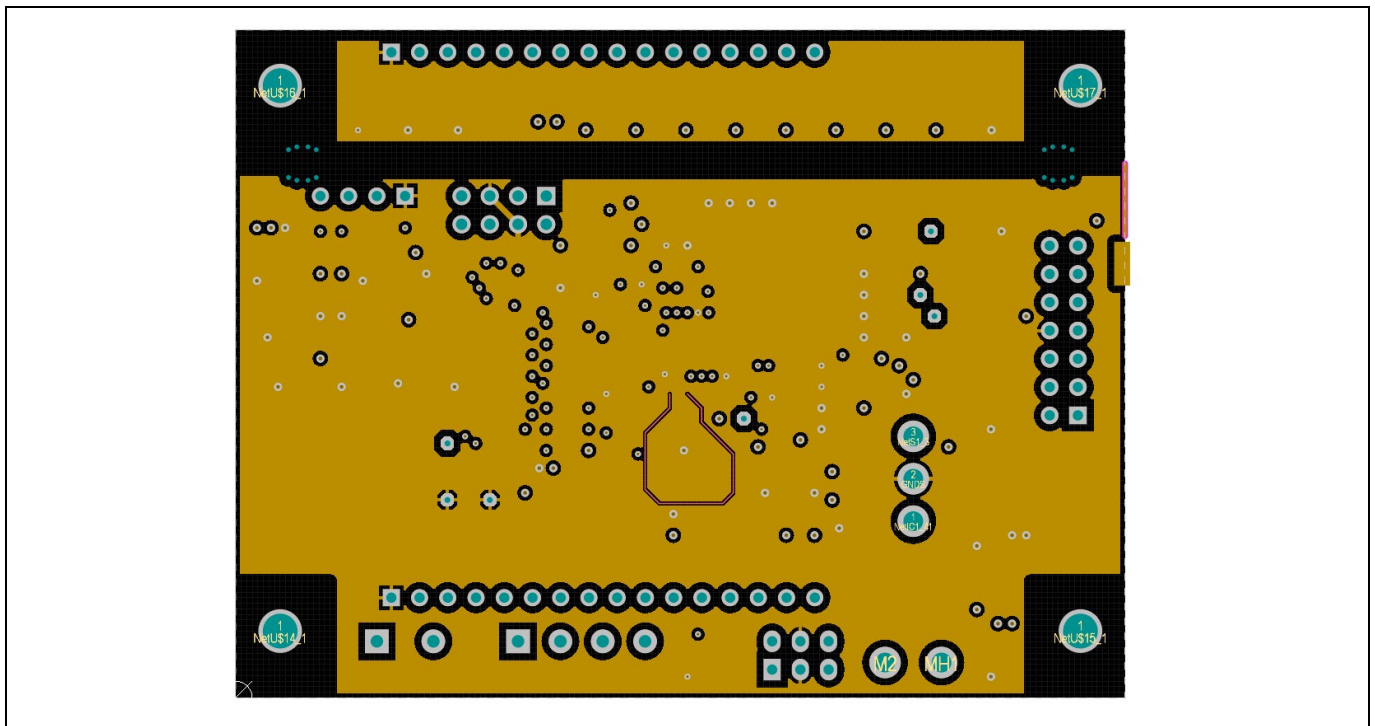
Figure 55   View of control PCB inner 1 layer
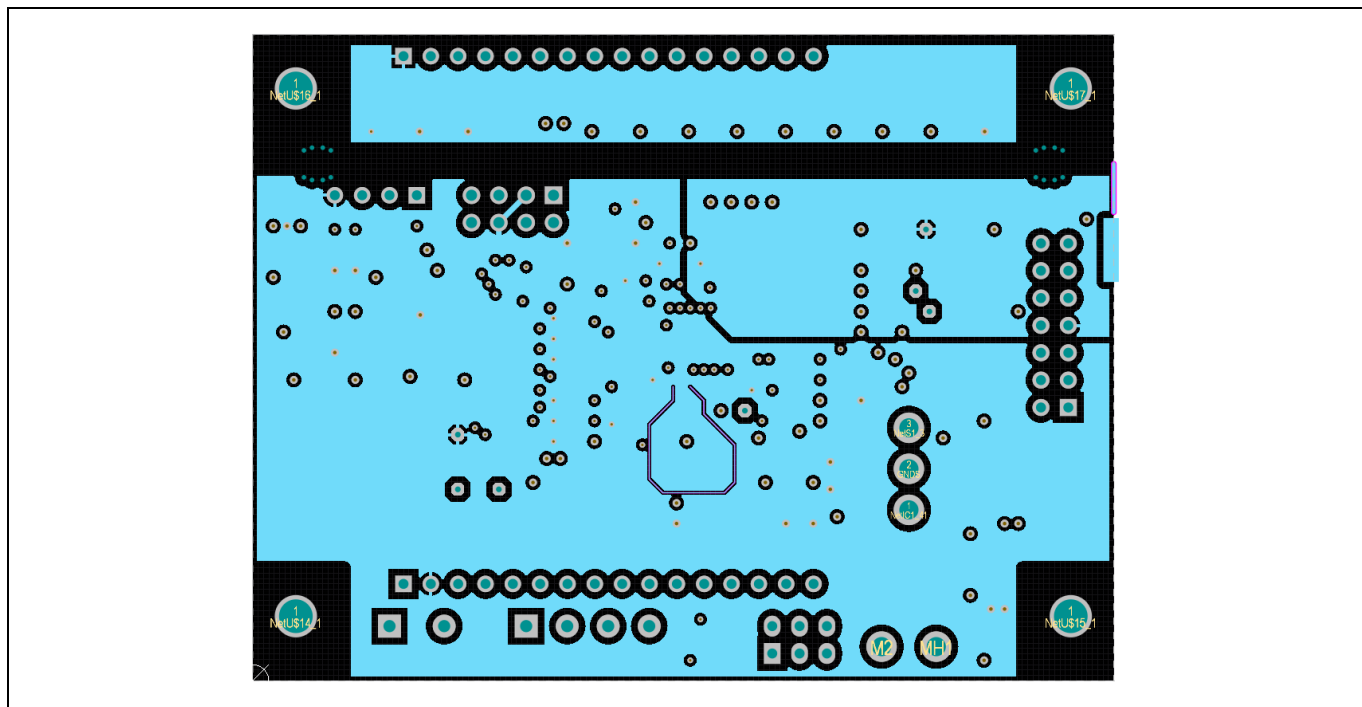
Figure 56   View of control PCB inner 2 layer
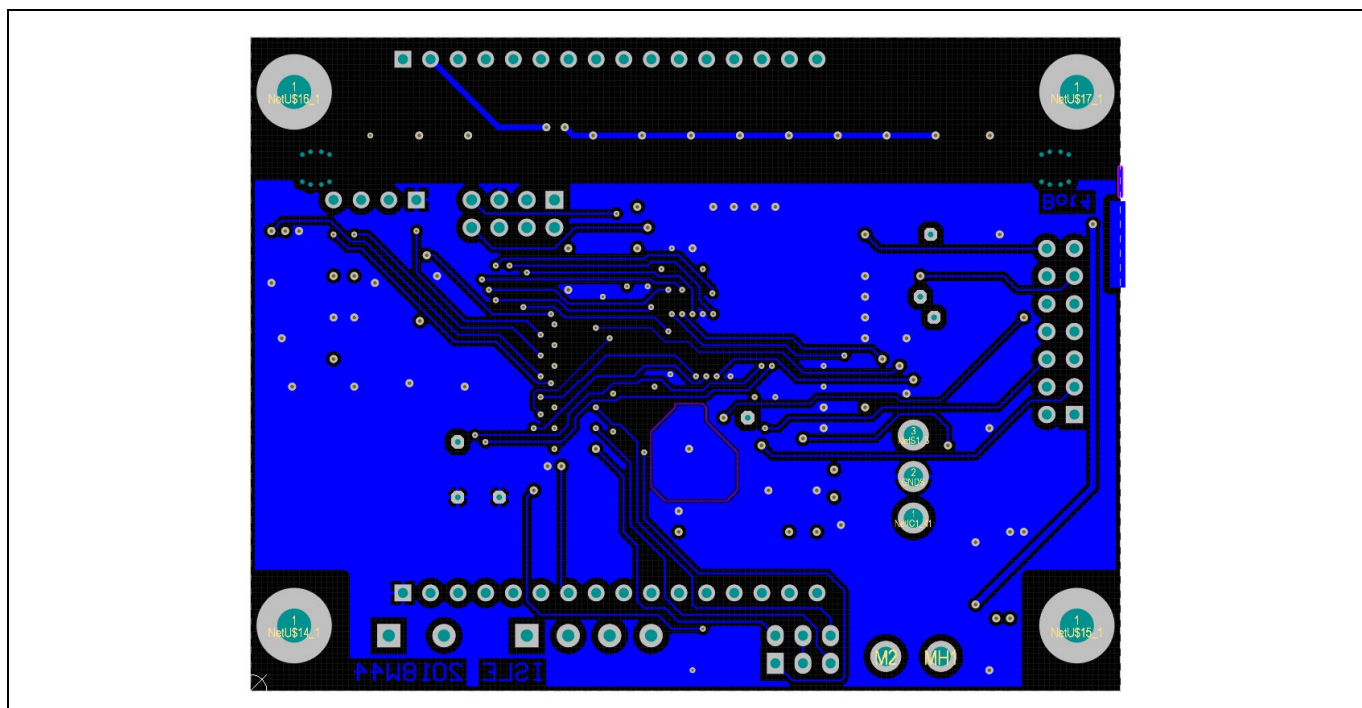
Figure 57   View of control PCB bottom layer

9.6 Control board BOM

Table 16   **Control board BOM**

Comment	Description	Designator	Quantity
100 nf	Capacitor	C1, C4, C5, C6, C21, C24, C31, C37, C38, C39, C40	11
18 pF	Capacitor	C2, C3	2
1.0 µF	Capacitor	C7	1
1.0 nF	Capacitor	C8, C9, C10, C11, C15	5
3.3 nF	Capacitor	C12, C13, C14	3
4.7 nF	Capacitor	C20	1
47 nF	Capacitor	C22, C23	2
10 µF	Capacitor	C29, C33, C34, C35	4
220 nF	Capacitor	C47	1
LYY876	LED	D0, D1, D2, D3, D4, D5, D6, D7	8
LBY8SG	LED	D8	1
LGY876	LED	D9, D10	2
LWY8SG	LED	D11, D15	2
BAS70-04	Schottky double diode SOT23	D12	1
LSY876	LED	D13	1
LOY876	LED	D14	1
1N4448WS-7-F		D16, D18, D19, D22, D23	5
PESD1CAN	Transil array for CAN ESD protection	D17	1
SMAJ6.5A		D20, D21	2
HSMG-C170	LED	D24	1
PLVA650A	Z-diode SOT23	D25	1
XMC1403-Q064X0128 AA	IFX XMC1000 family microcontroller	IC1	1
25LC040AT-E/OT	SPI serial EEPROM	IC2	1
74AHC138D	Dual peripheral driver	IC3	1
LP2950ACDT-5.0	Micropower voltage regulator	IC4	1
IFX1050G	CAN transceiver for 24 V systems	IC5	1
SN65HVD3082ED	Multi-point RS485/RS422 transceiver	IC6	1
B82793C0225N265	Magnetic core CM inductor	L1, L2	2
BLM21PG331SN1D	Inductor	L4, L6	2
Z-PCB unbest_5808-CNT_1	Unsoldered board	PCB1	1
ZZ-PCB best_5808-CNT	Soldered board	PCB2	1

Comment	Description	Designator	Quantity
BC847C	Amplifier transistor NPN silicon	Q1	1
10 K	Resistor	R1, R2, R3, R4, R5, R22, R27, R28, R29, R47, R48, R56, R57, R58, R62, R63, R64, R66, R67	19
0R0	Resistor	R6, R7	2
n.b.	Resistor	R8, R9, R37, R46	4
1K0	Resistor	R10, R11, R12, R18, R19, R21, R49, R50	8
470 R	Resistor	R13, R16, R17, R20, R23	5
22 K	Resistor	R14	1
2K2	Resistor	R15	1
8K2	Resistor	R24, R26, R31, R39, R43, R45, R52	7
27 K	Resistor	R25	1
10 R	Resistor	R30	1
4K7	Resistor	R32	1
1K5	Resistor	R33, R59, R61	3
47 R	Resistor	R34, R35, R36, R38, R40, R41, R42, R44	8
180 R	Resistor	R60	1
120 R	Resistor	R65	1
1MS1T2B4M7RE	Sub-miniature SPDT toggle switch	S1	1
PT65 5 26 L254	DIP switch, four-position, SPST	S2	1
HAR-09185146324	Flat cable connector (IDC), standard male header, pin, 14 contacts	X1	1
MC 1.5/2-G-5.08	Header, two-pin	X2	1
MC 1.5/4-G-3.81	Header, four-pin	X3	1
SL 11 112 16 G	Header, 16-pin	X4, X5	2
SL 22 139 8 G	Header, four-pin, dual row	X6	1
SL 11 112 4 G	Header, four-pin	X7	1
ABM3-20.000MHZ-D2Y-T	Quartz crystal	Y1	1

Revision history

Major changes since the last revision

Page or reference	Description of change

Other Trademarks
All referenced product or service names and trademarks are the property of their respective owners.